AD-A123 858 HYDROCODE CALCULATIONS OF HIGH LENGTH-TO-DIAMETER CYLINDRICAL EXPLOSIONS IN SAND(U) ORLANDO TECHNOLOGY INC SHALIMAR FL J J OSBORN FEB 82 AFATL-TR-82-10 1/1

UNCLASSIFIED F08635-81-C-0050 F/G 19/4 NL

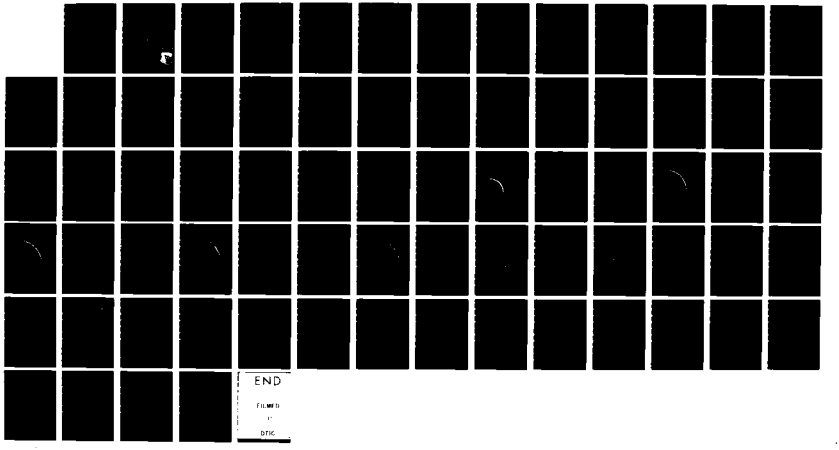

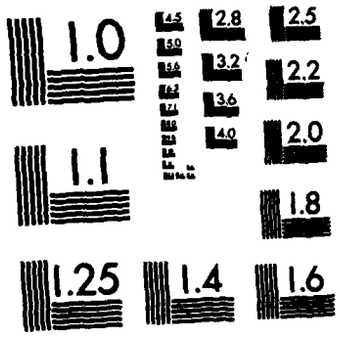

AFATL-TR-82-10

Hydrocode Calculations of High Length-to-Diameter Cylindrical Explosions in Sand

John J Osborn

ORLANDO TECHNOLOGY, INC
P O BOX 855
SHALIMAR, FLORIDA 32579

FEBRUARY 1982

FINAL REPORT FOR PERIOD MAY 1981-JUNE 1981

Approved for public release; distribution unlimited

Air Force Armament Laboratory
AIR FORCE SYSTEMS COMMAND ★ UNITED STATES AIR FORCE ★ EGLIN AIR FORCE BASE, FLORIDA

UNCLASSIFIED

SECURITY CLASSIFICATION OF THIS PAGE *(When Data Entered)*

REPORT DOCUMENTATION PAGE	READ INSTRUCTIONS BEFORE COMPLETING FORM
1. REPORT NUMBER: AFATL-TR-82-10	2. GOVT ACCESSION NO.: AD-A123858
3. RECIPIENT'S CATALOG NUMBER	
4. TITLE *(and Subtitle)*: HYDROCODE CALCULATIONS OF HIGH LENGTH-TO-DIAMETER CYLINDRICAL EXPLOSIONS IN SAND	5. TYPE OF REPORT & PERIOD COVERED: FINAL REPORT 1 May 1981 - 30 June 1981
	6. PERFORMING ORG. REPORT NUMBER
7. AUTHOR(s): John J. Osborn	8. CONTRACT OR GRANT NUMBER(s): F08635-81-C-0050 Purchase Order 2000-3-1
9. PERFORMING ORGANIZATION NAME AND ADDRESS: Orlando Technology, Incorporated P.O. Box 855 Shalimar, Florida 32579	10. PROGRAM ELEMENT, PROJECT, TASK AREA & WORK UNIT NUMBERS: PE: 62602F JON: 2543-19-24
11. CONTROLLING OFFICE NAME AND ADDRESS: Air Force Armament Laboratory Armament Division Eglin Air Force Base, Florida 32542	12. REPORT DATE: February 1982
	13. NUMBER OF PAGES: 72
14. MONITORING AGENCY NAME & ADDRESS *(if different from Controlling Office)*	15. SECURITY CLASS. *(of this report)*: UNCLASSIFIED
	15a. DECLASSIFICATION/DOWNGRADING SCHEDULE

16. DISTRIBUTION STATEMENT *(of this Report)*

Approved for public release; distribution unlimited.

17. DISTRIBUTION STATEMENT *(of the abstract entered in Block 20, if different from Report)*

18. SUPPLEMENTARY NOTES

Availability of this report is specified on verso of front cover.

19. KEY WORDS *(Continue on reverse side if necessary and identify by block number)*

Cylindrical Explosives
Sand
Reflected Pressure
Incident Pressure
Hydrocode

20. ABSTRACT *(Continue on reverse side if necessary and identify by block number)*

This document presents wave propagation computer code (hydrocode) calculations of infinitely long Composition B explosive cylinders detonated in a dry, highly porous, sand medium. Scaled free-field pressure and pressure impulse predictions are presented along with reflected pressures.

DD FORM 1 JAN 73 1473

UNCLASSIFIED

SECURITY CLASSIFICATION OF THIS PAGE *(When Data Entered)*

PREFACE

The calculations in this report were performed by Orlando Technology, Incorporated, P.O. Box 855, Shalimar, Florida 32579, under subcontract to Datatec, Incorporated of Fort Walton Beach, 182 Green Acres Road, Fort Walton Beach, Florida 32548. Purchase Order 2000-13-1 applies. The Datatec, Inc. contract is F08635-81-C-0050 with the Air Force Armament Laboratory, Armament Division, Eglin Air Force Base, Florida 32542. Program Manager on the Datatec, Inc. contract is Mr. James R. Holder (DLYV). This work was accomplished during the period from 1 May 1981 to 30 June 1981.

The Public Affairs (PA) office has reviewed this report, and it is releasable to the National Technical Information Service (NTIS), where it will be available to the general public, including foreign nationals.

This technical report has been reviewed and is approved for publication.

FOR THE COMMANDER

JAMES L. THOREEN
Chief, Analysis Division

(The reverse of this page is blank)

TABLE OF CONTENTS

LIST OF FIGURES

LIST OF FIGURES (CONCLUDED)

LIST OF TABLES

LIST OF SYMBOLS

R = Distance or Range

R_{HE} = Radius of Explosive Charge

P = Pressure

P_I = Incident Pressure

P_R = Reflected Pressure

ρ = Density

ρ_o = Initial Density

μ = Excess Compression = $\frac{\rho}{\rho_o} - 1$

η = Volumetric Strain = $1-\rho_o/\rho$

s = Slope of Shock Velocity/Particle Velocity Curve

(The reverse of this page is blank)

SECTION I

INTRODUCTION/SUMMARY

Recent experiments have been sponsored by the Air Force Armament Laboratory (AFATL) to measure pressure against buried structures from high length-to-diameter buried explosives. Hydrocode calculations were required to help understand anomalous high pressure results of models built from low pressure measurements. This report documents the several calculations performed.

All calculations were performed using a model of Eglin AFB dry sand (40-percent porosity). The calculations predict reflected pressure for several incident pressures, free-field pressure in the sand as a function of explosive size and reflected pressure on a plate placed in the soil at a distance of 6 charge radii.

The calculations show that the ratio of reflected pressure to incident pressure in sand is a function of the incident pressure, reaching an almost steady value of 3.8 at an incident pressure level of 50,000 PSI. The pressure ratio is slightly less than 3 at an incident pressure of 10,000 PSI.

SECTION II

HYDROCODE SAND MODEL

Calculations were performed using the AFATL version of the TOODY IV Lagrangian wave propagation code (Reference 1) and the AFATL HULL Eulerian code (Reference 2). Both employed the same sand model. The model is based on high pressure data from Van Thiel's Hugoniot data handbook (Reference 3) and low pressure data taken from low strain rate hydrostatic measurements (Reference 4). The sand is assumed to be a dry quartz sand with 40 percent porosity. Its initial density is 1.6 gm/cc (100 lb/ft^3).

The complete pressure versus excess compression curve is seen in Figure 1. Arrows indicate whether paths can be used for loading or unloading or both. Yield strength is assumed to be zero for the sand (it is believed to actually reach only a few hundred PSI under very high pressure levels and hence is neglected). The Gruneisen ratio for sand is very low (perhaps 0.2 to 0.3), and the internal energy contribution to pressure is ignored.

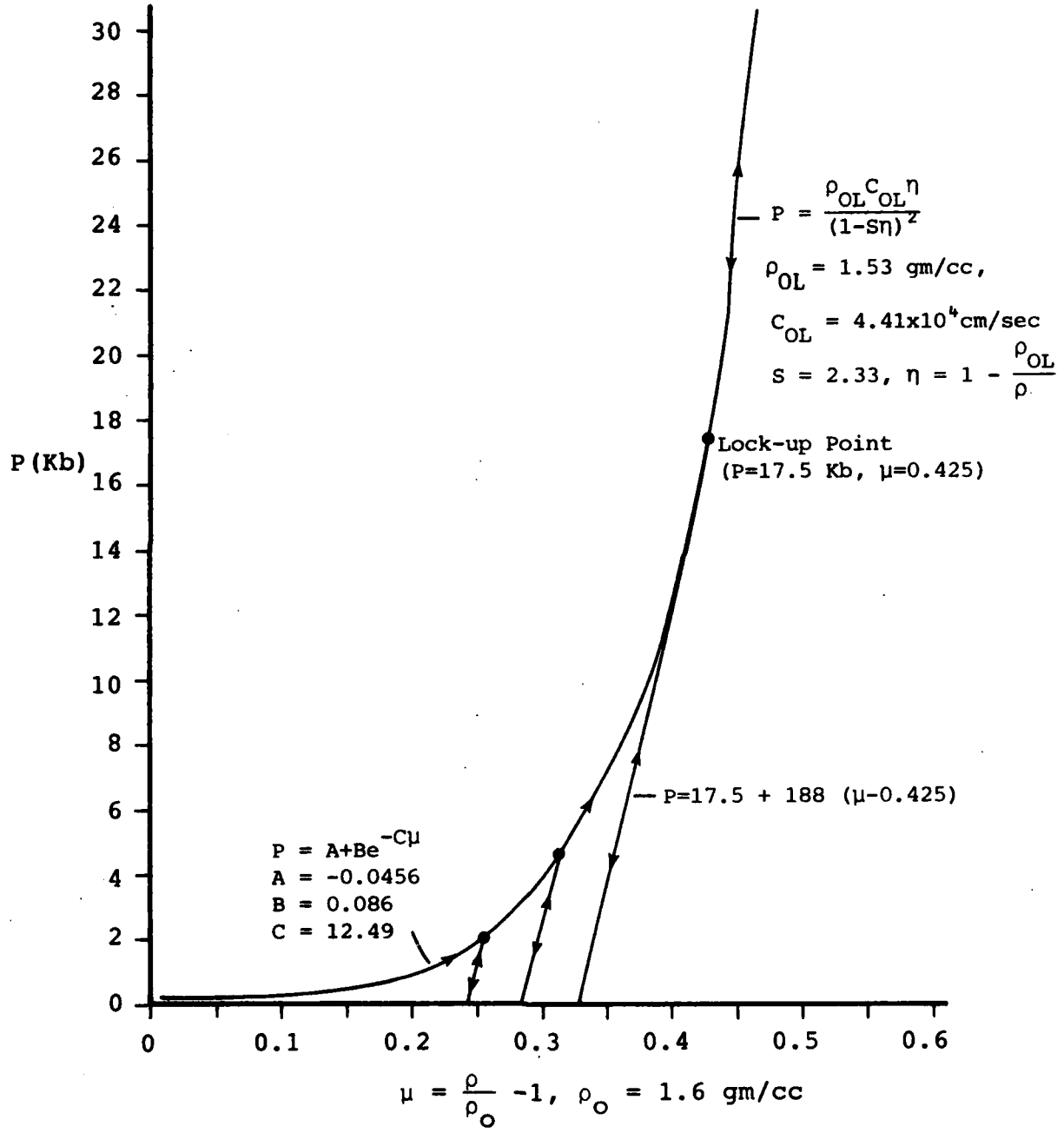

Figure 1. Sand Model

SECTION III
CALCULATIONS

The first series of calculations were performed using TOODY and square wave pressure inputs at various levels from 5,000 to 100,000 PSI. The calculation modeled sand backed with 2-cm thick steel. The pressure in the sand was calculated next to the steel. The calculations were performed in one-dimensional plane geometry using symmetry boundaries in the two-dimensional TOODY code.

Figures 2 through 7 present pressure, pressure impulse, density, and velocity versus time for incident pressures of 5,000, 10,000, 20,000, 30,000, 50,000, and 100,000 PSI. Plotted pressures are in terms of kilobars. These values can be multiplied by 14,500 to convert them to PSI. For example, 10 kilobars is 145,000 PSI. Impulse is in units of dyne-sec/cm^2 (10^9 dynes/cm^2 is 1 kilobar). Drops in pressure levels in the plots from the peak reflected pressures are due to relief waves from the free surface of the steel plate. The plots provide Table 1 which relates the reflected to incident pressure ratio to incident pressure.

TABLE 1. REFLECTED TO INCIDENT PRESSURE RATIO

P_I(PSI)	P_R(PSI)	P_R/P_I
5,000	11,600	2.32
10,000	28,320	2.83
20,000	65,940	3.30
30,000	106,275	3.54
50,000	189,710	3.79
100,000	391,450	3.91

These ratios are plotted in Figure 8 and demonstrate that P_R/P_I reaches an almost steady value of 3.8 at the 50,000 PSI incident level.

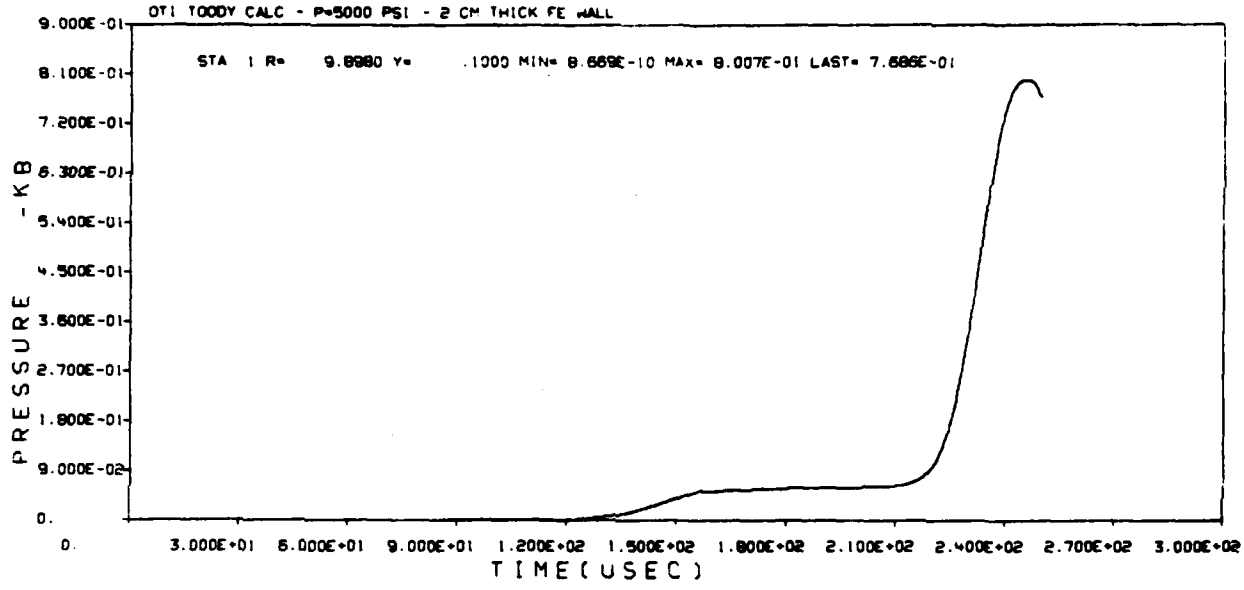

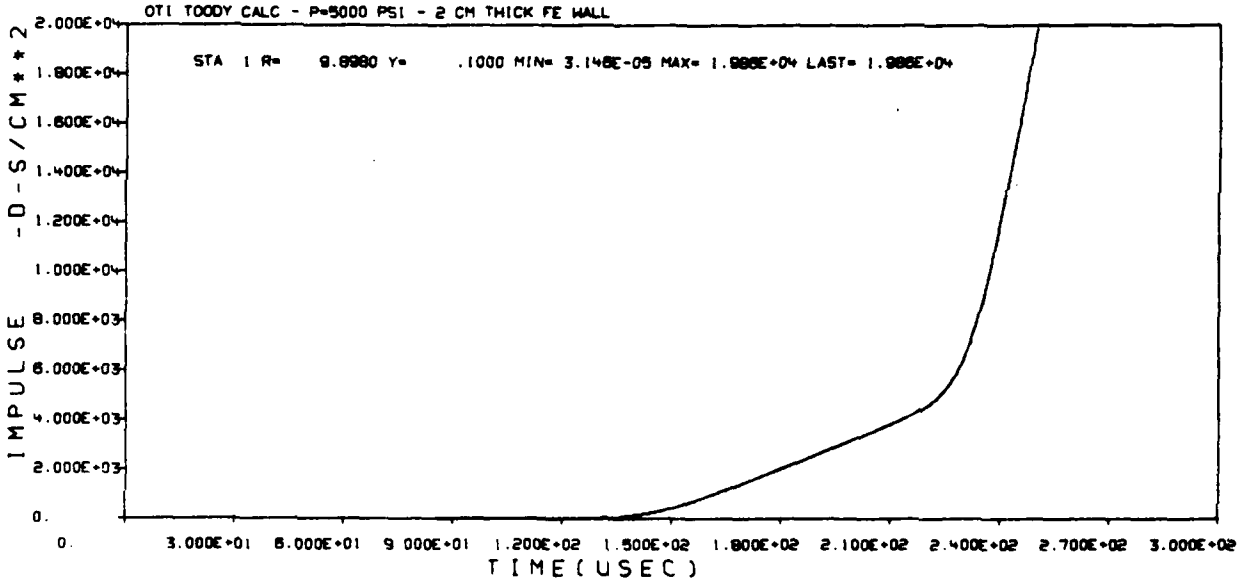

Figure 2. Reflected Pressure and Impulse at 5000 PSI

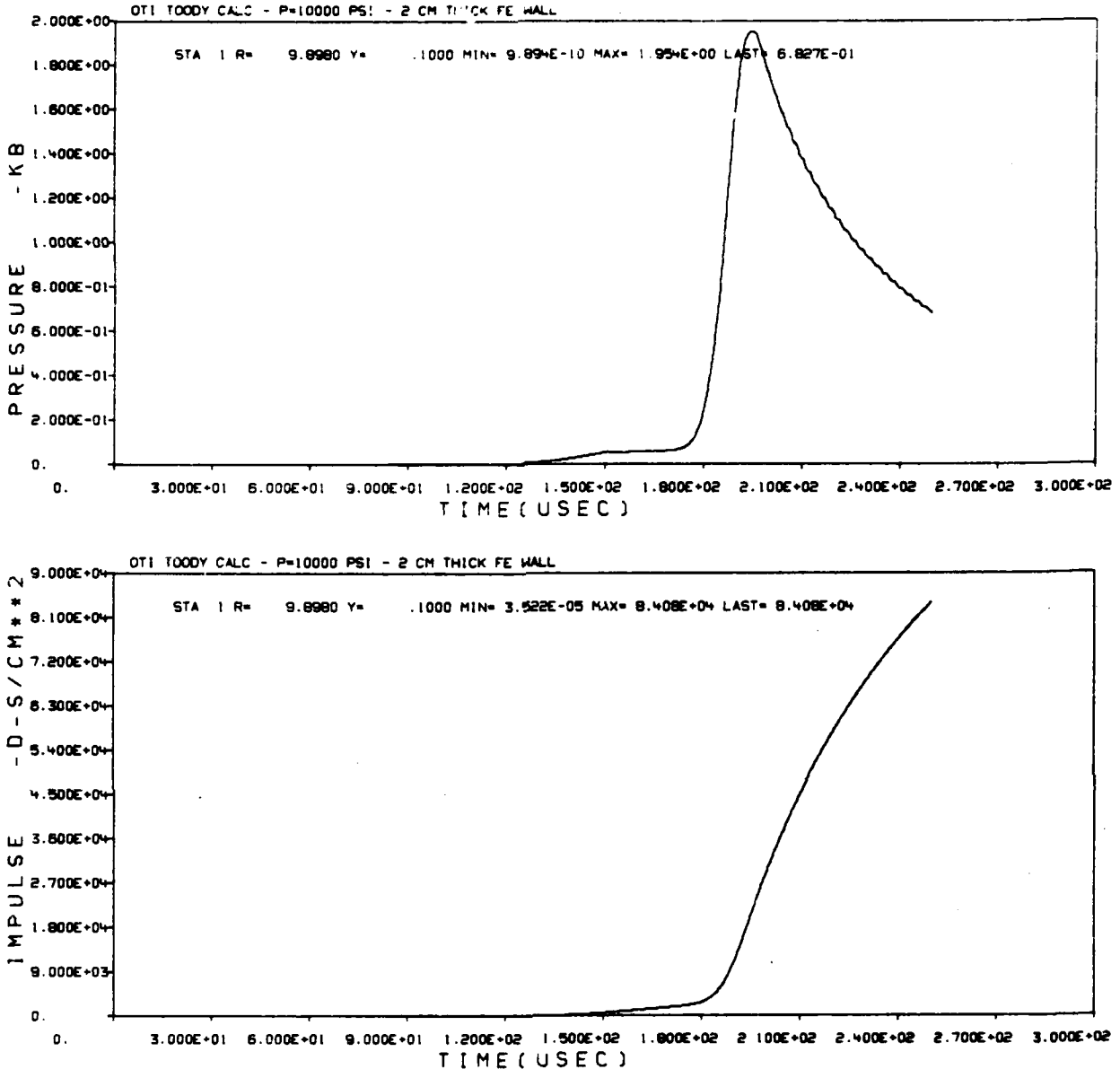

Figure 3. Reflected Pressure and Impulse at 10,000 PSI

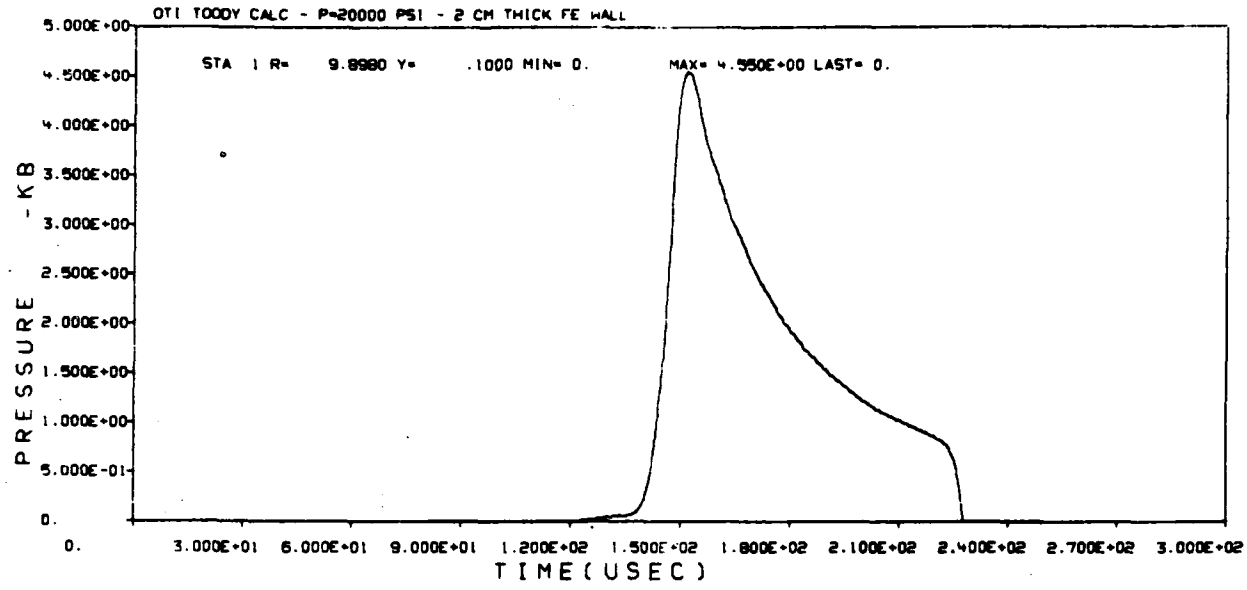

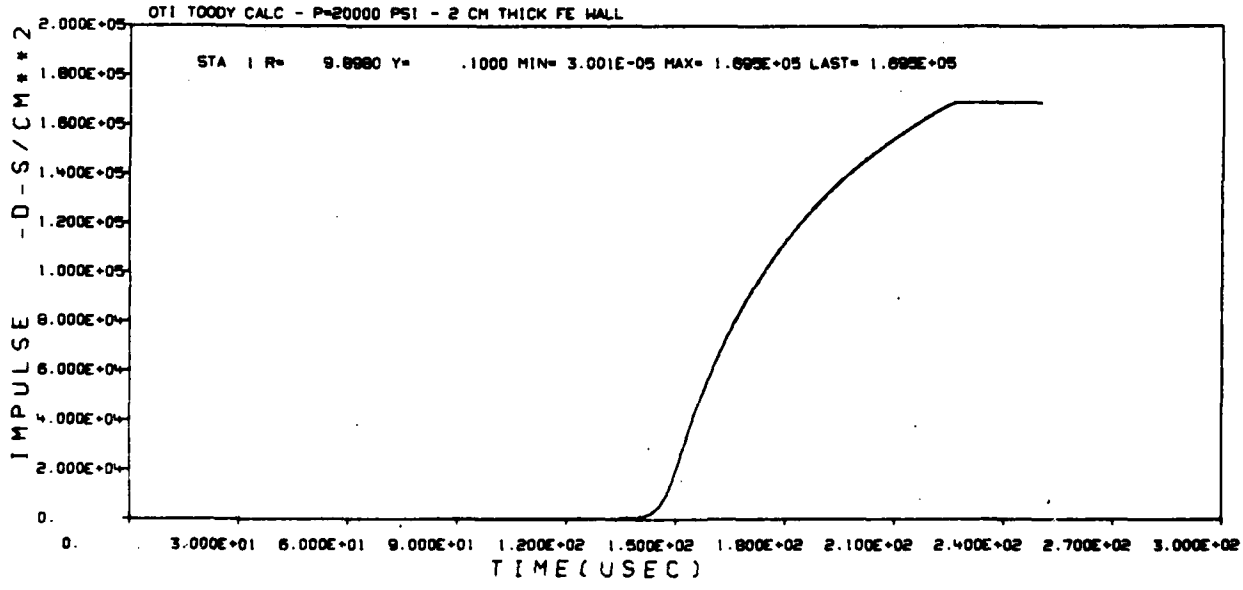

Figure 4. Reflected Pressure and Impulse at 20,000 PSI

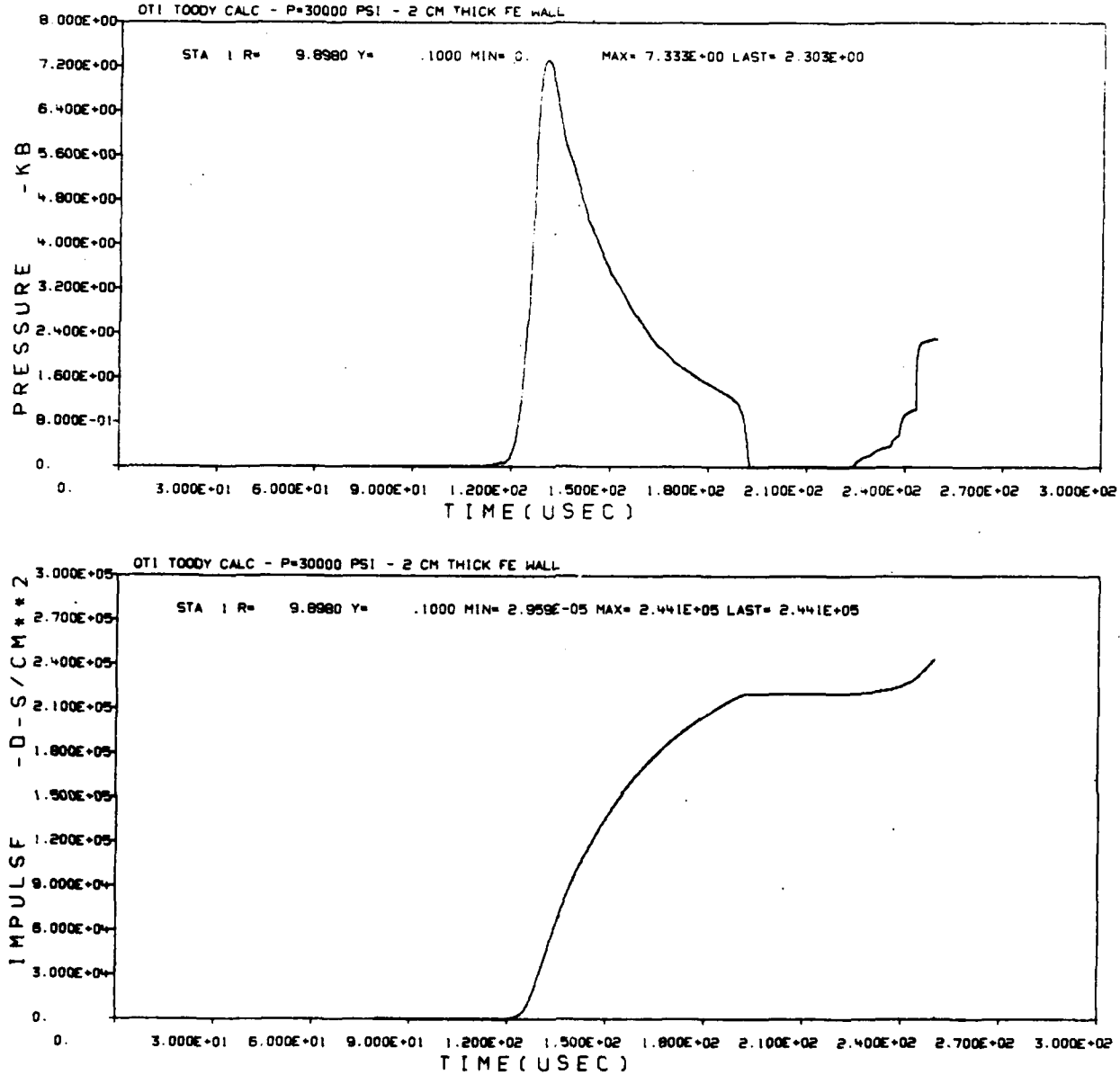

Figure 5. Reflected Pressure and Impulse at 30,000 PSI

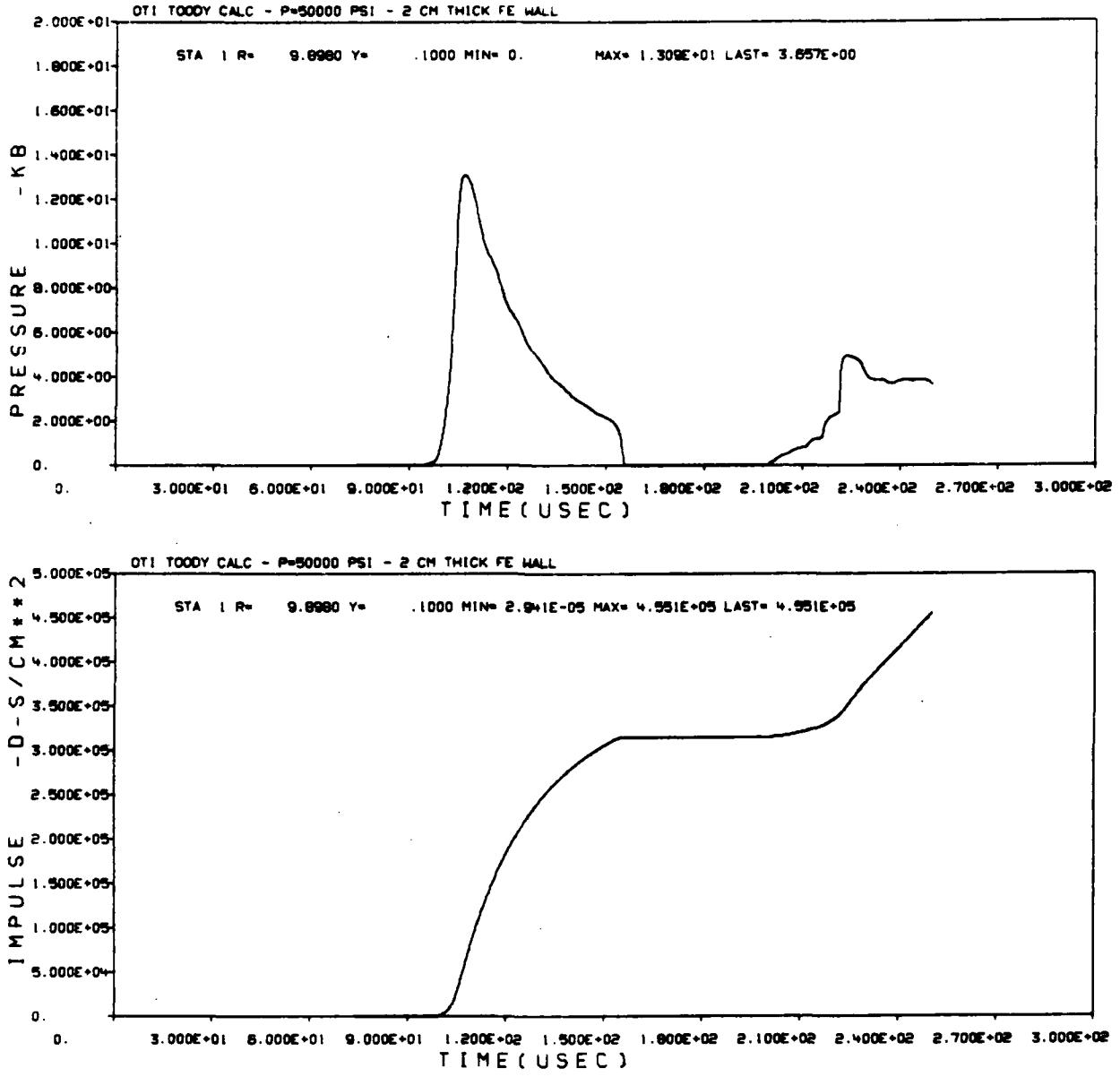

Figure 6. Reflected Pressure and Impulse at 50,000 PSI

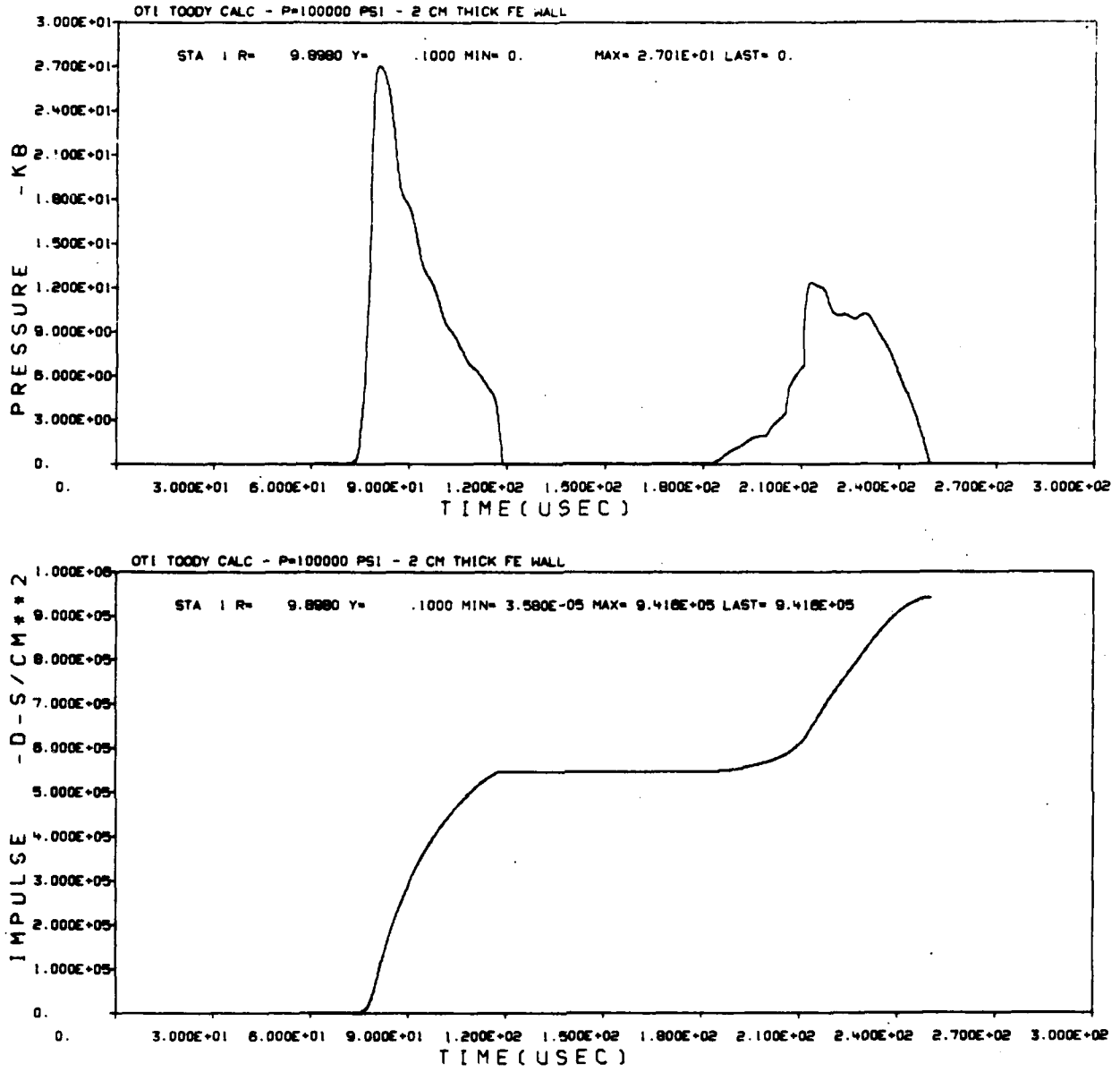

Figure 7. Reflected Pressure and Impulse at 100,000 PSI

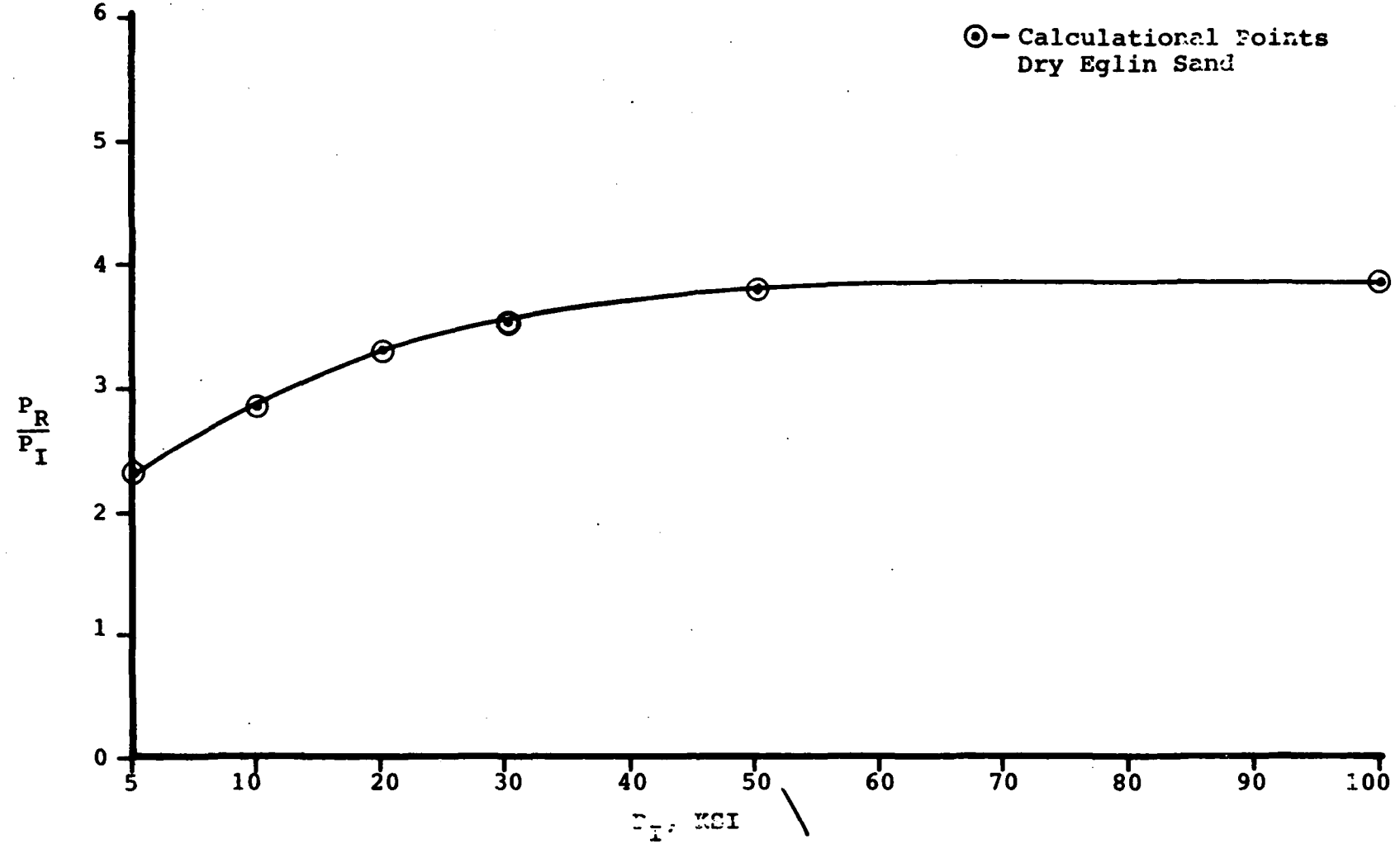

Figure 8. Reflected/Incident Pressure Versus Incident Pressure at Normal Incidence

To apply these reflection factors to the experiment of interest, one must know the value of incident pressure level in the sand as a function of the size of the explosive. TOODY calculations were performed to obtain this information. The calculations assumed an infinitely long cylinder of Composition B explosive. Two cylindrical sizes were run (4.0-cm and 5.6-cm radii). Figures 9 through 18 are pressure and impulse time history plots from the 5.6-cm radius calculation. The R value given on each plot is the initial distance of the time history point from the center of the charge. The time history points move with the flow. Note that stations 1 and 2 are inside the explosive. Stations in the sand sometimes exhibit unrealistic peak pressure values, especially near the explosive. These large peaks could be damped out with additional viscosity. The average value of the first few oscillations represents the true pressure at the station. In Table 2, the pressure data has been adjusted to take these oscillations into account by extrapolating back from the smooth slope of the pressure curve to the time of wave arrival.

TABLE 2. FREE-FIELD PRESSURE LEVELS

Explosive Radius (cm)	Station Location (cm)	Peak Pressure (kb)	PSI
5.6	10	300	4,347,820
	14	18	260,870
	16	14	202,900
	20	9.5	137,680
	24	5.3	76,810
	28	3.7	53,620
	32	2.7	39,130

The calculation with the explosive radius set to 4 centimeters yields the same incident pressure levels when plotted versus R/R_{HE} where R is the distance to the station measured from the axis of the explosive and R_{HE} is the explosive radius. The scaling factor for an infinitely long explosive then is R/R_{HE}. Figure 19 presents incident pressure versus R/R_{HE} data from these two calculations. The pressure from R/R_{HE}=5 to 7 (and it is assumed to extend to 8) can

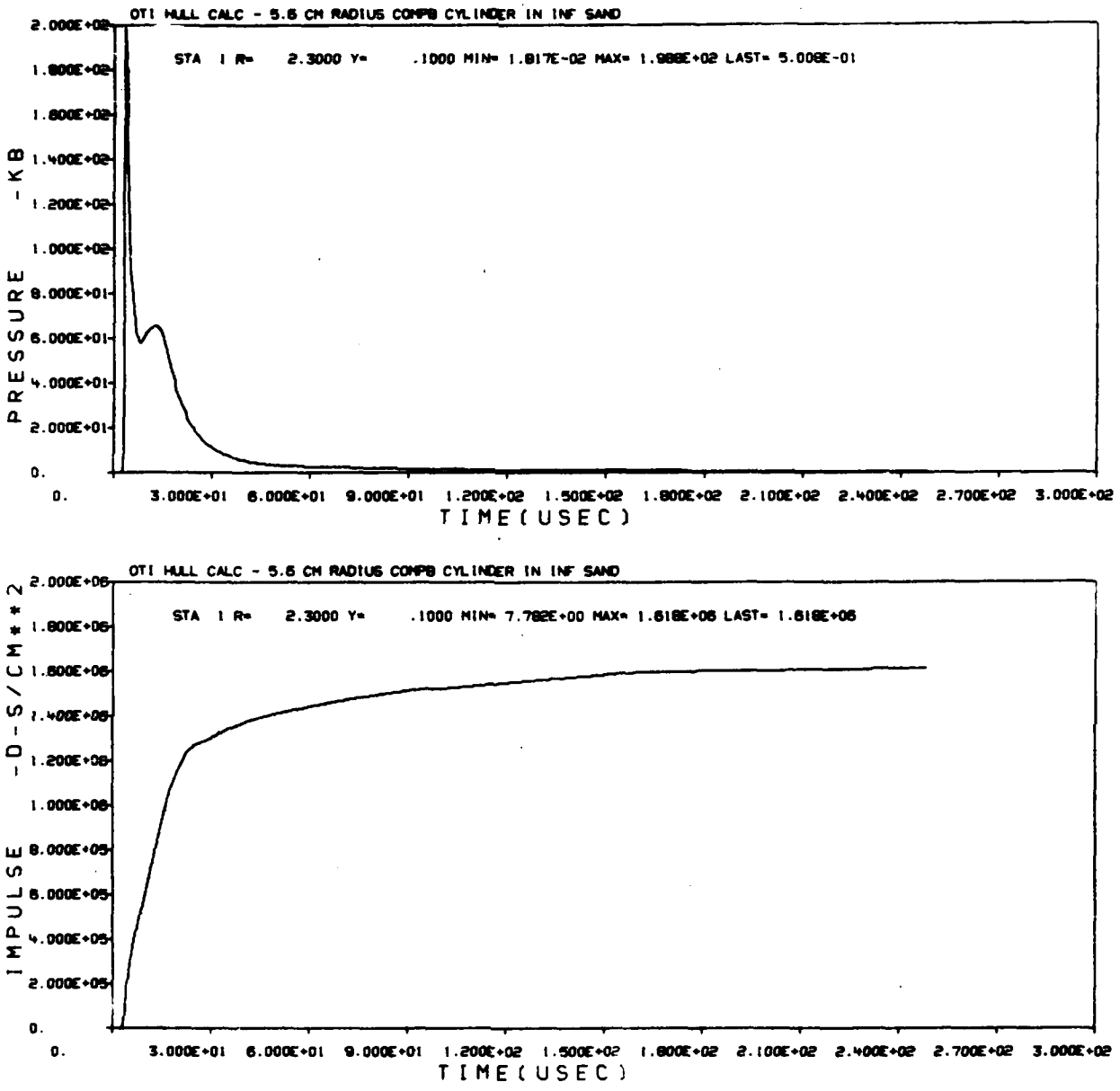

Figure 9. Station 1 Free-Field Pressure and Impulse

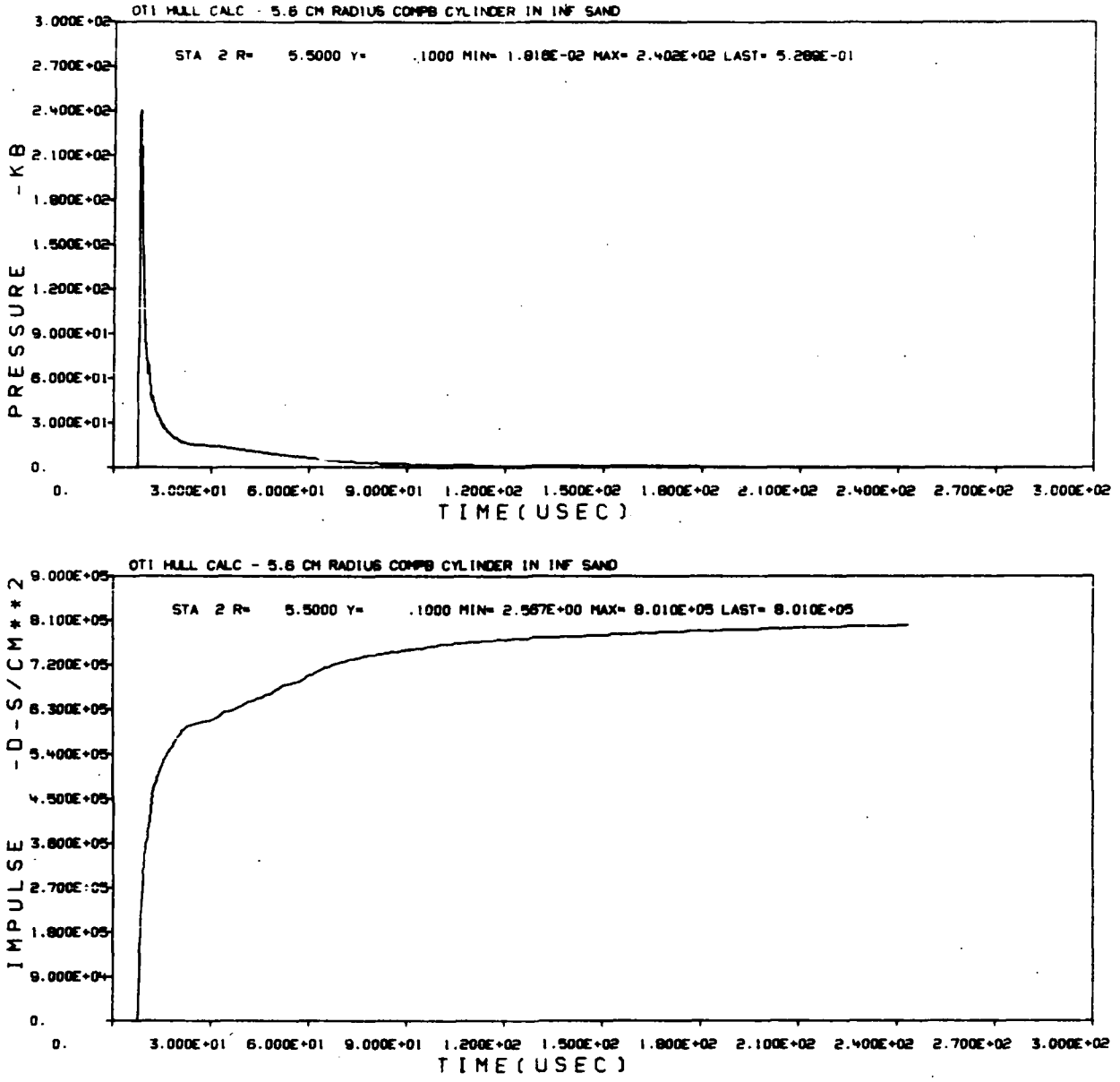

Figure 10. Station 2 Free-Field Pressure and Impulse

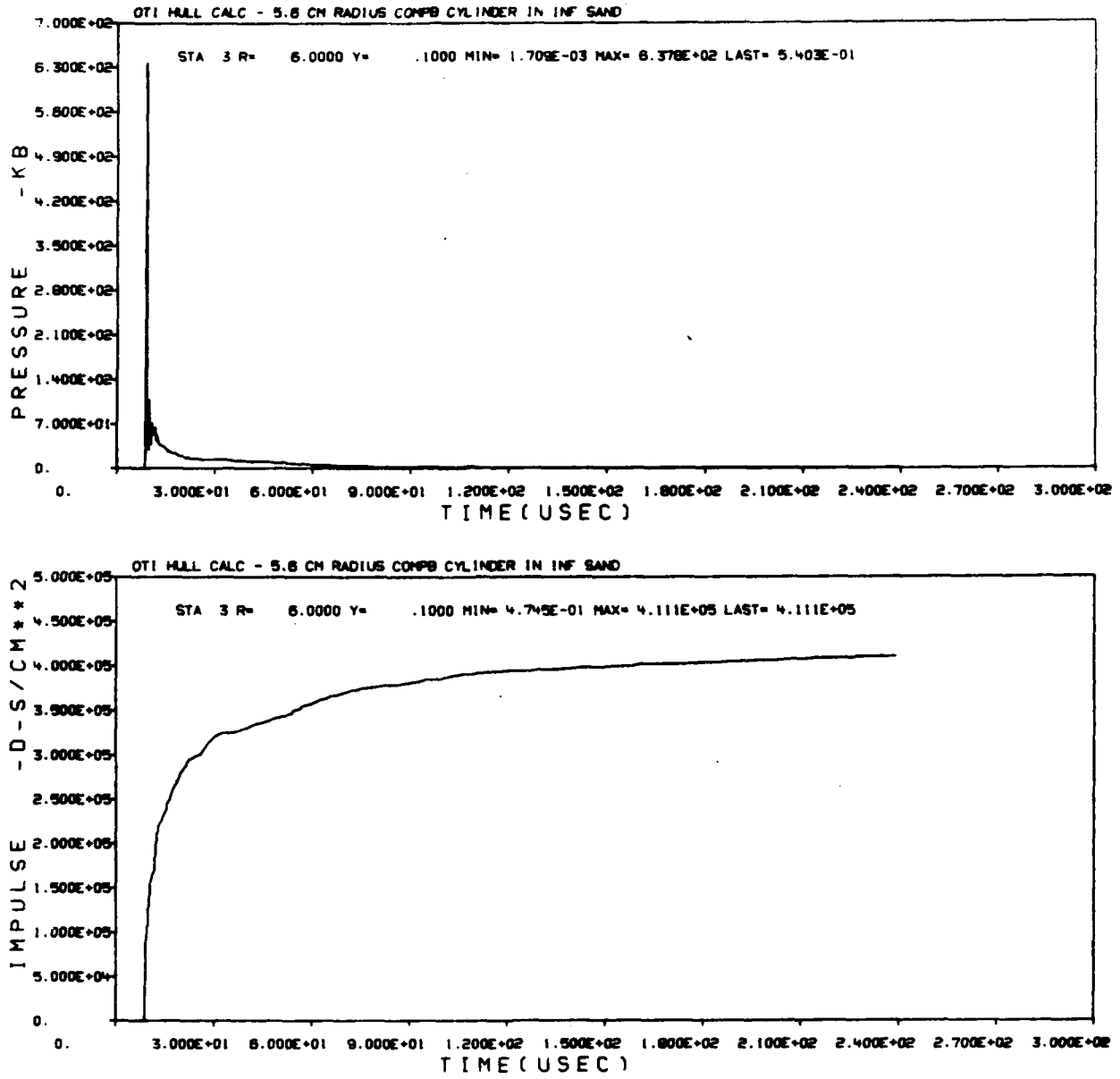

Figure 11. Station 3 Free-Field Pressure and Impulse

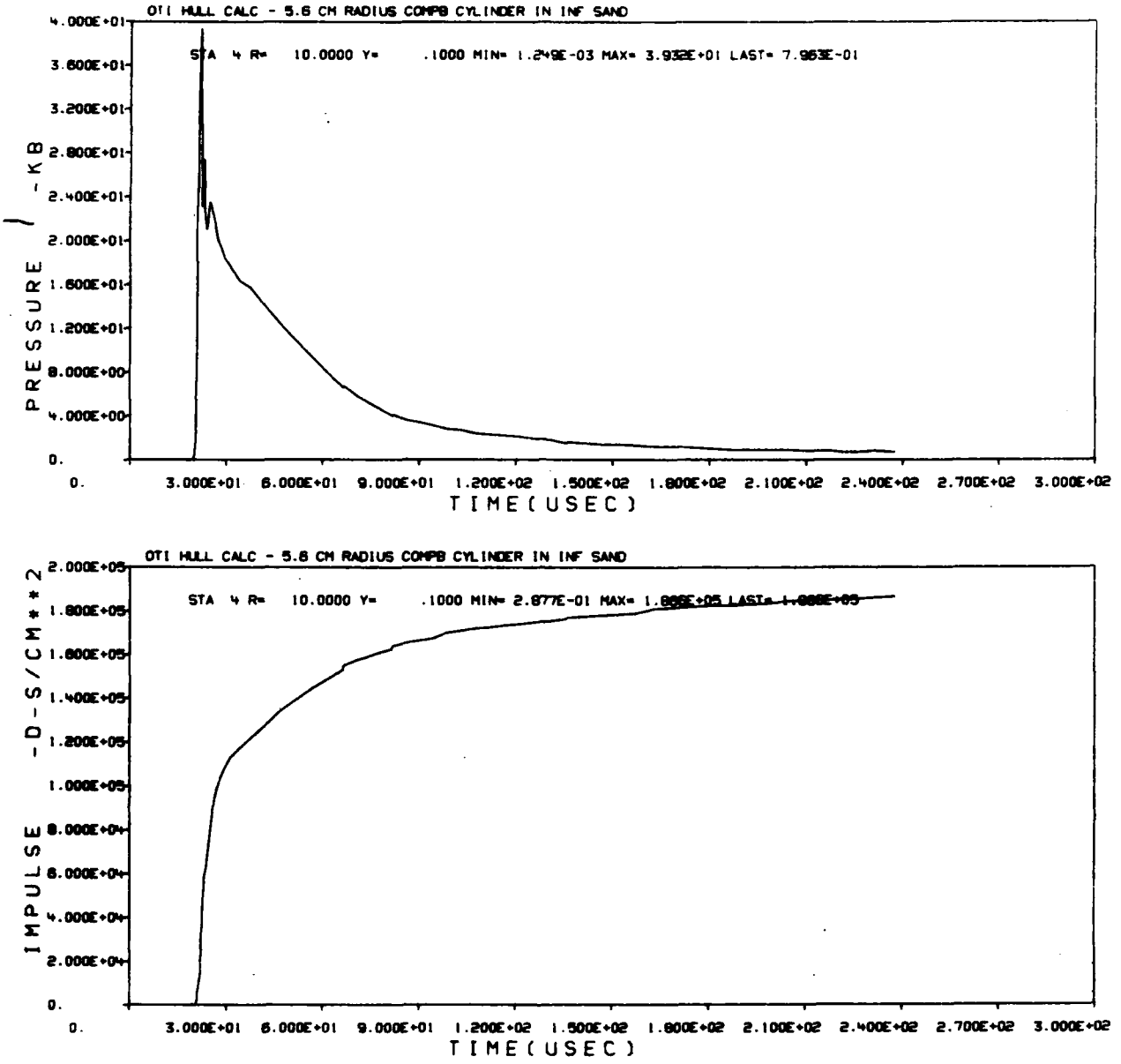

Figure 12. Station 4 Free-Field Pressure and Impulse

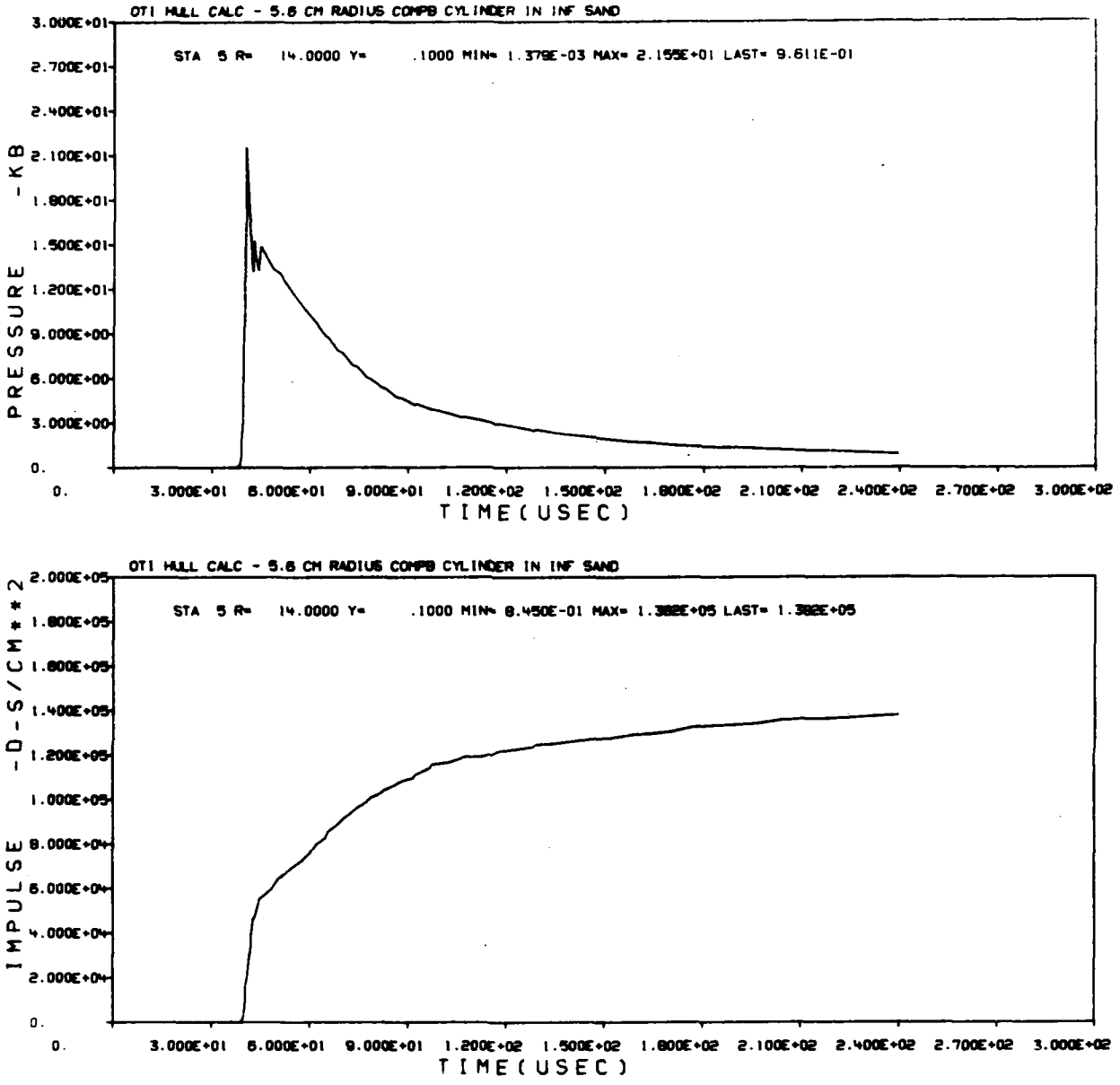

Figure 13. Station 5 Free-Field Pressure and Impulse

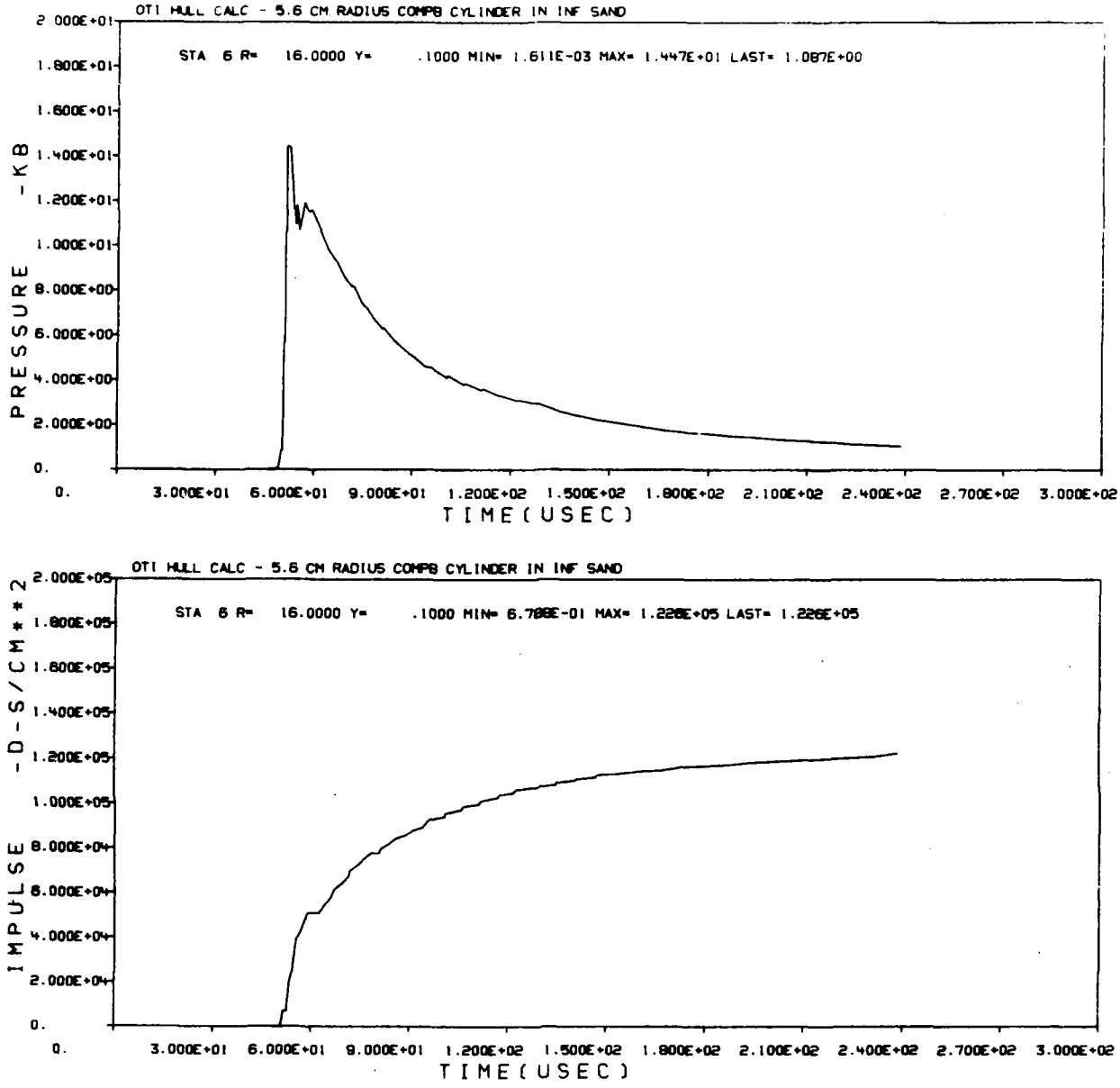

Figure 14. Station 6 Free-Field Pressure and Impulse

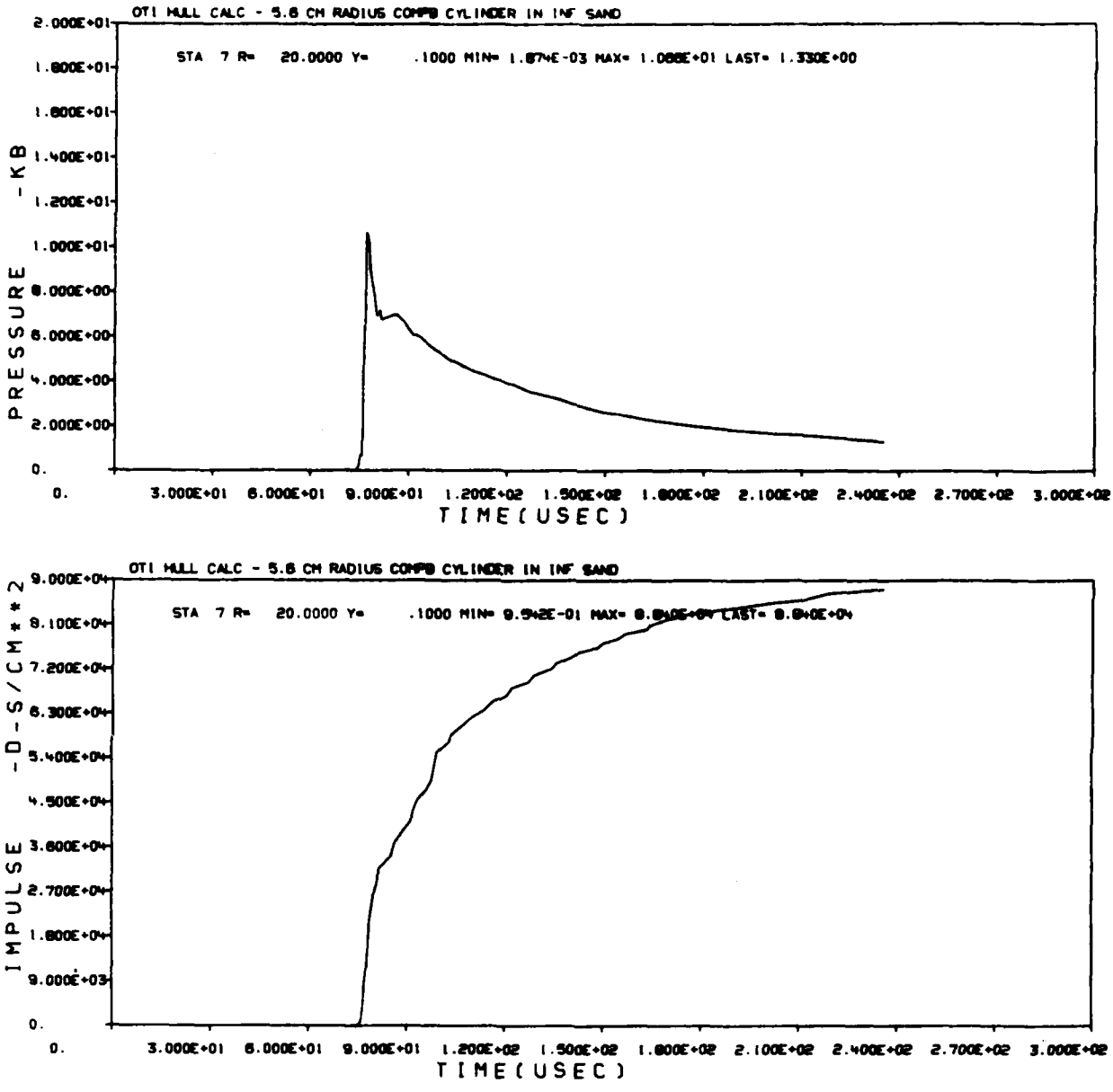

Figure 15. Station 7 Free-Field Pressure and Impulse

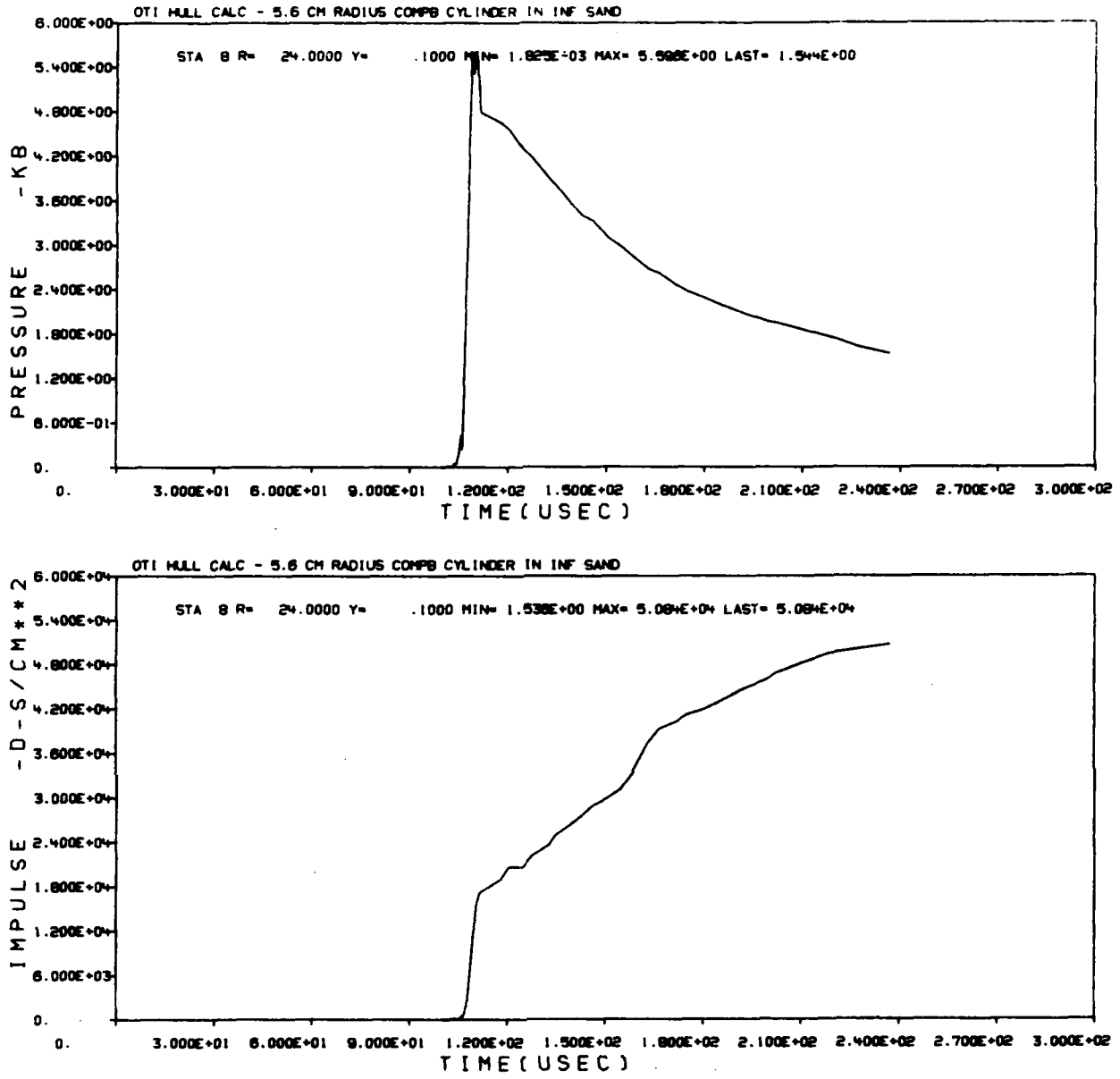

Figure 16. Station 8 Free-Field Pressure and Impulse

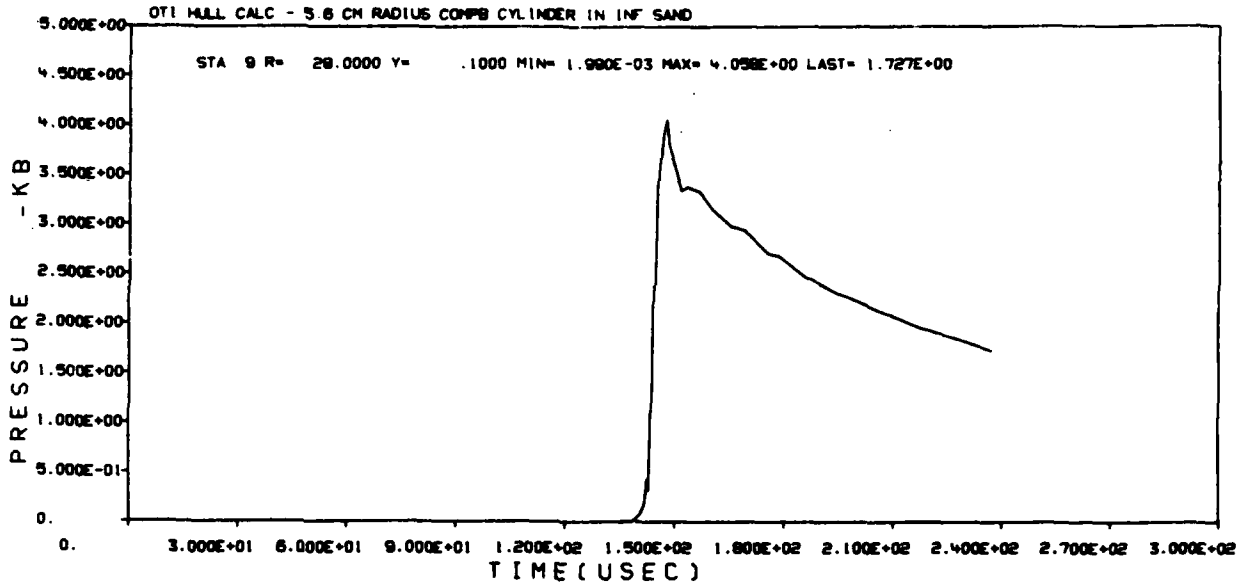

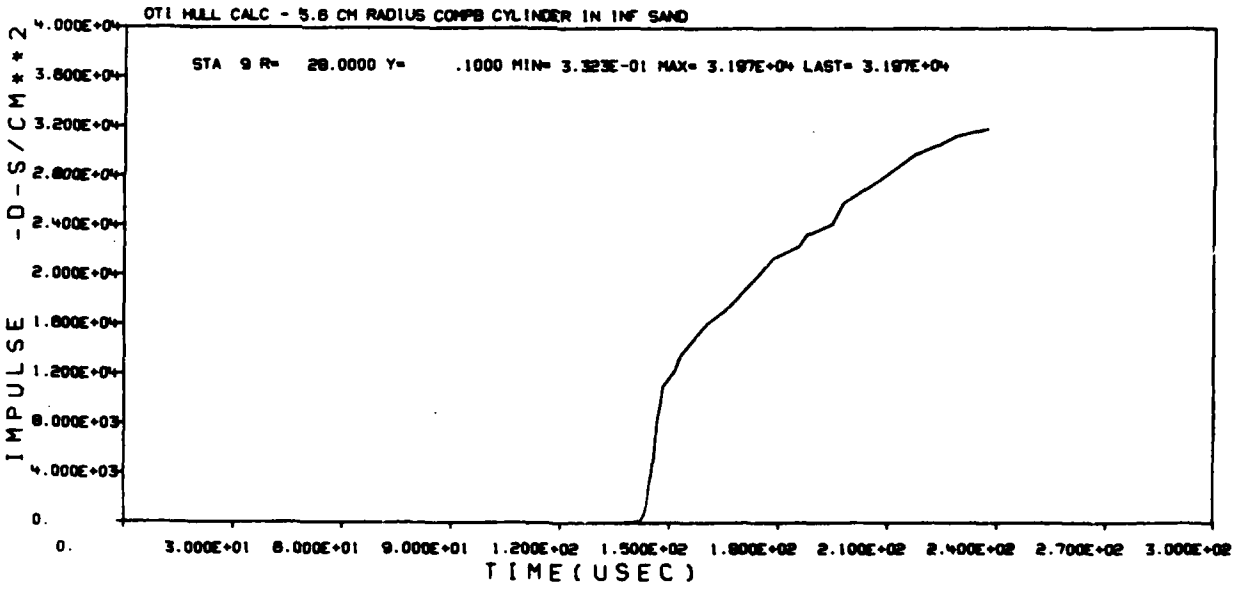

Figure 17. Station 9 Free-Field Pressure and Impulse

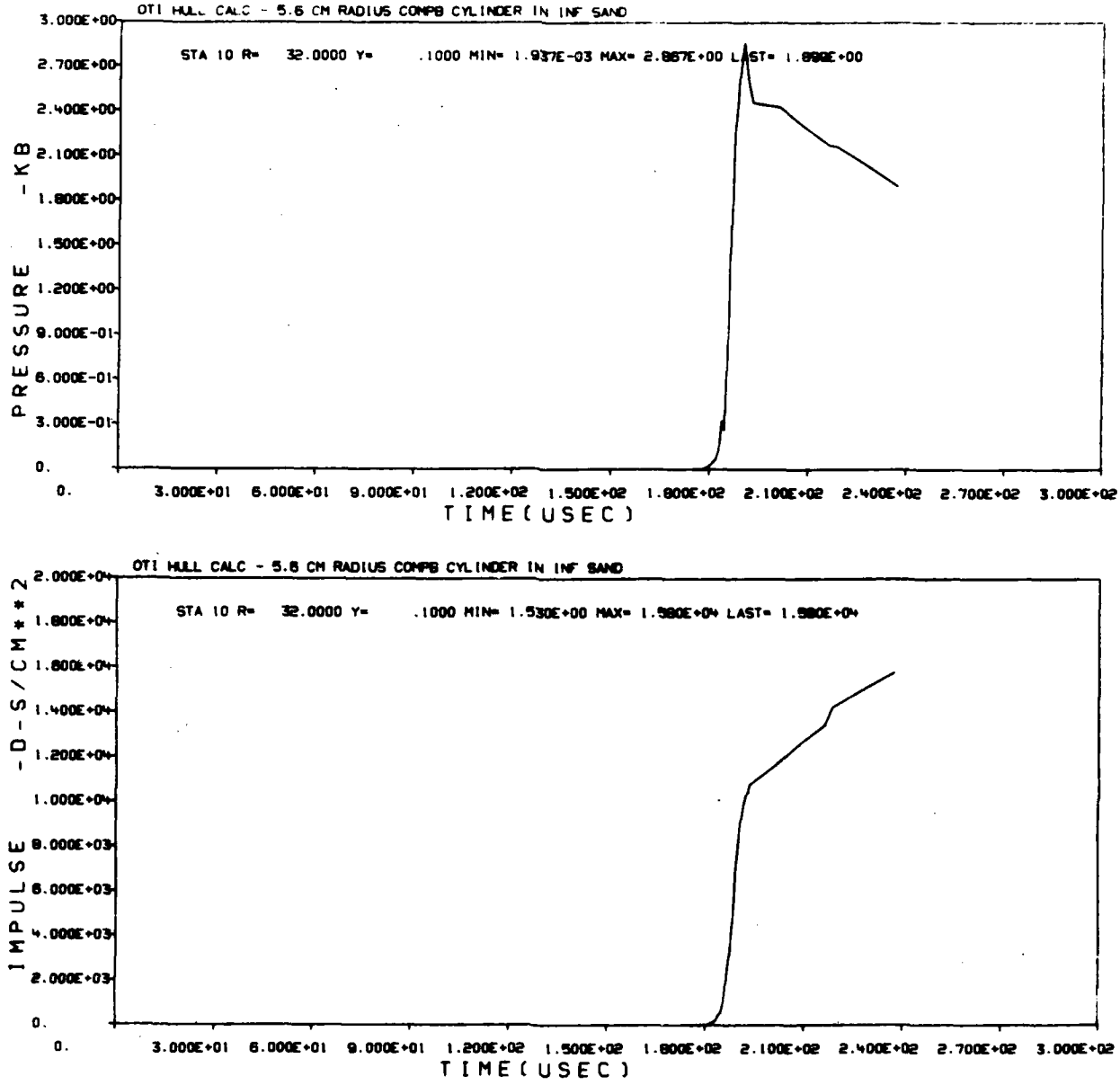

Figure 18. Station 10 Free-Field Pressure and Impulse

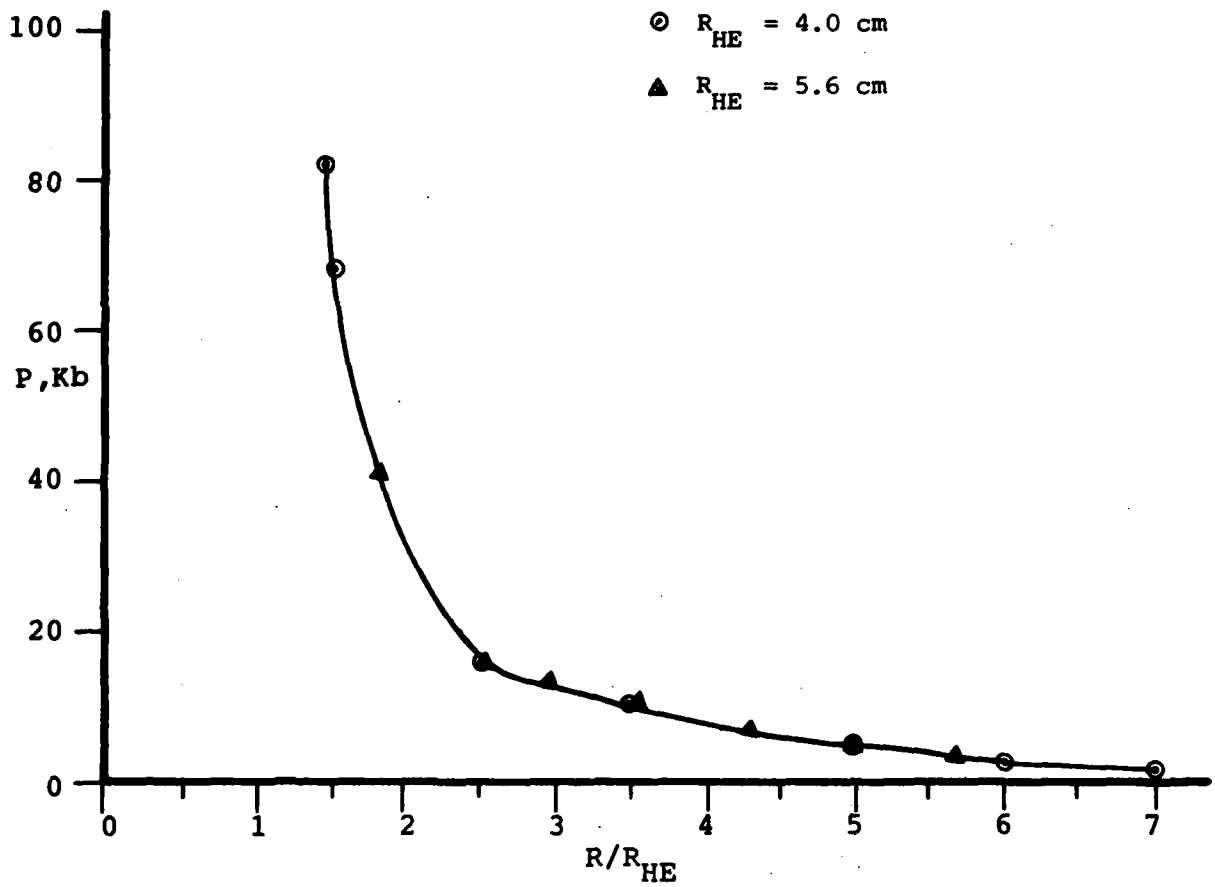

Figure 19. Incident Pressure in Sand From Infinitely Long Composition B Cylinders Versus R/R_{HE}

be approximately fit with the equation:

$$P_I = 23.4\ e^{-0.376\ R/R_{HE}} \quad (kb)$$

This equation is not valid for R/R_{HE} values less than 5. For normal incidence of the sand shock wave with a thick steel plate, the reflected pressures given in Table 3 can be expected at scaled distances of 5 to 8. The pressures are calculated from using the incident pressure equation above with P_R/P_I values from Table 1.

TABLE 3. REFLECTED PRESSURE VERSUS SCALED DISTANCE

R/R_{HE}	P_I(PSI)	P_R(PSI)
5	51,750	196,650
6	35,530	127,910
7	24,395	83,080
8	16,750	52,720

The next calculation utilized the HULL code and was designed to investigate the variation of pressure along a flat plate established at a scaled distance of 6 from the center of a 5.6-cm radius Composition B charge. Figure 20 is a density contour plot showing the undetonated explosive in sand. The two axes (Y vertical and R horizontal) are planes of symmetry and the equations solved are those applying to plane geometry. The charge is therefore an infinitely long bare explosive. The wall is a rigid, perfectly reflecting plane at an R value of 33.6 cm (R/R_{HE}=6.0). It does not show up in the contour plots until impacted by a shock wave at approximately 200 microseconds. Figures 21 through 47 are density contours, pressure contours, and pressure histograms along the Y (vertical) axis at approximately 50-microsecond intervals to 400 microseconds. Note that the pressure histogram describes free-field pressure since it presents values along the vertical axis. Reflected pressures will be seen in time history plots presented later in this report. The discontinuities in pressure halfway up the pressure histograms are oscillations at the explosive/sand interface. Numbers on the right side

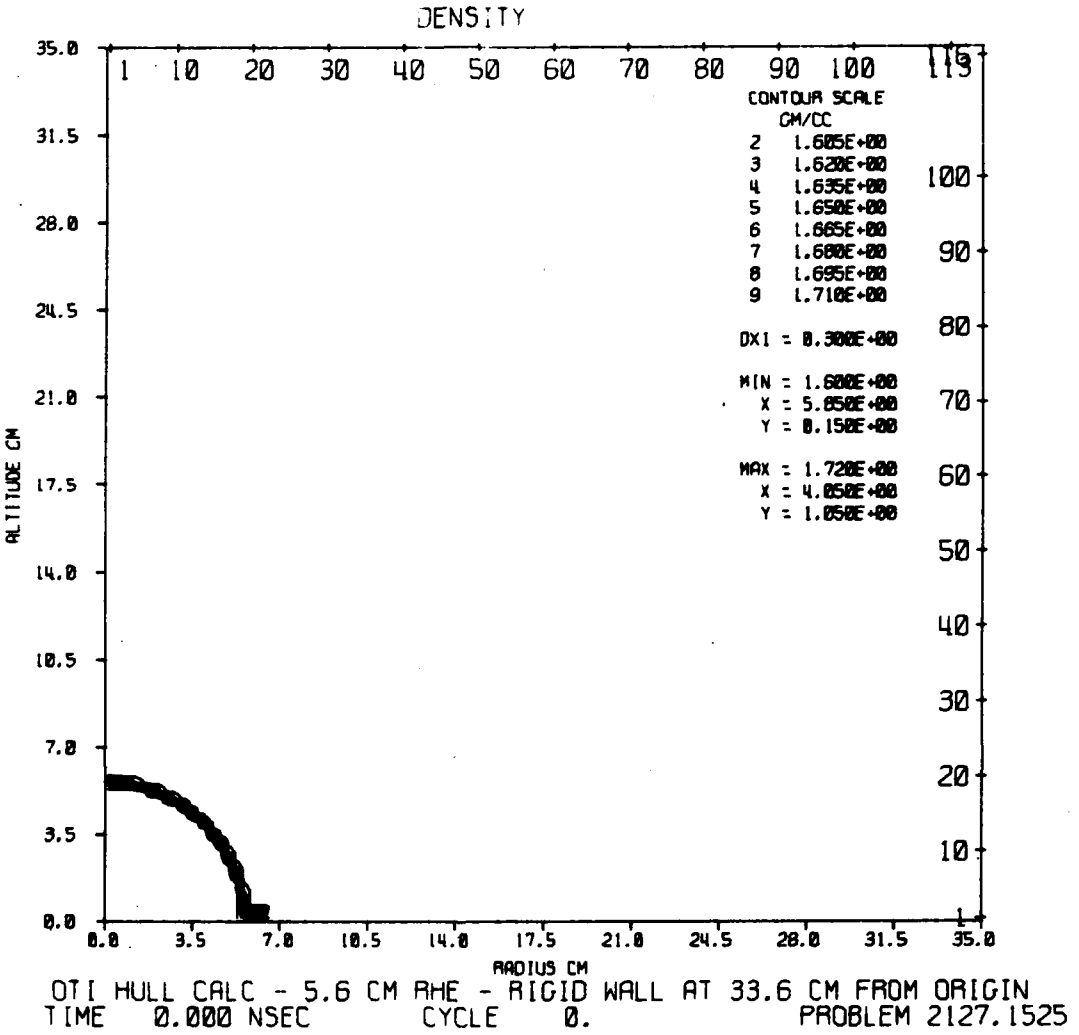

Figure 20. Initial Setup: Composition B in Sand

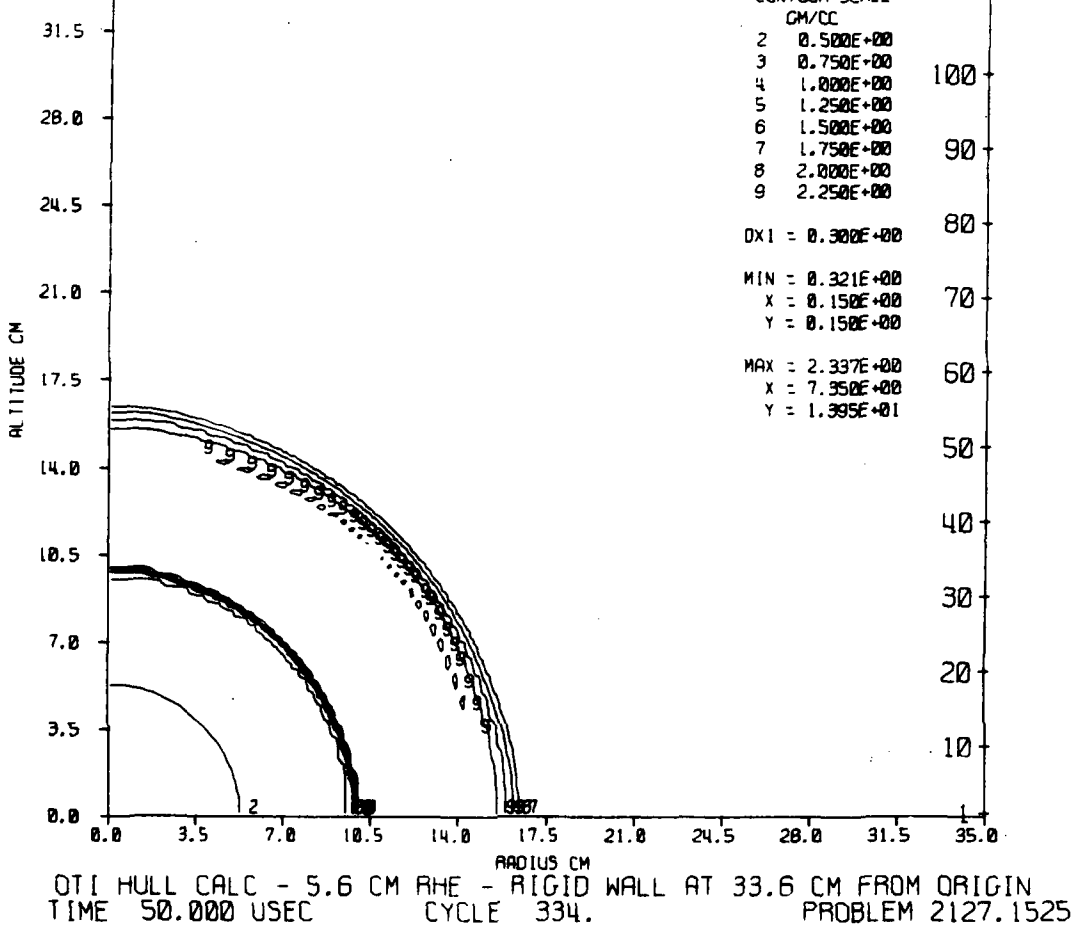

Figure 21. Density Contours at 50 Microseconds

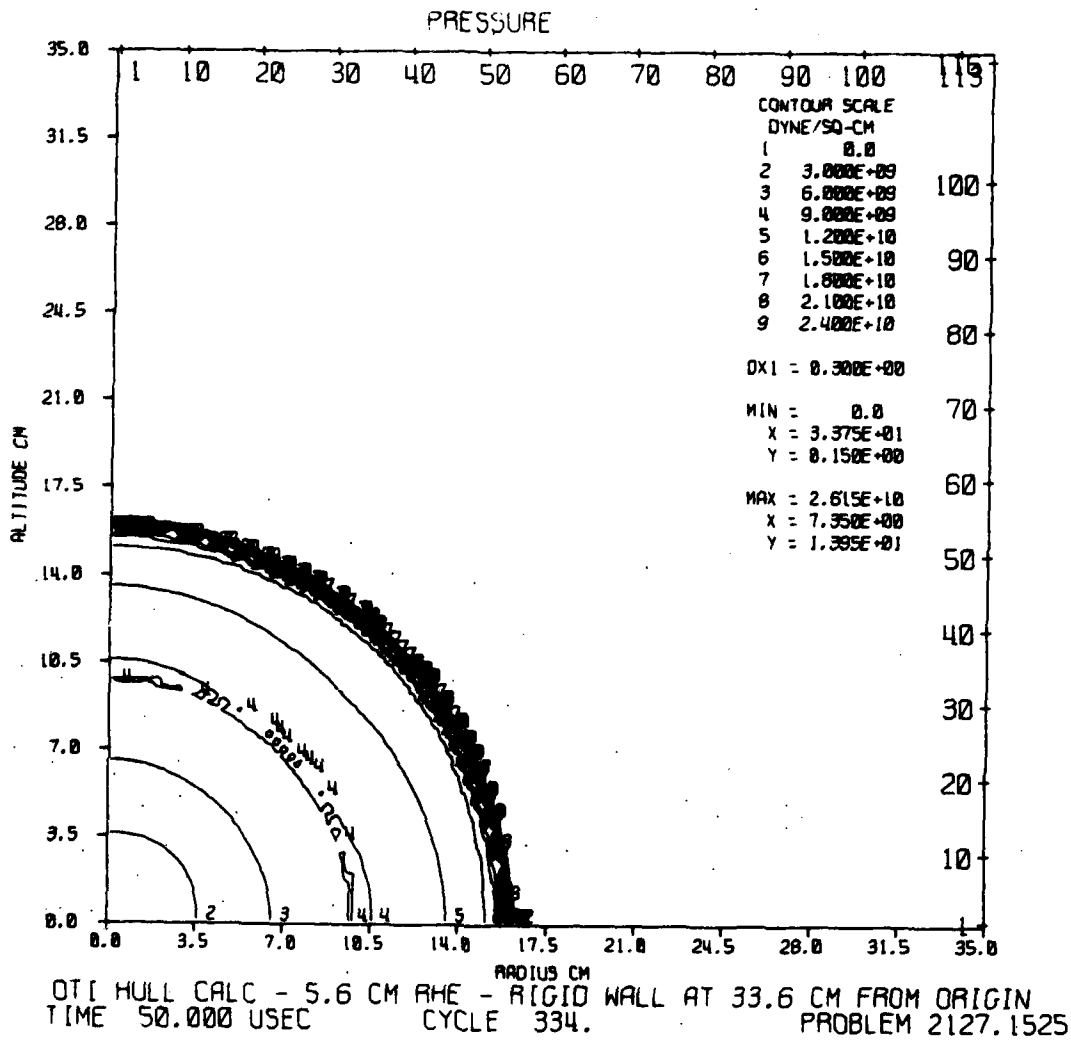

Figure 22. Pressure Contours at 50 Microseconds

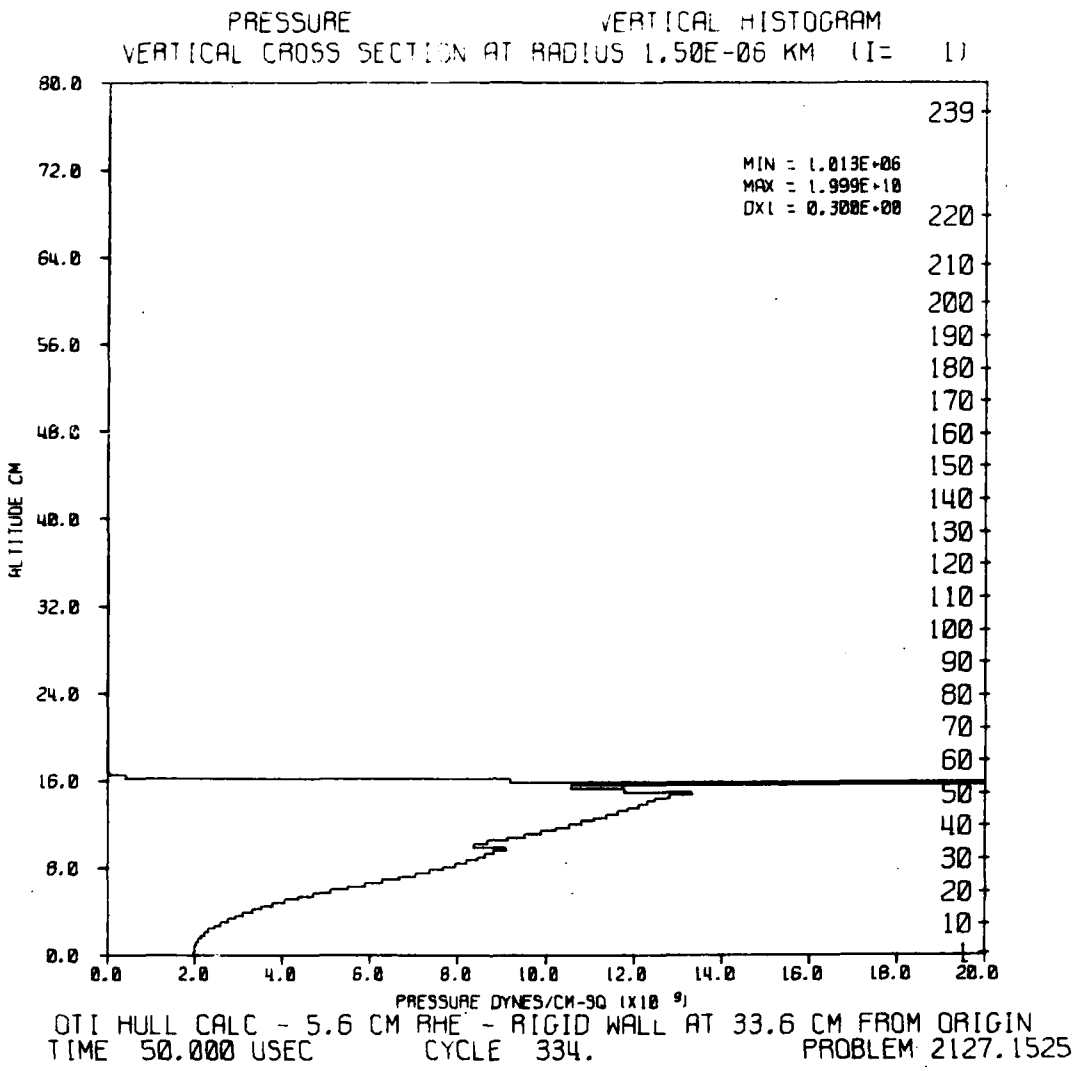

Figure 23. Pressure Histogram at 50 Microseconds

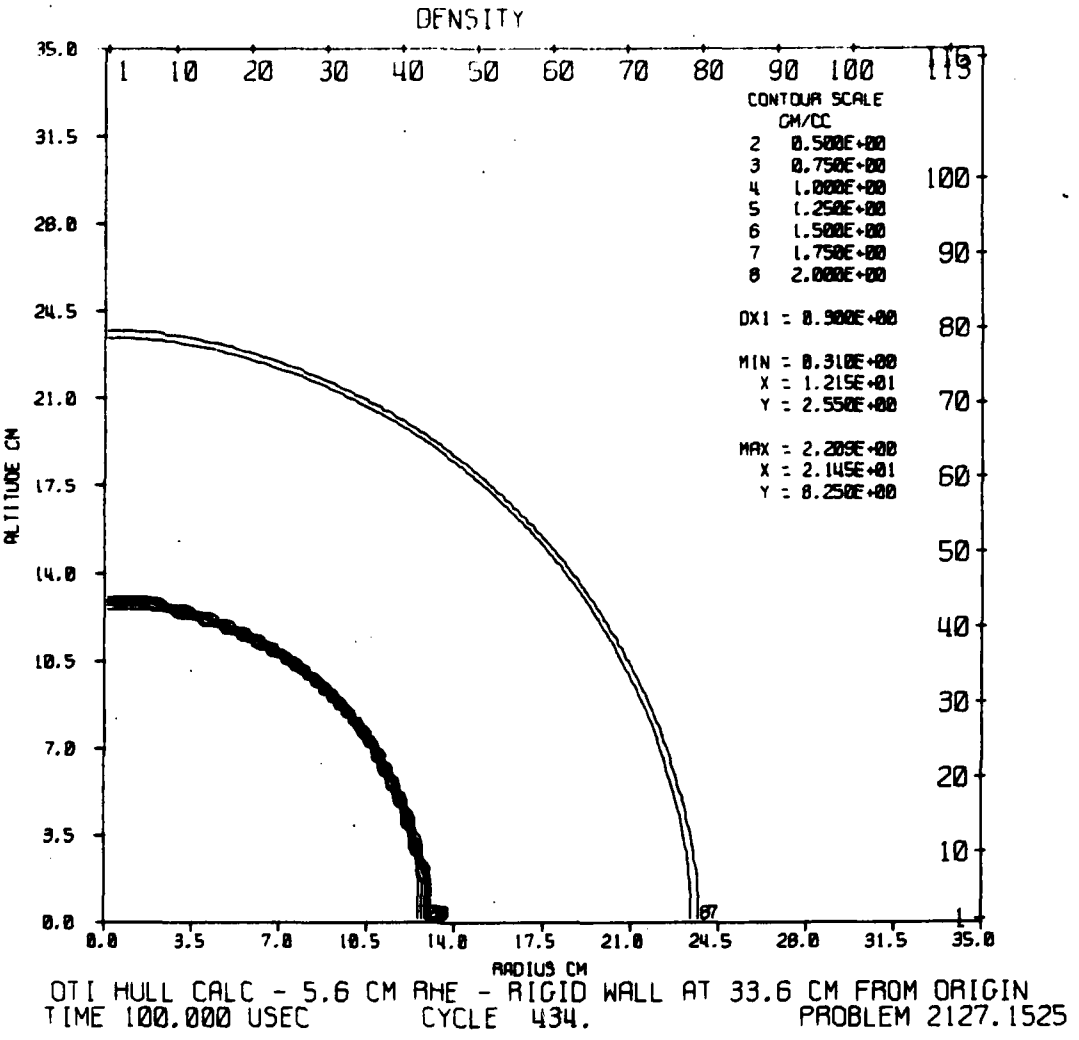

Figure 24. Density Contours at 100 Microseconds

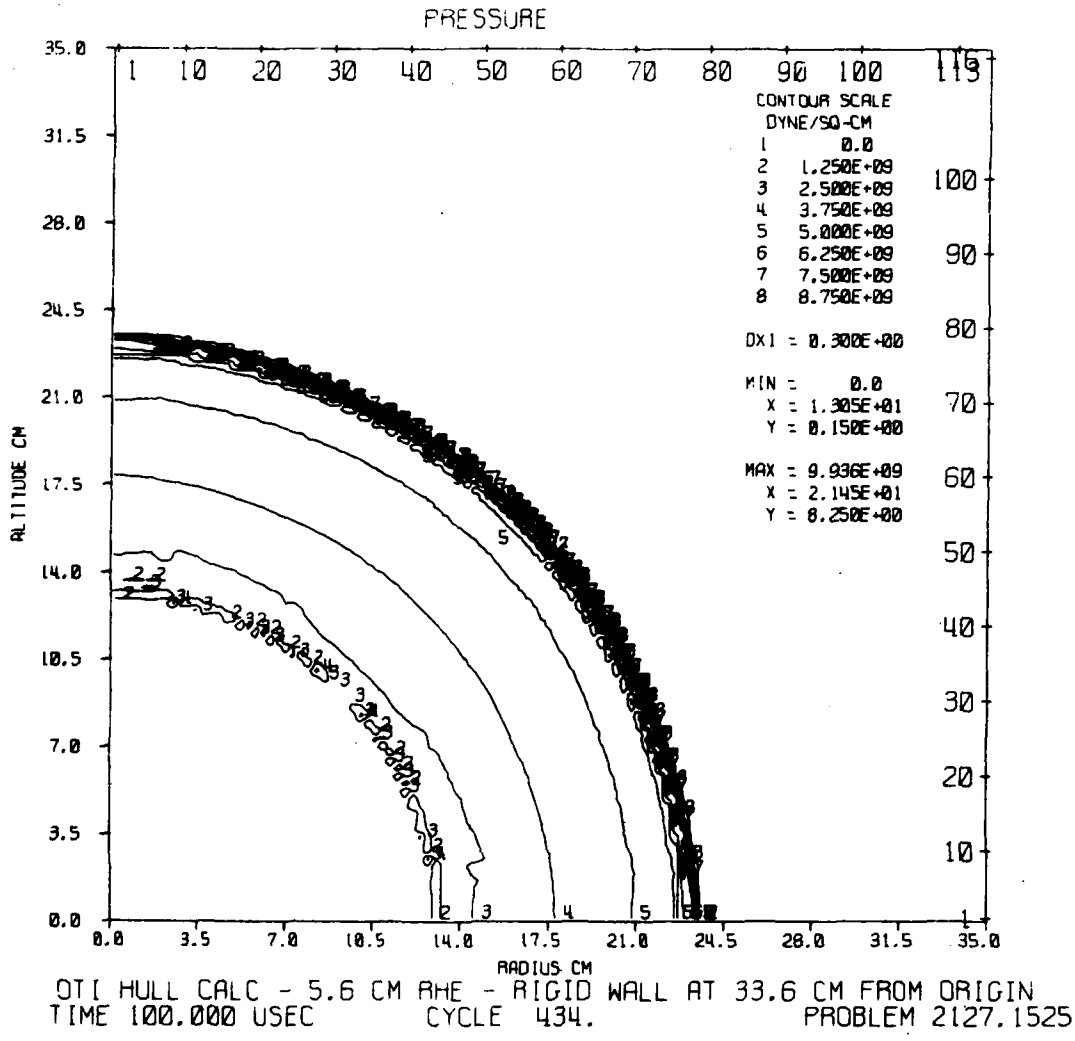

Figure 25. Pressure Contours at 100 Microseconds

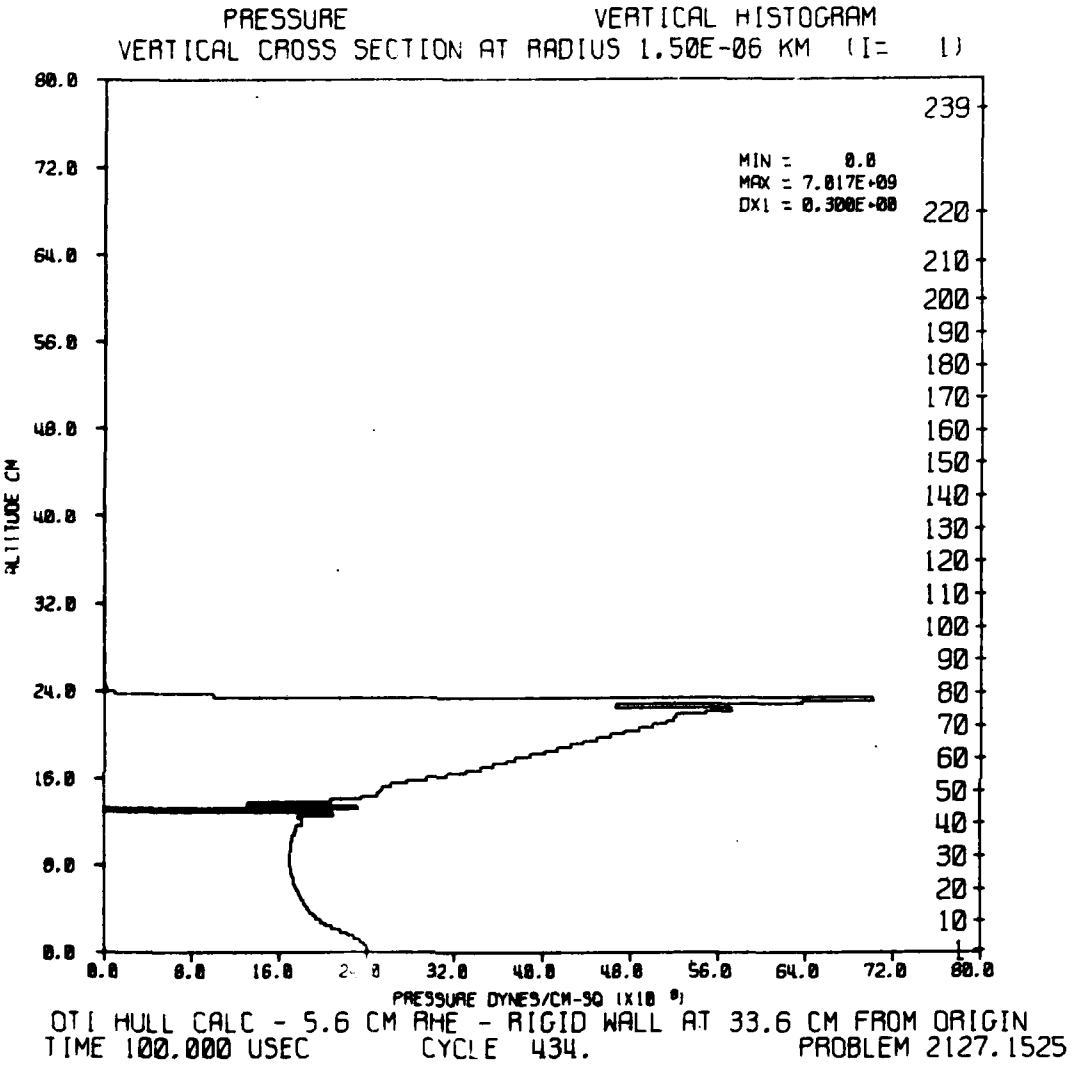

Figure 26. Pressure Histogram at 100 Microseconds

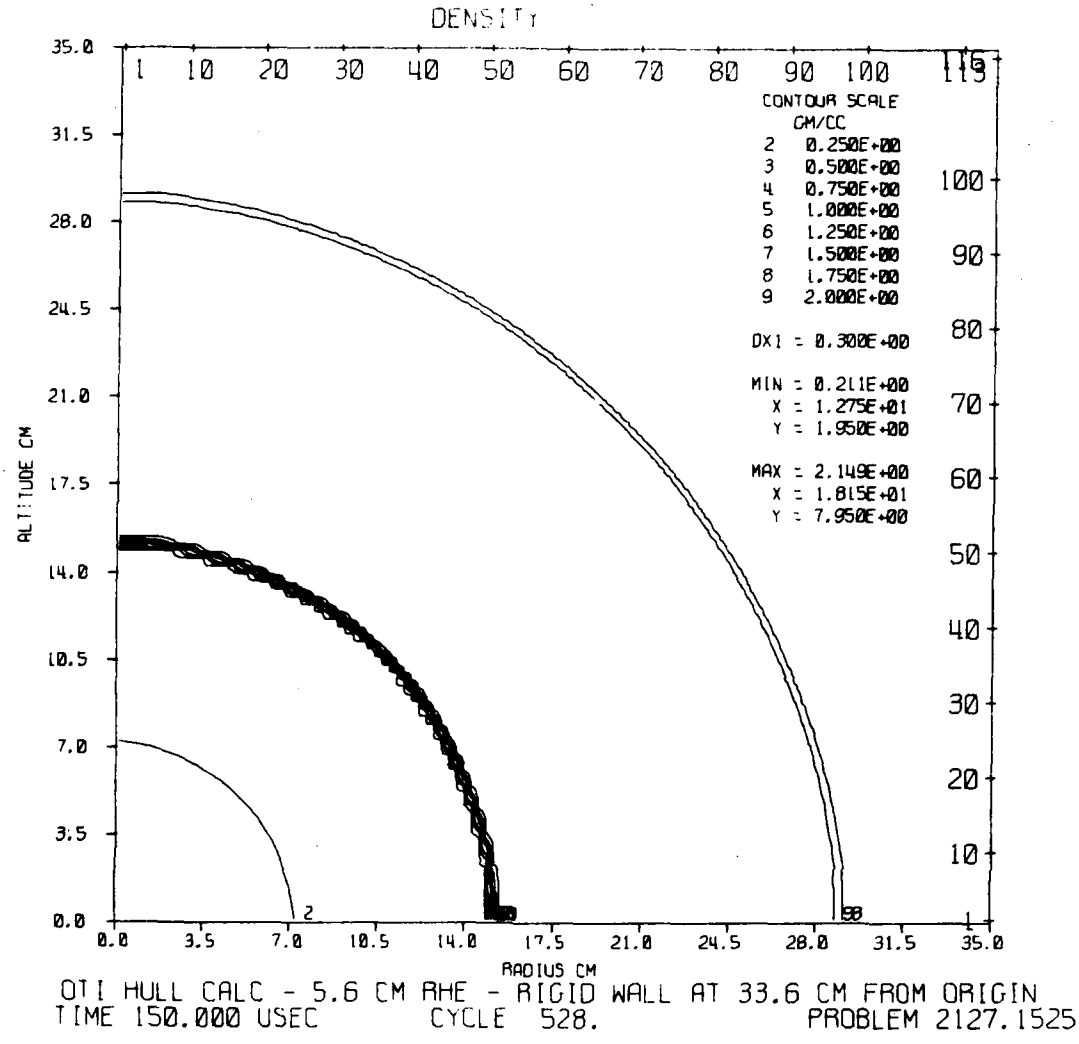

Figure 27. Density Contours at 150 Microseconds

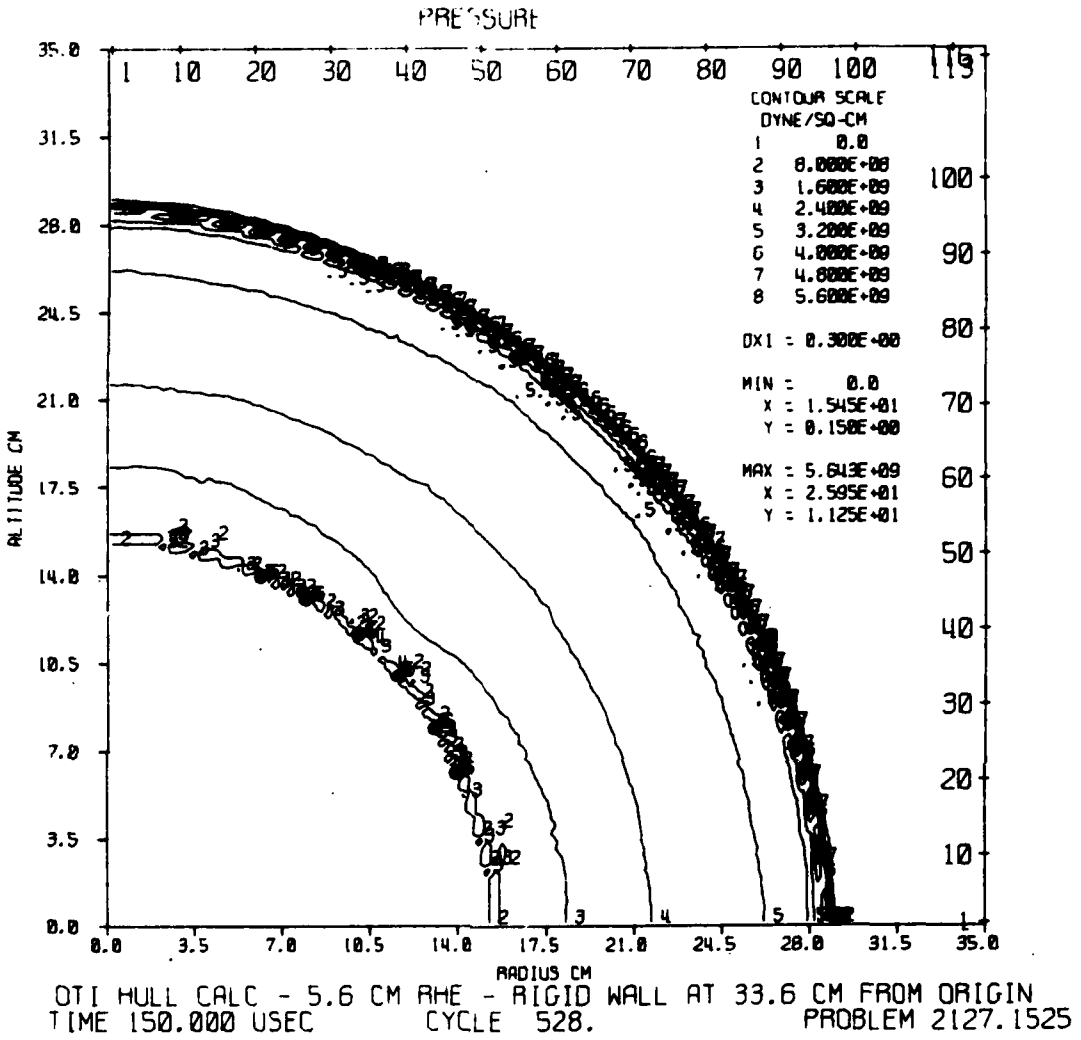

Figure 28. Pressure Contours at 150 Microseconds

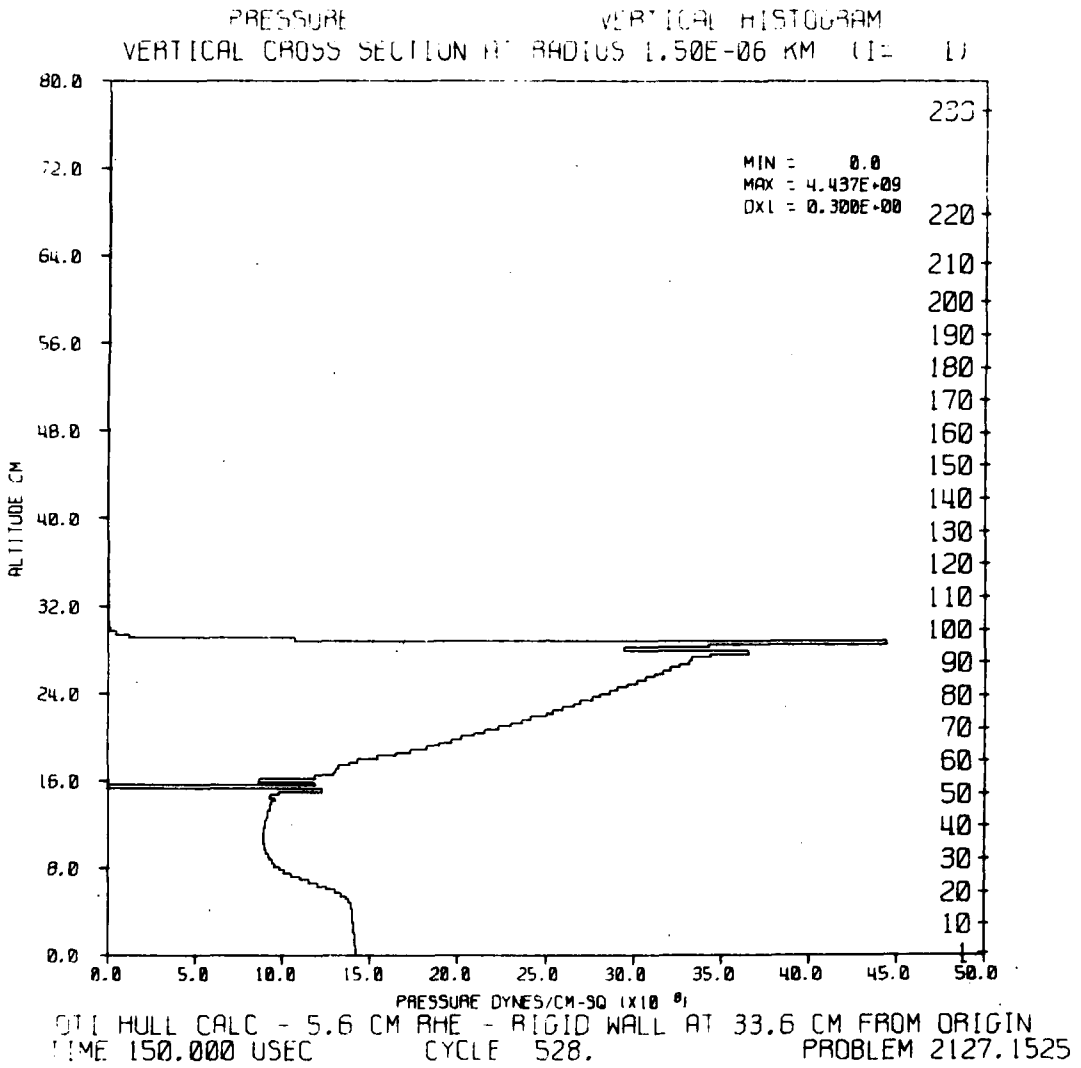

Figure 29. Pressure Histogram at 150 Microseconds

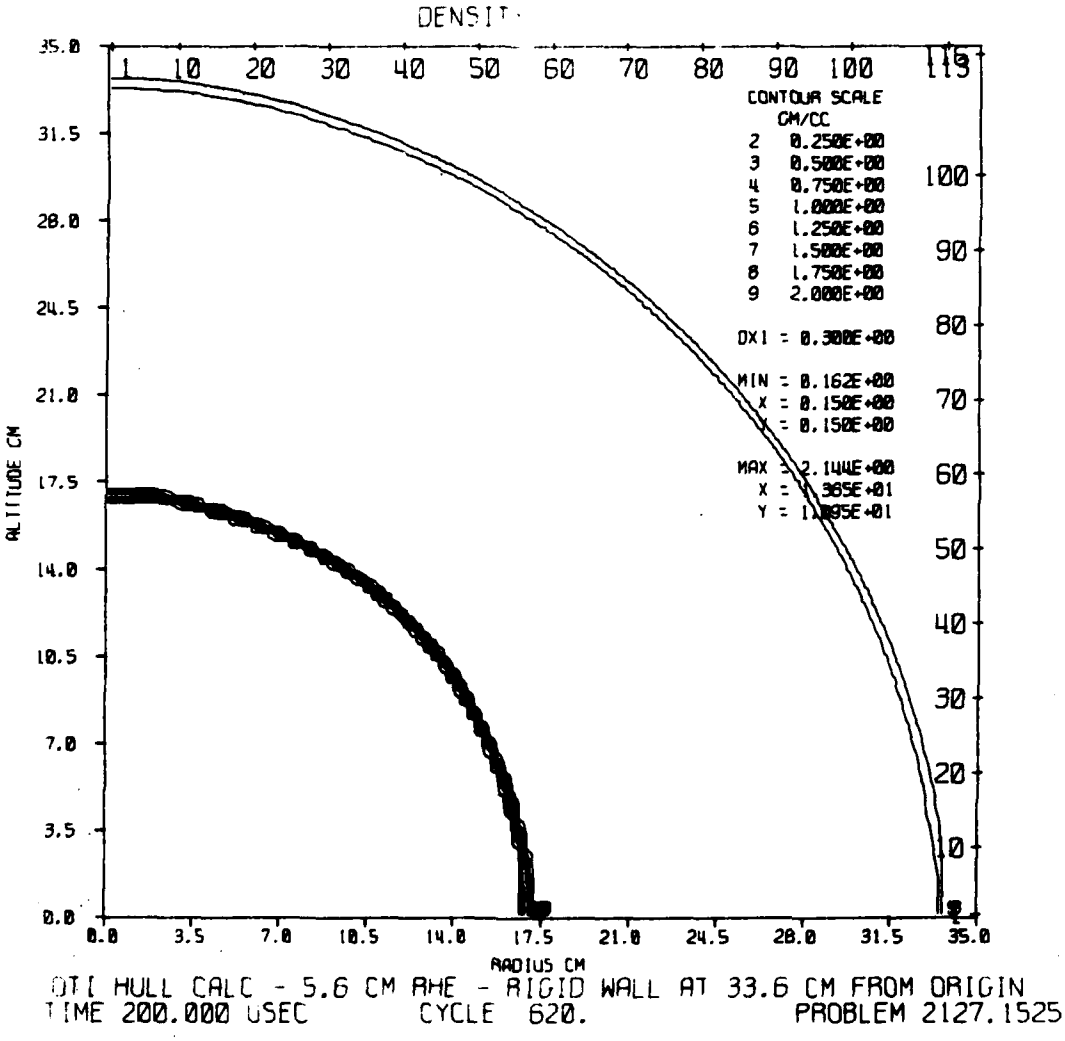

Figure 30. Density Contours at 200 Microseconds

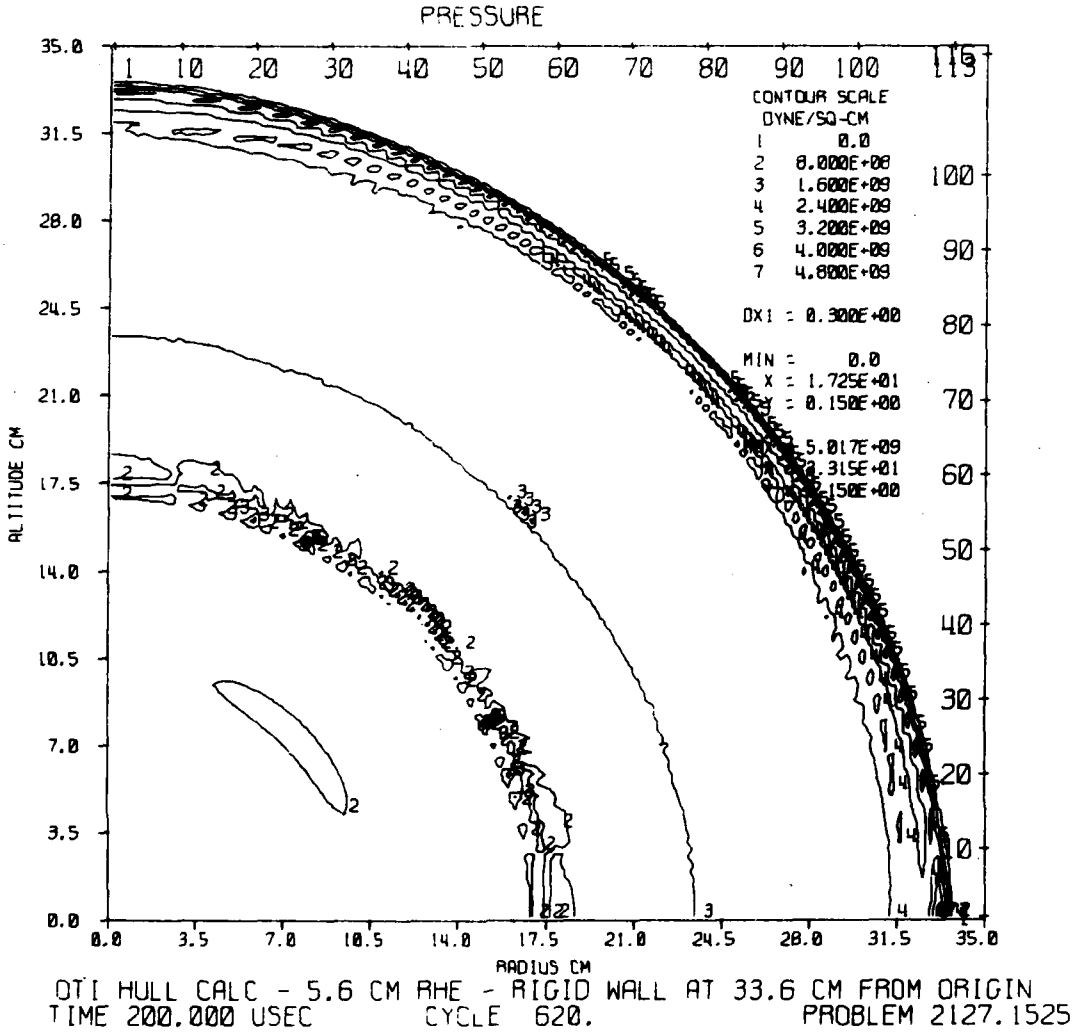

Figure 31. Pressure Contours at 200 Microseconds

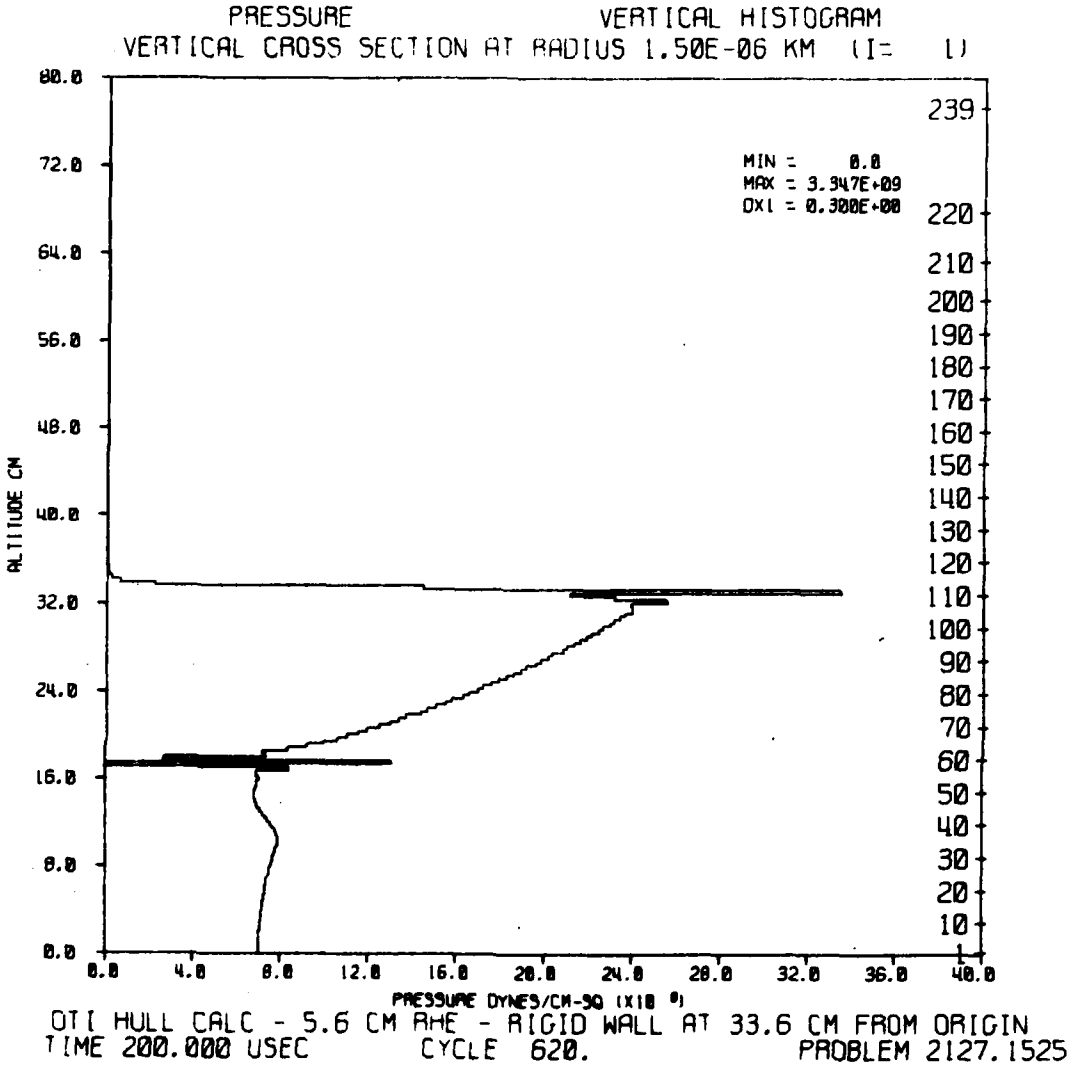

Figure 32. Pressure Histogram at 200 Microseconds

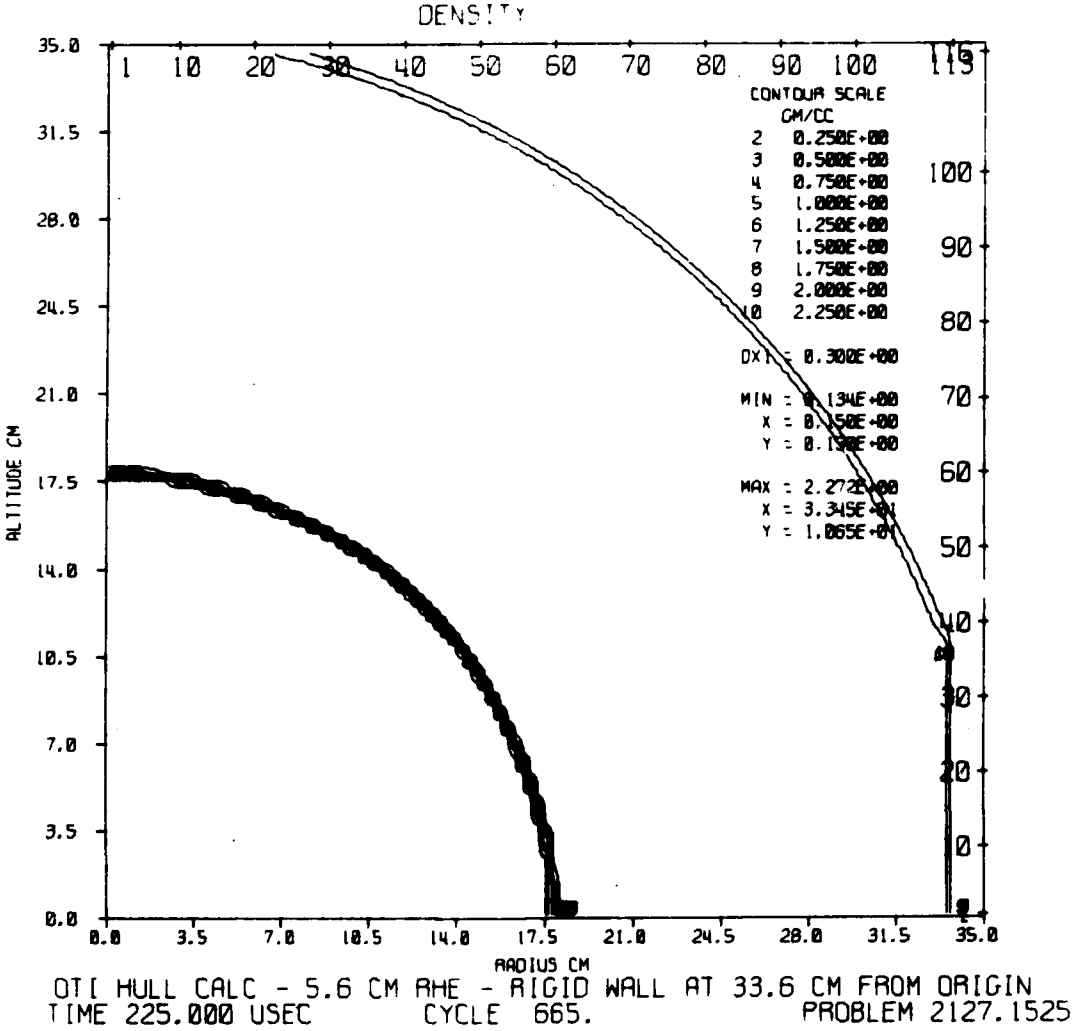

Figure 33. Density Contours at 225 Microseconds

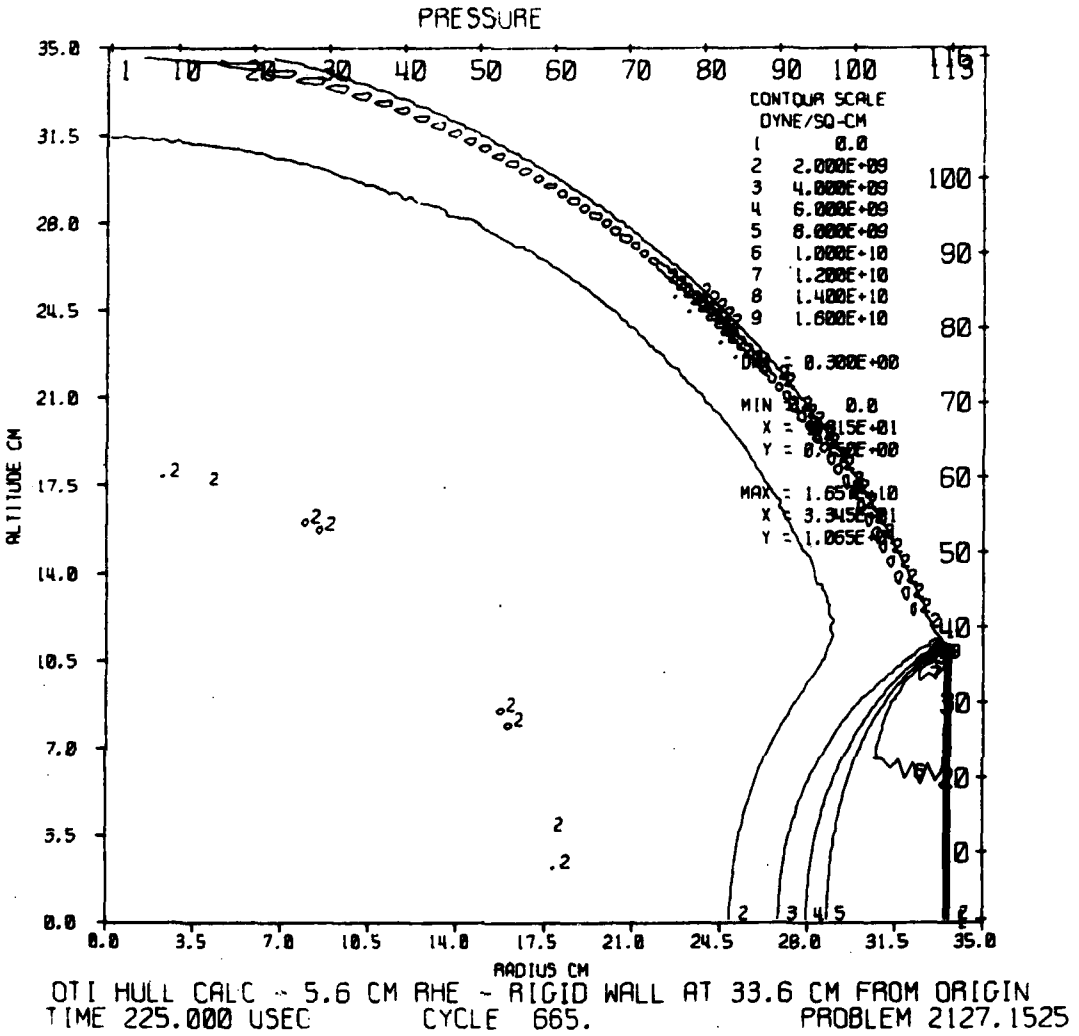

Figure 34. Pressure Contours at 225 Microseconds

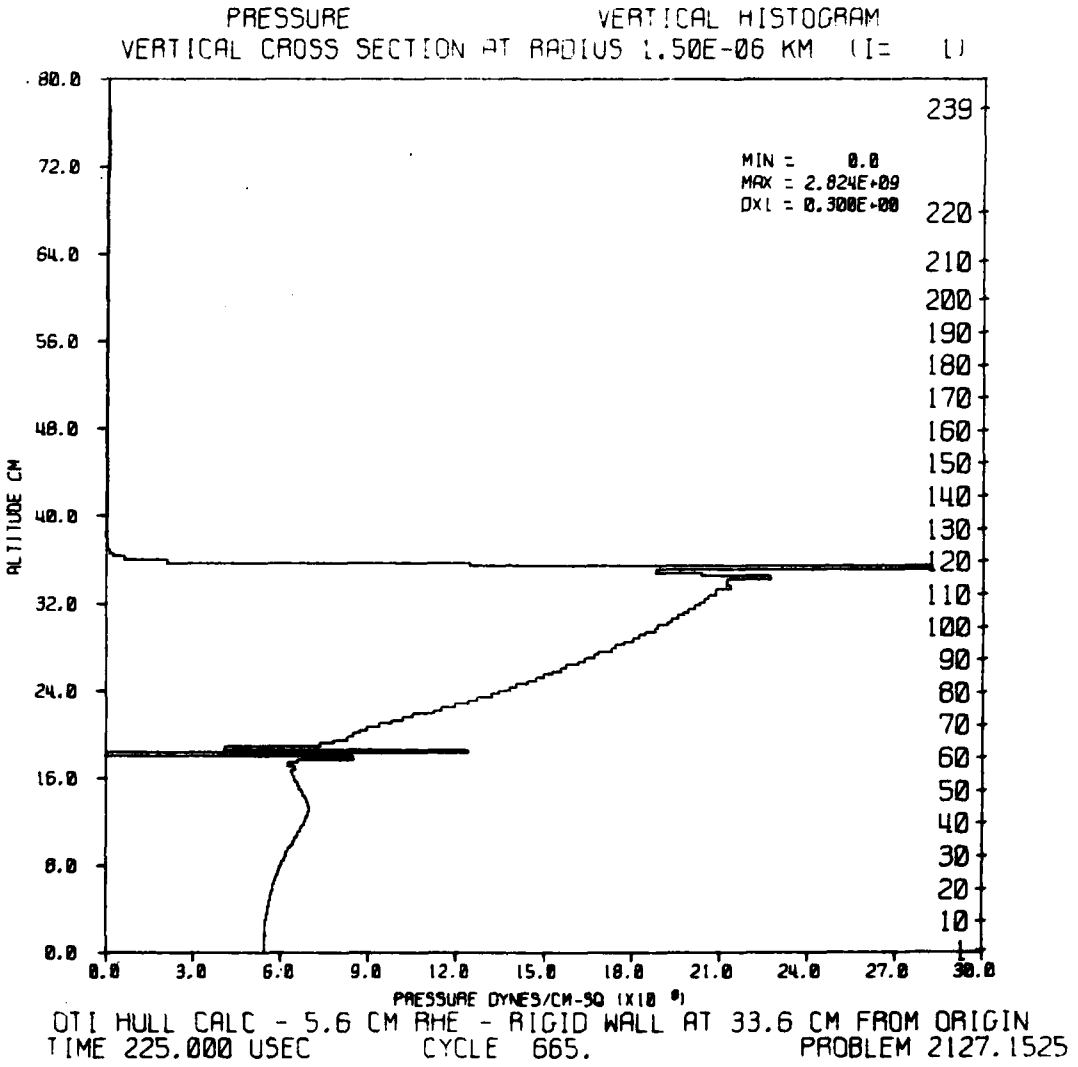

Figure 35. Pressure Histogram at 225 Microseconds

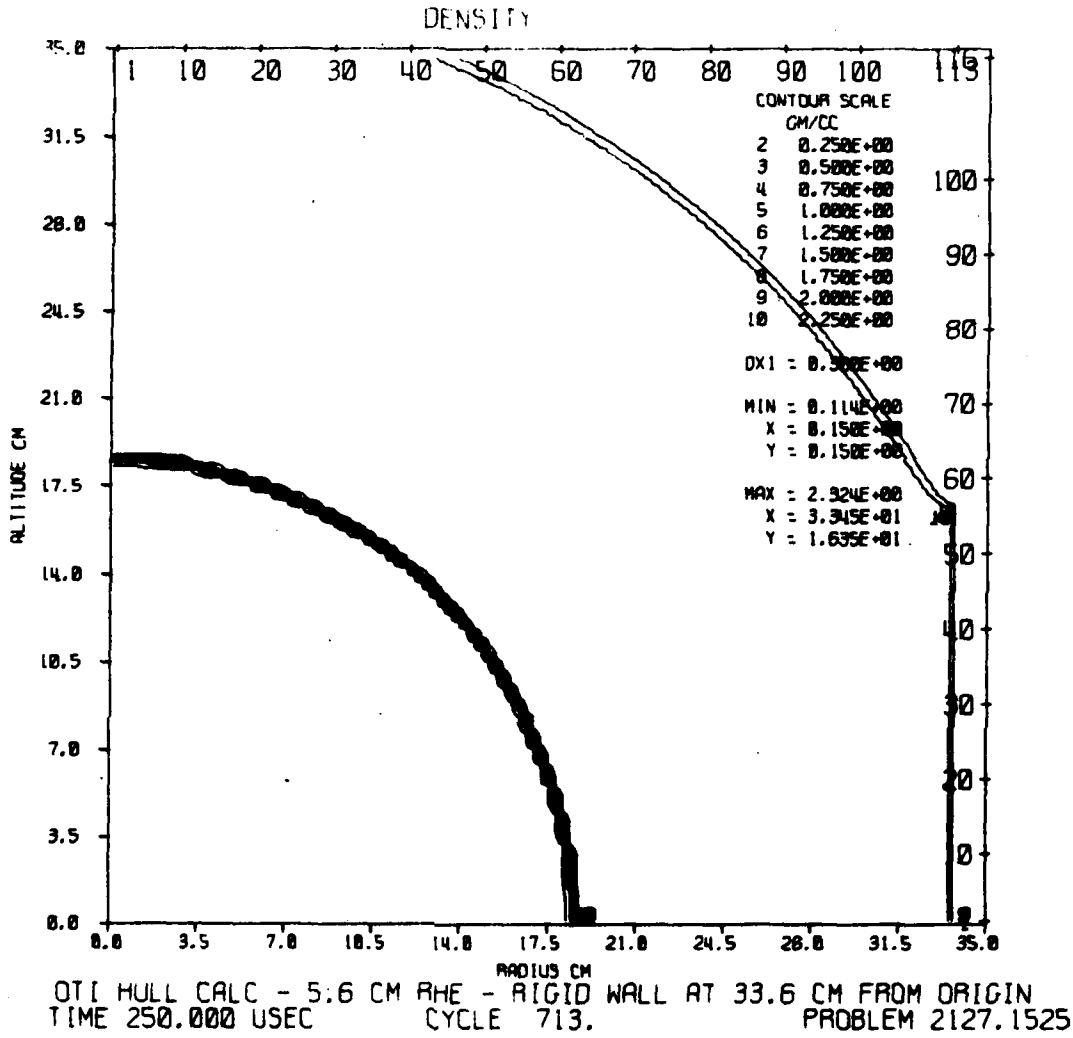

Figure 36. Density Contours at 250 Microseconds

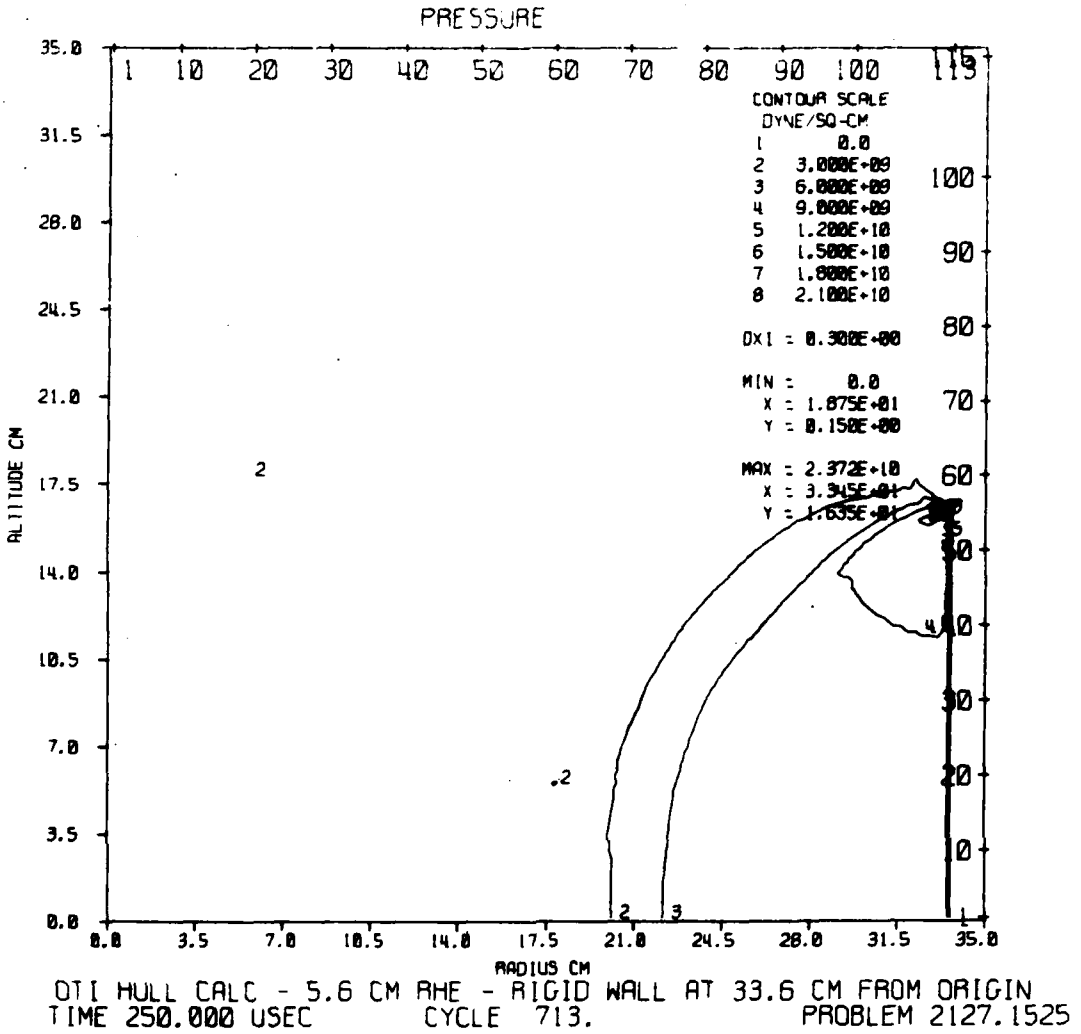

Figure 37. Pressure Contours at 250 Microseconds

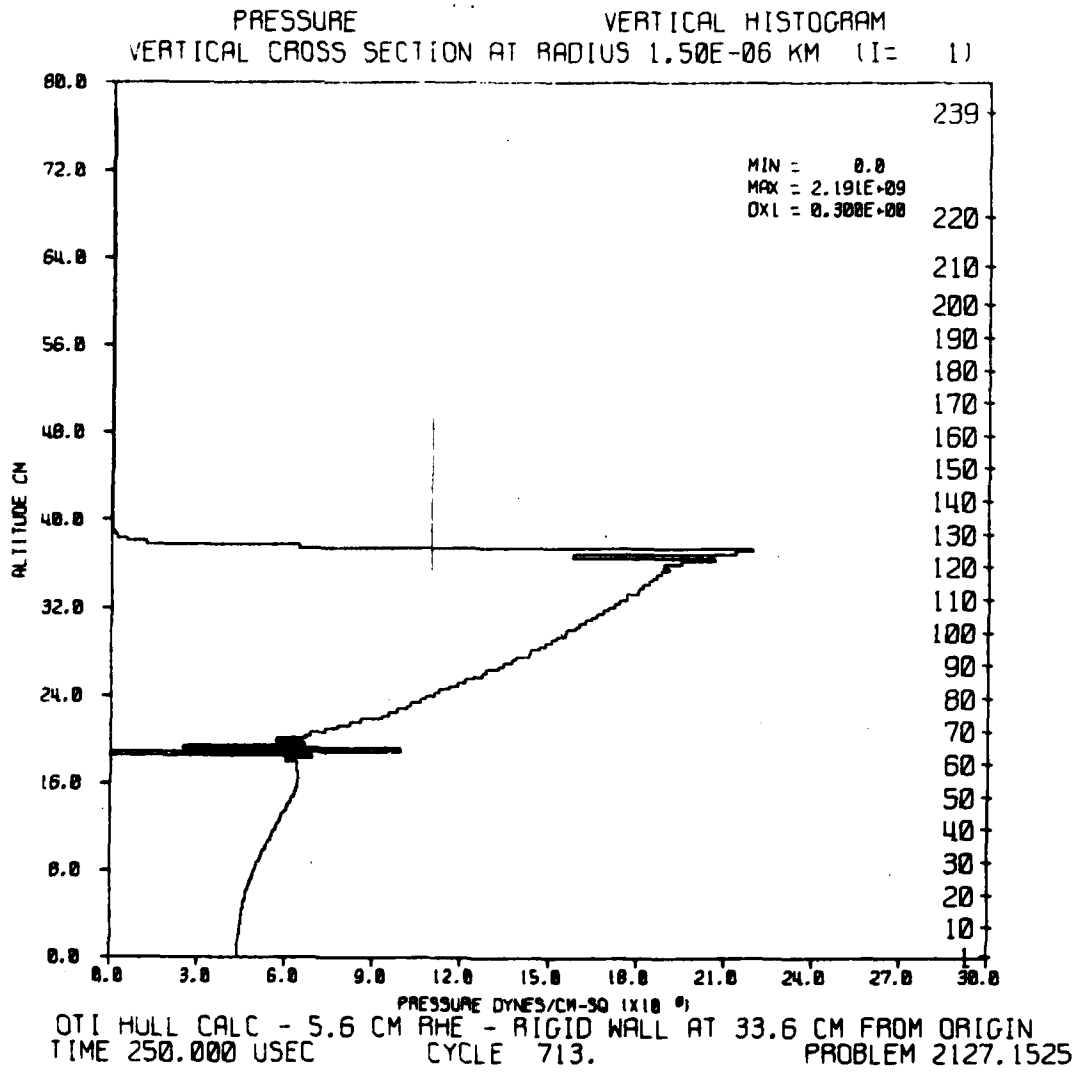

Figure 38. Pressure Histogram at 250 Microseconds

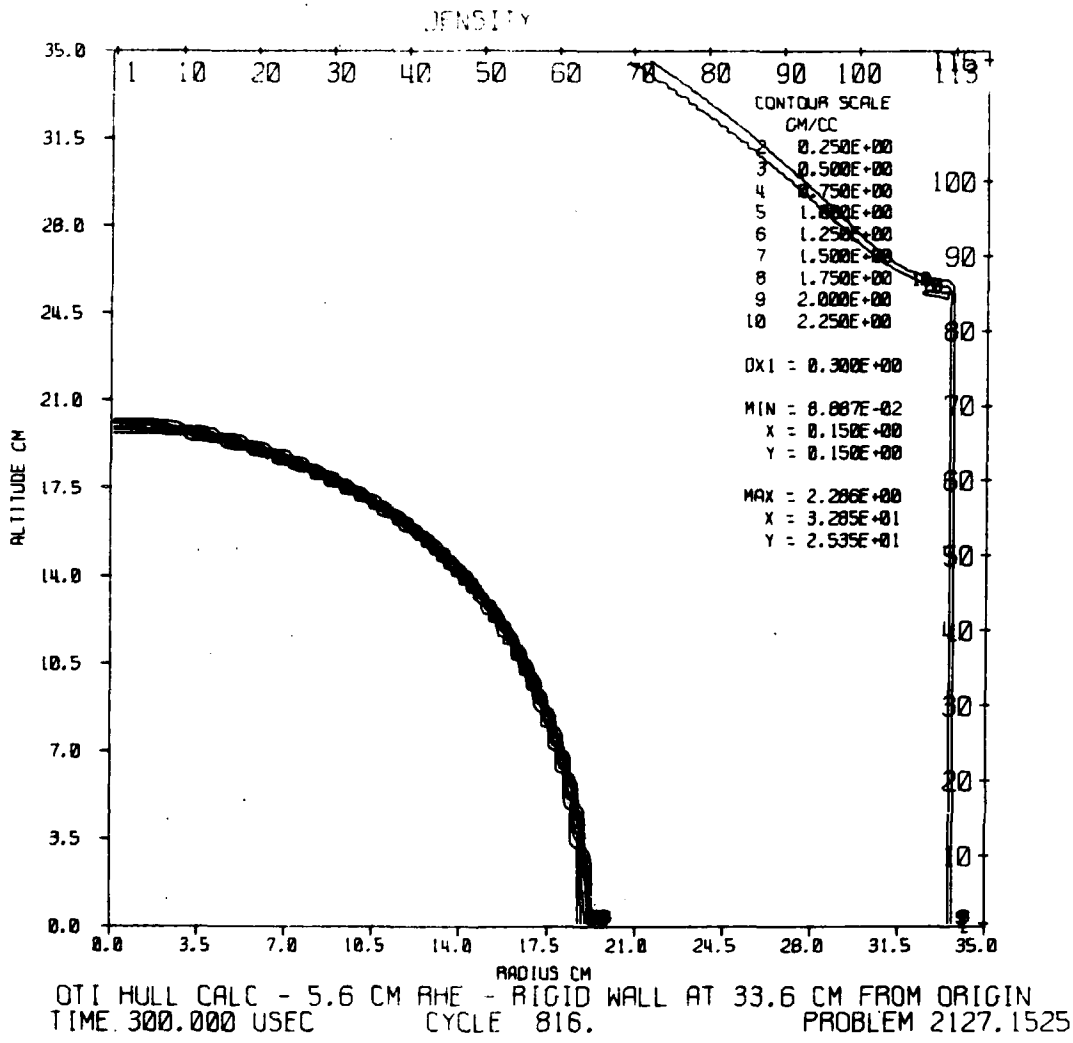

Figure 39. Density Contours at 300 Microseconds

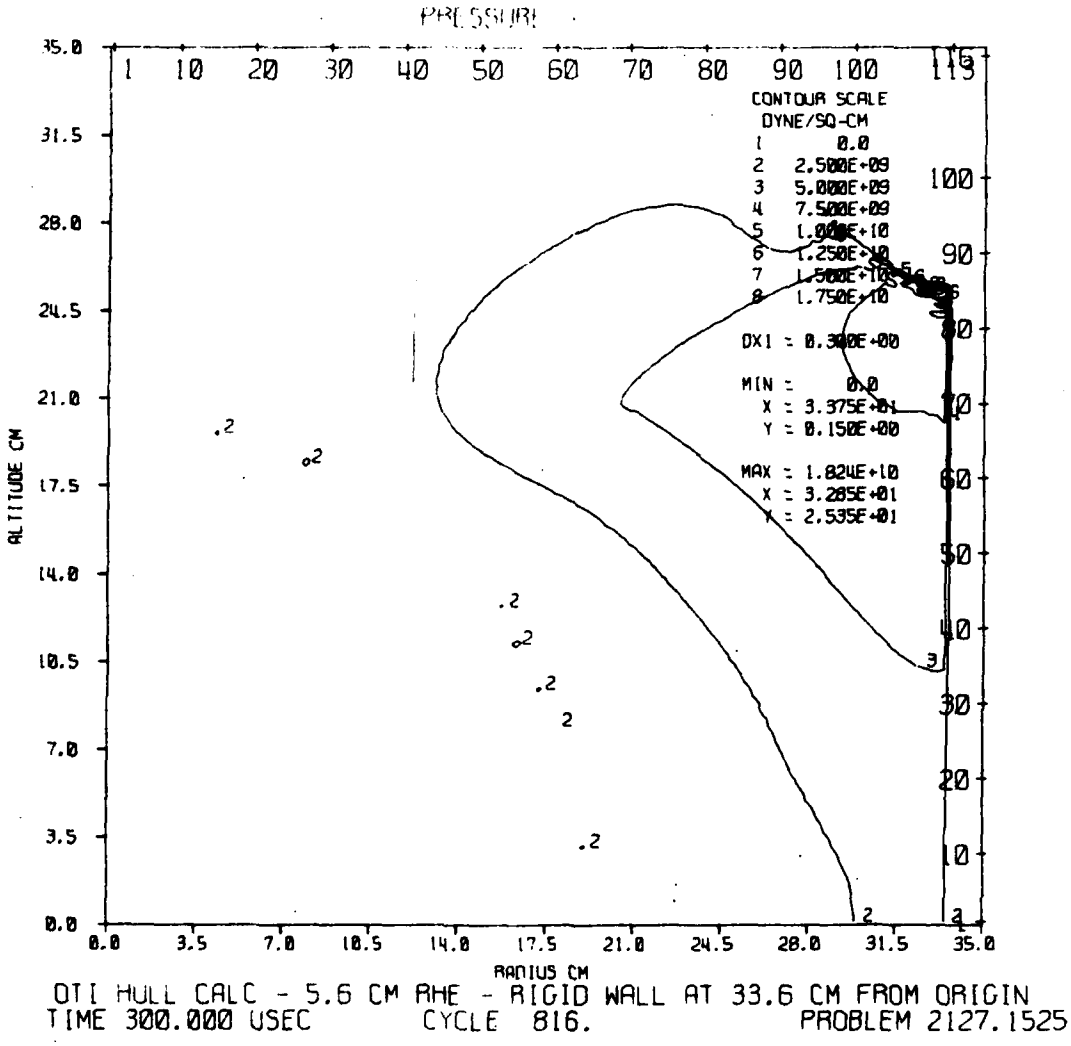

Figure 40. Pressure Contours at 300 Microseconds

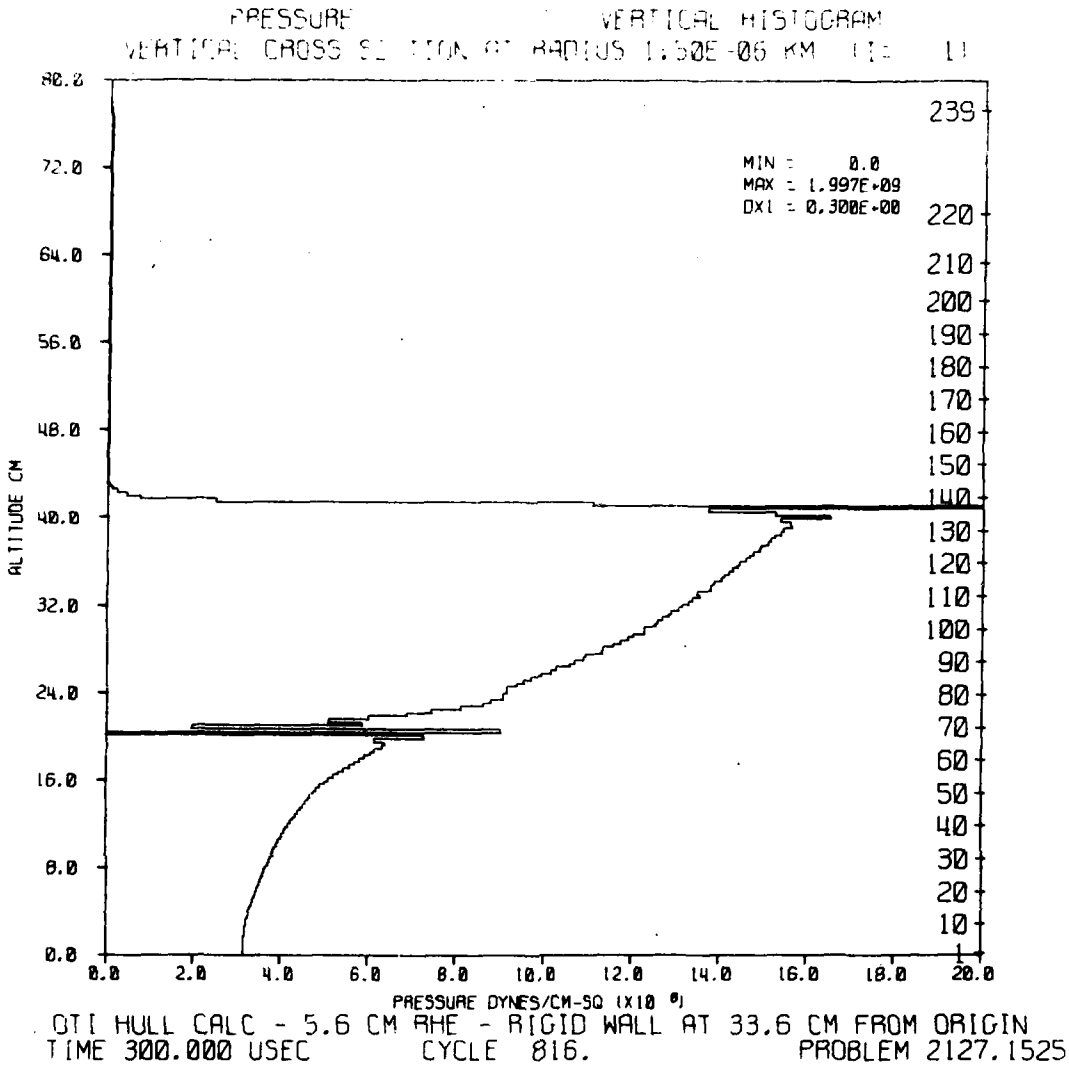

Figure 41. Pressure Histogram at 300 Microseconds

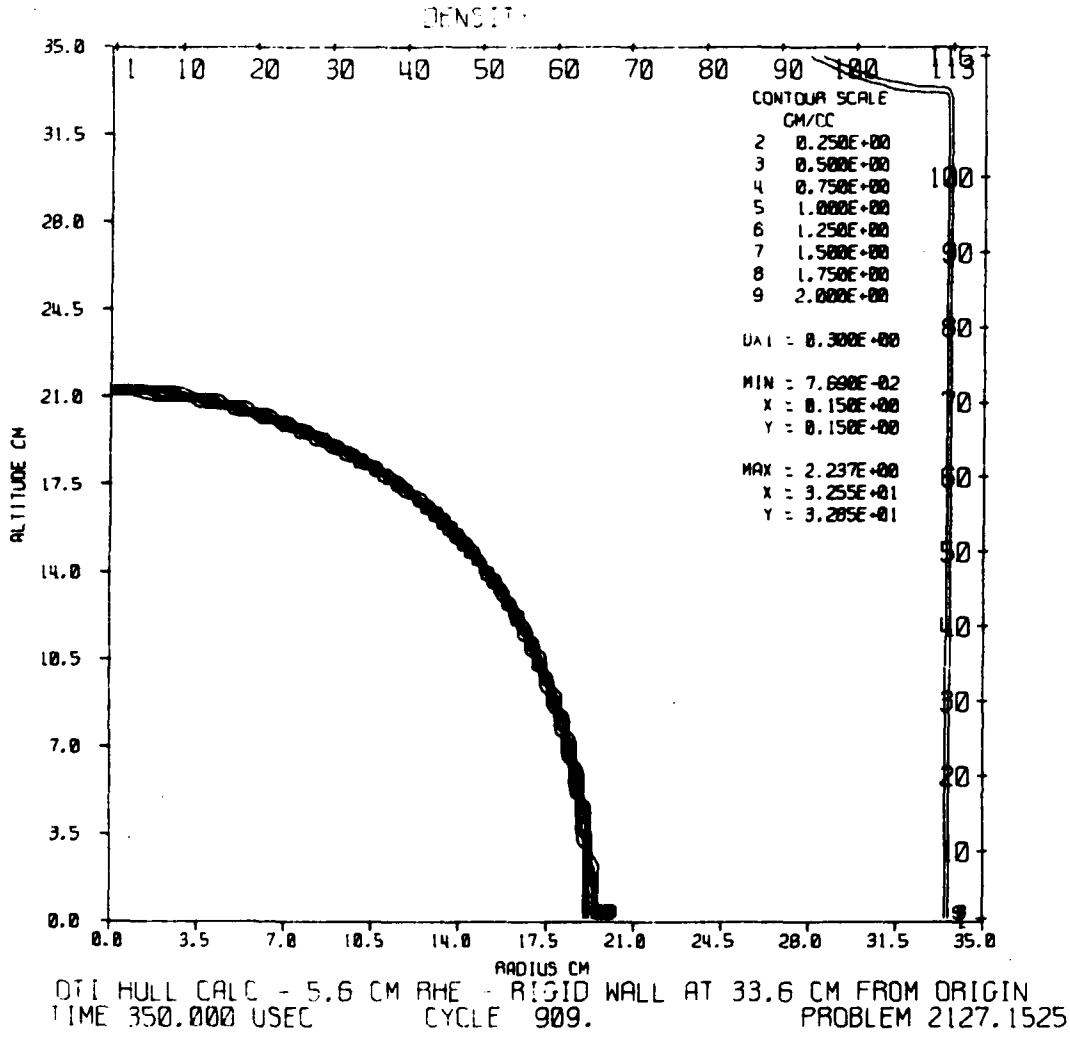

Figure 42. Density Contours at 350 Microseconds

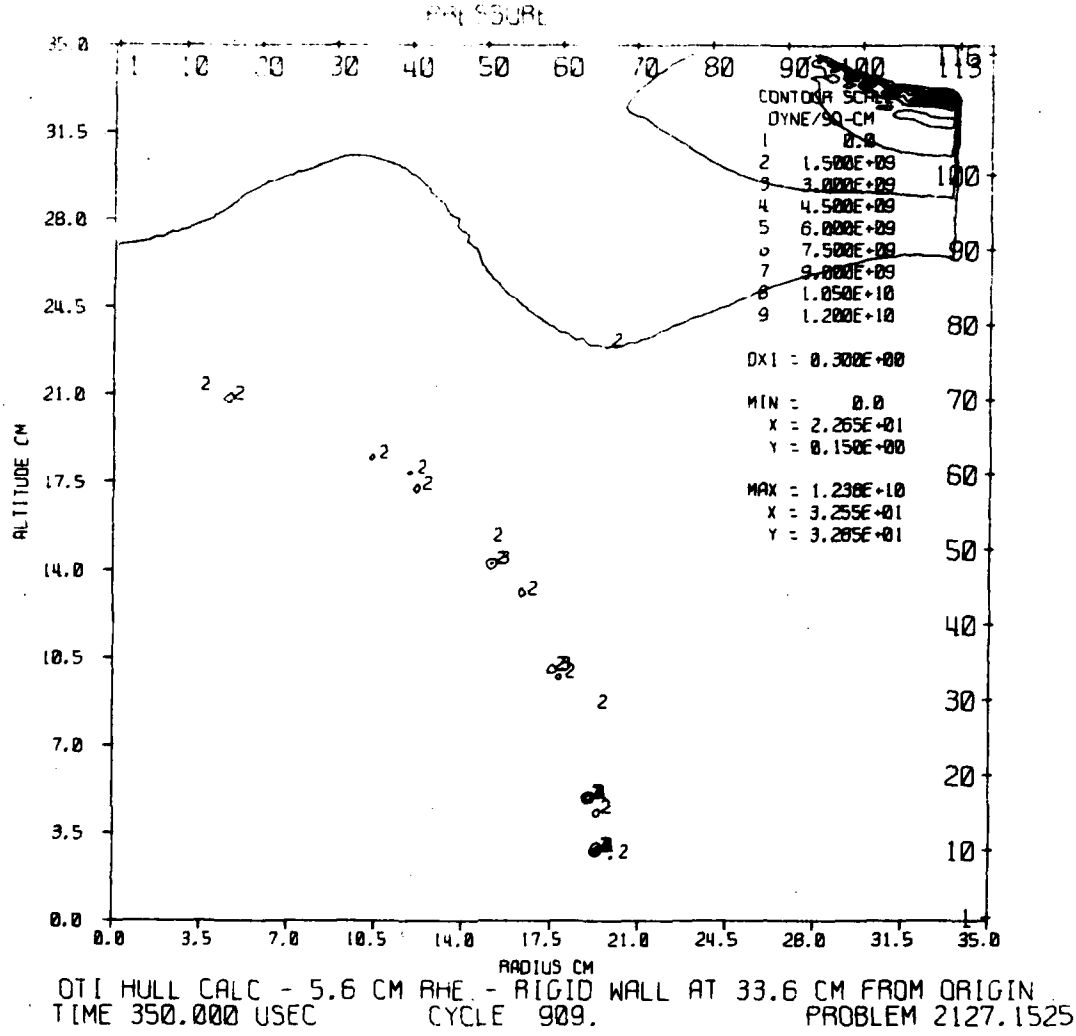

Figure 43. Pressure Contours at 350 Microseconds

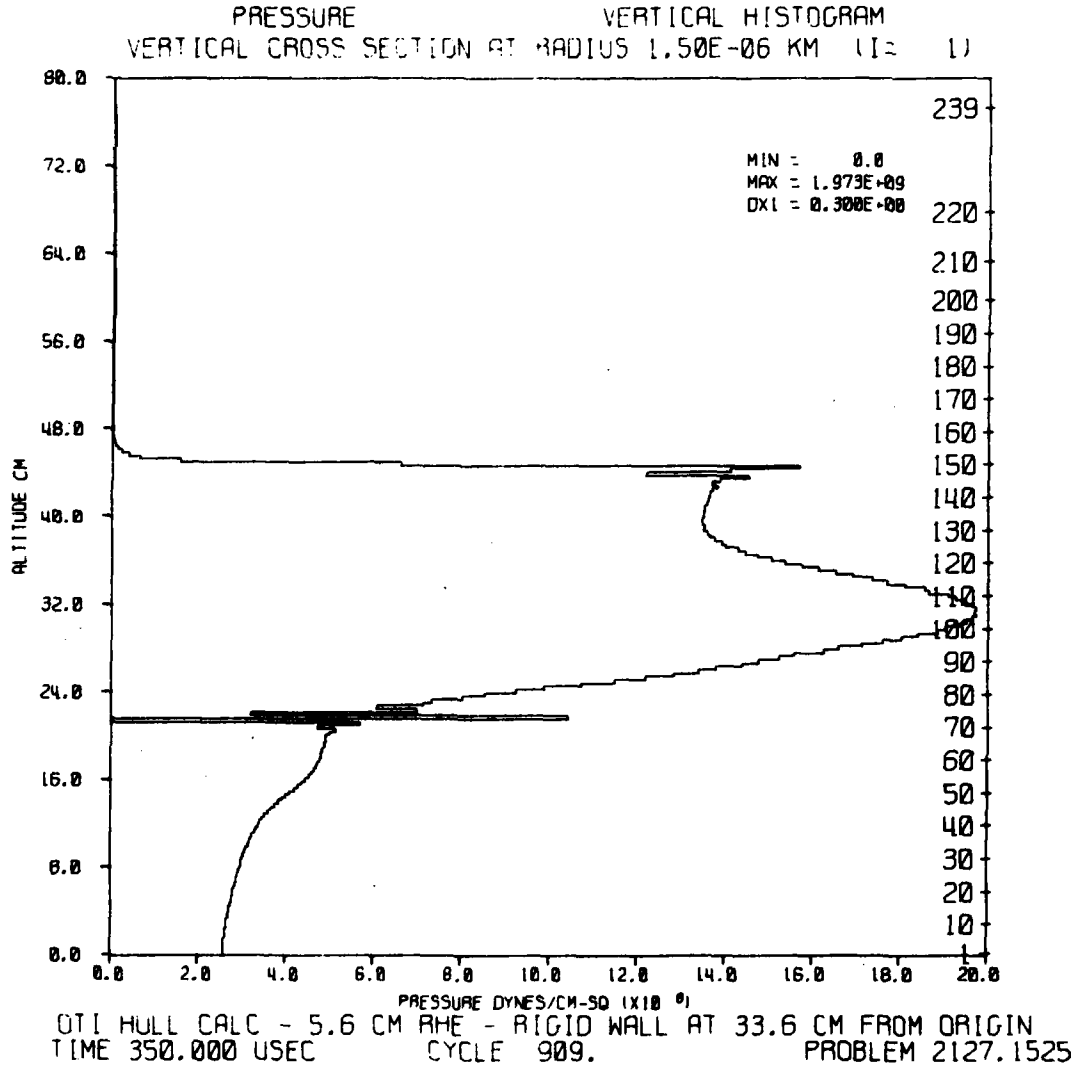

Figure 44. Pressure Histogram at 350 Microseconds

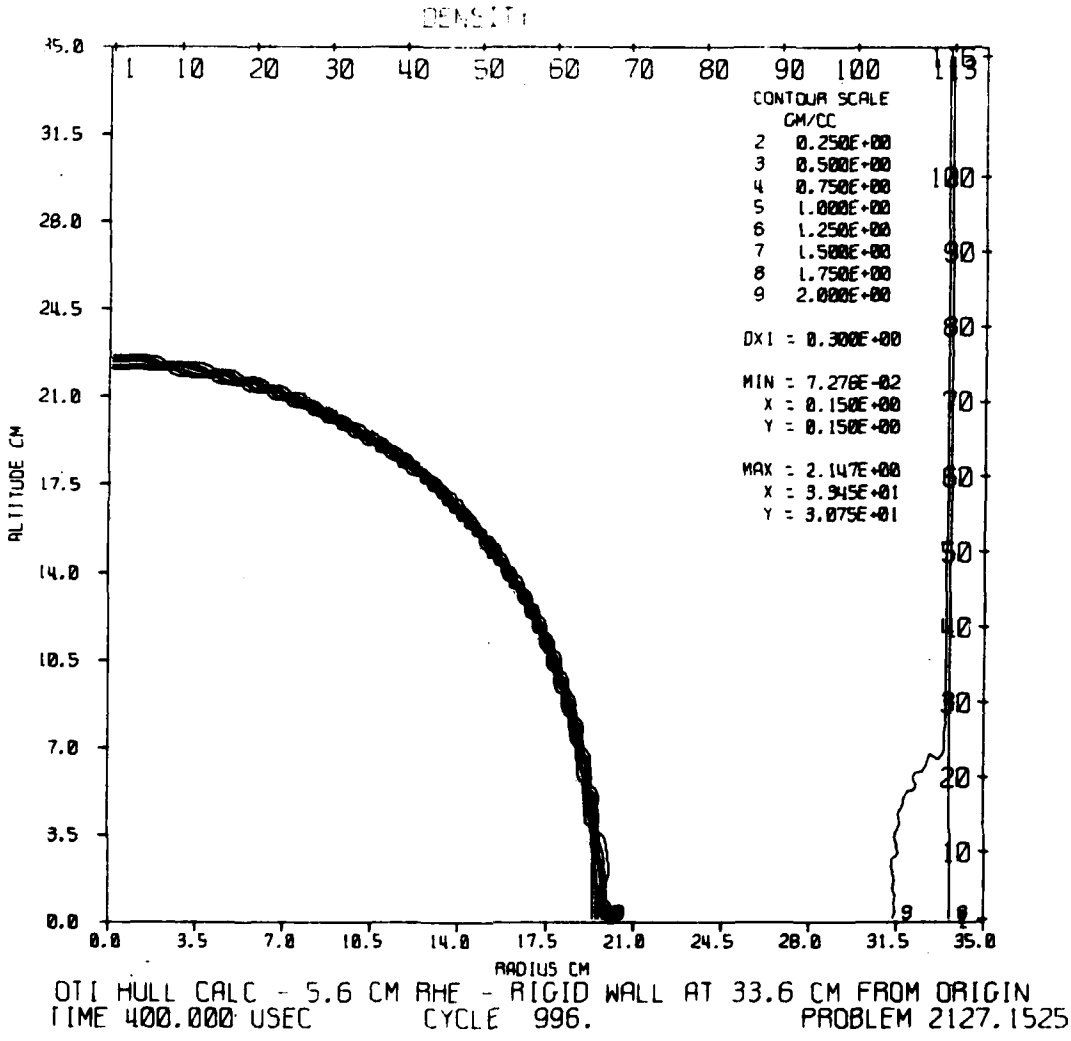

Figure 45. Density Contours at 400 Microseconds

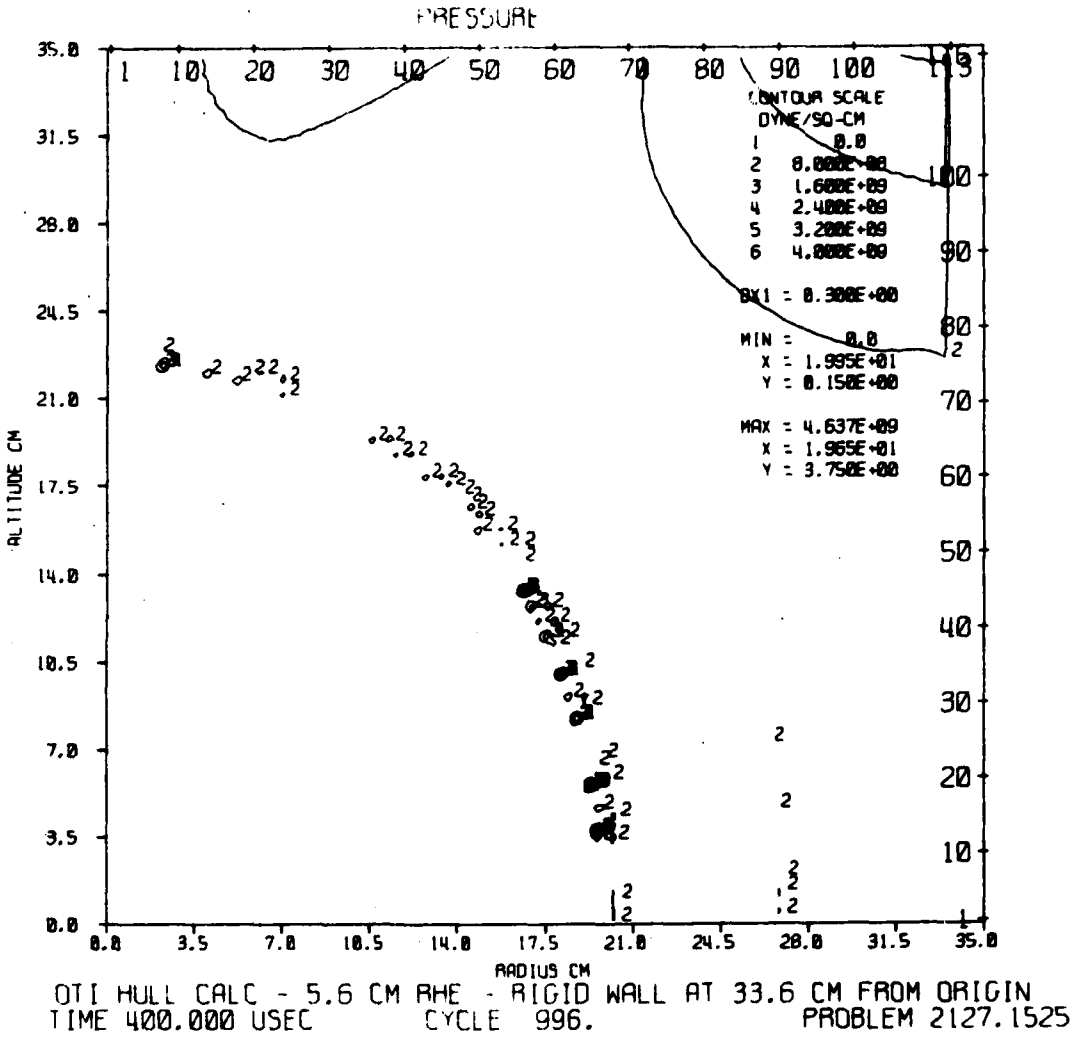

Figure 46. Pressure Contours at 400 Microseconds

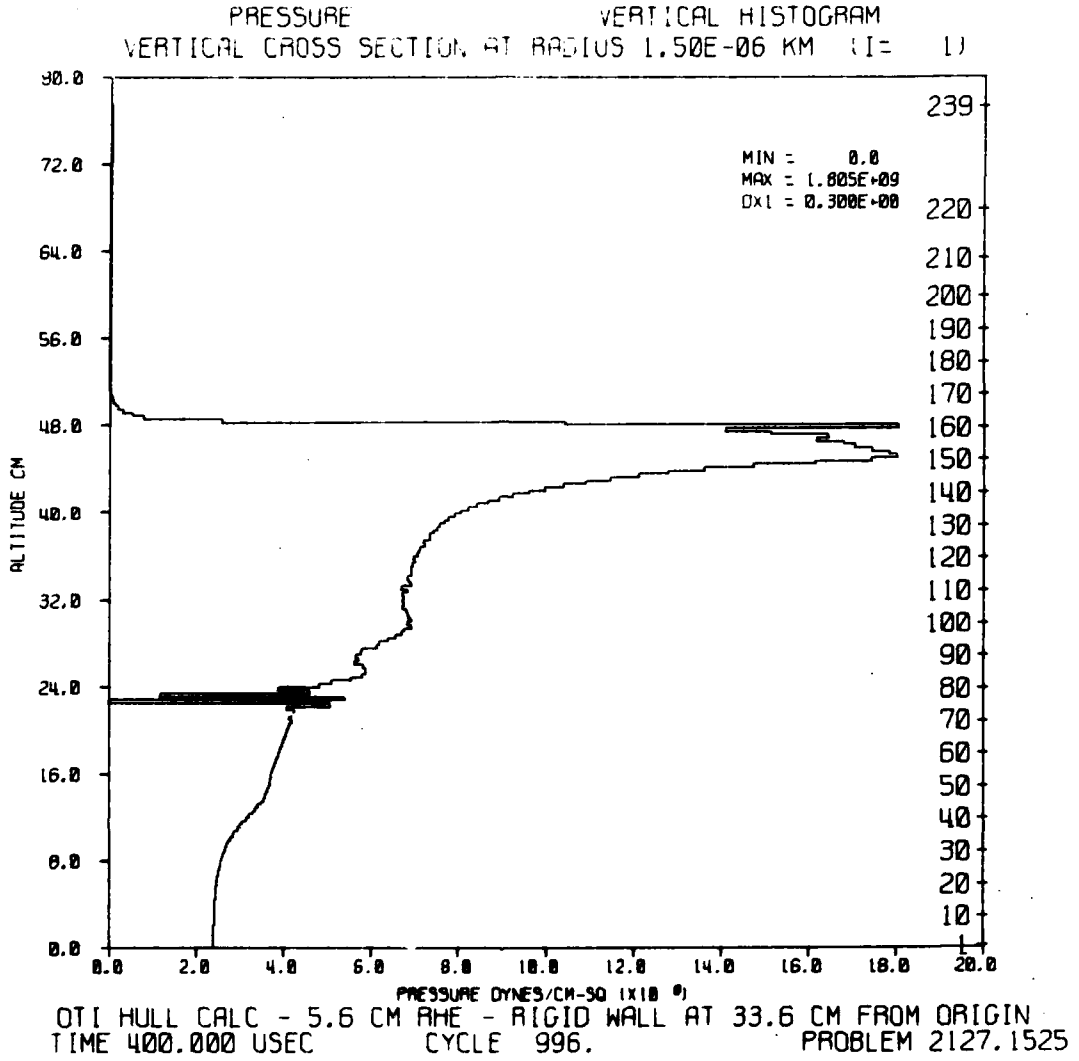

Figure 47. Pressure Histogram at 400 Microseconds

and across the tops of some of these figures refer to zone numbers in the calculation. The (I=1) on the histograms means that the data apply to the first radial zone. This report has used R and Y as axis descriptors. Minimum and maximum contour values in the figures are indicated as existing at X and Y positions. In this case, the X axis is the same as the R axis.

The first shock wave is seen to hit the wall between 200 and 225 microseconds (see Figures 29 and 32). Figure 34 shows that a mild Mach-stem has developed along the wall at the intersection of the reflected and incident waves. This behavior continues as seen in subsequent pressure contour plots, although one must mentally draw in the incident pressure curve from the lead location on the pressure histograms, since contour values chosen by the plotting program do not include it after 225 microseconds. The establishment of a Mach-stem leads to slightly higher pressures at positions away from the point closest to the explosive. This effect is seen in the pressure and impulse time histories recorded at locations near the wall.

Figures 48 through 55 are pressure and pressure impulse time histories for stations located in the sand next to the rigid wall. The stations are fixed with respect to the wall and do not move as the sand moves. For stations beyond the first two (48 and 49), judgement is again required to determine the actual peak as distinguished from the initial oscillations. Pressure-time slopes from the smooth part of each curve were extrapolated back to the time of arrival of the wave to generate Table 4.

Free-field pressures at various distances from the explosive can be determined by smoothing the peak pressures in the pressure histogram curves up to 300 microseconds. Beyond this time the reflected pressure from the wall has reached the Y axis and disturbed these values. Examination of the histogram values shows excellent agreement with the free-field data in Table 3. The incident peak pressure then at the wall is 35,530 PSI. The reflected pressure at the point of normal incidence is 158,116 PSI, yielding a P_R/P_I ratio of 4.45. It is believed that this reflected pressure ratio is larger than that obtained previously because of the nature of the absolutely rigid wall in this calculation. The steel in the previous calculations was able to move slightly and relieve peak pressure.

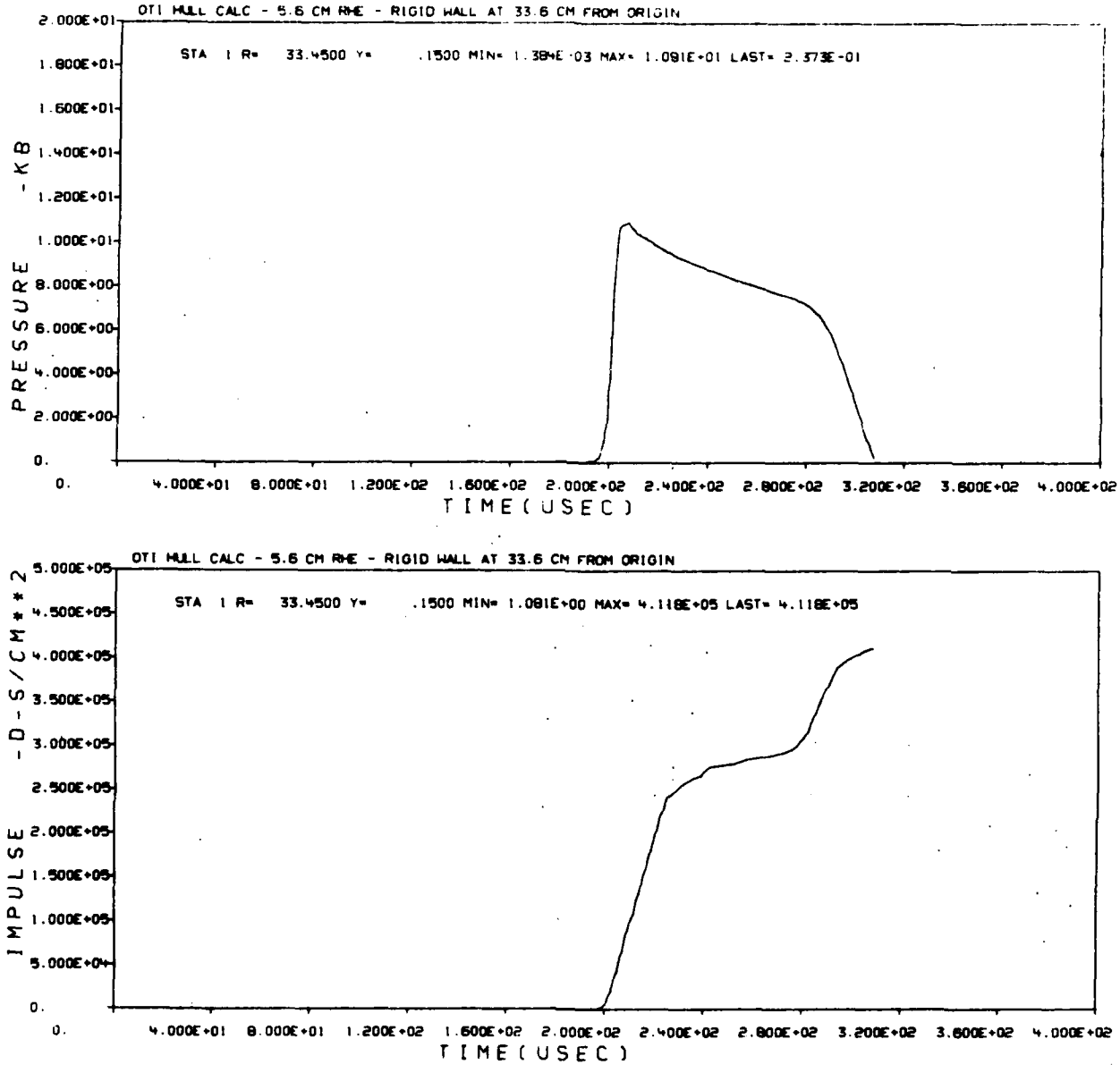

Figure 48. Station 1 Pressure/Impulse at Rigid Wall

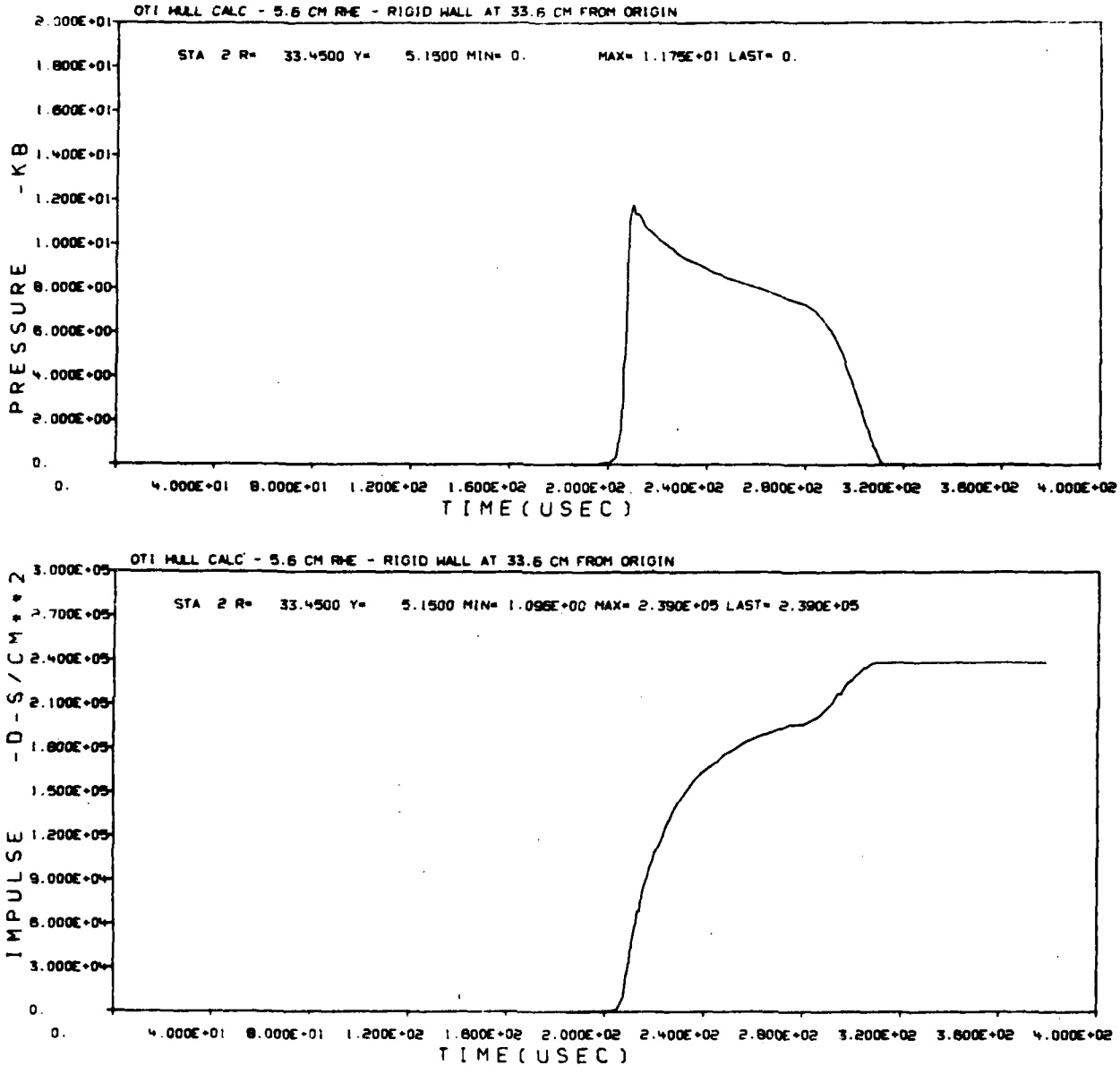

Figure 49. Station 2 Pressure/Impulse at Rigid Wall

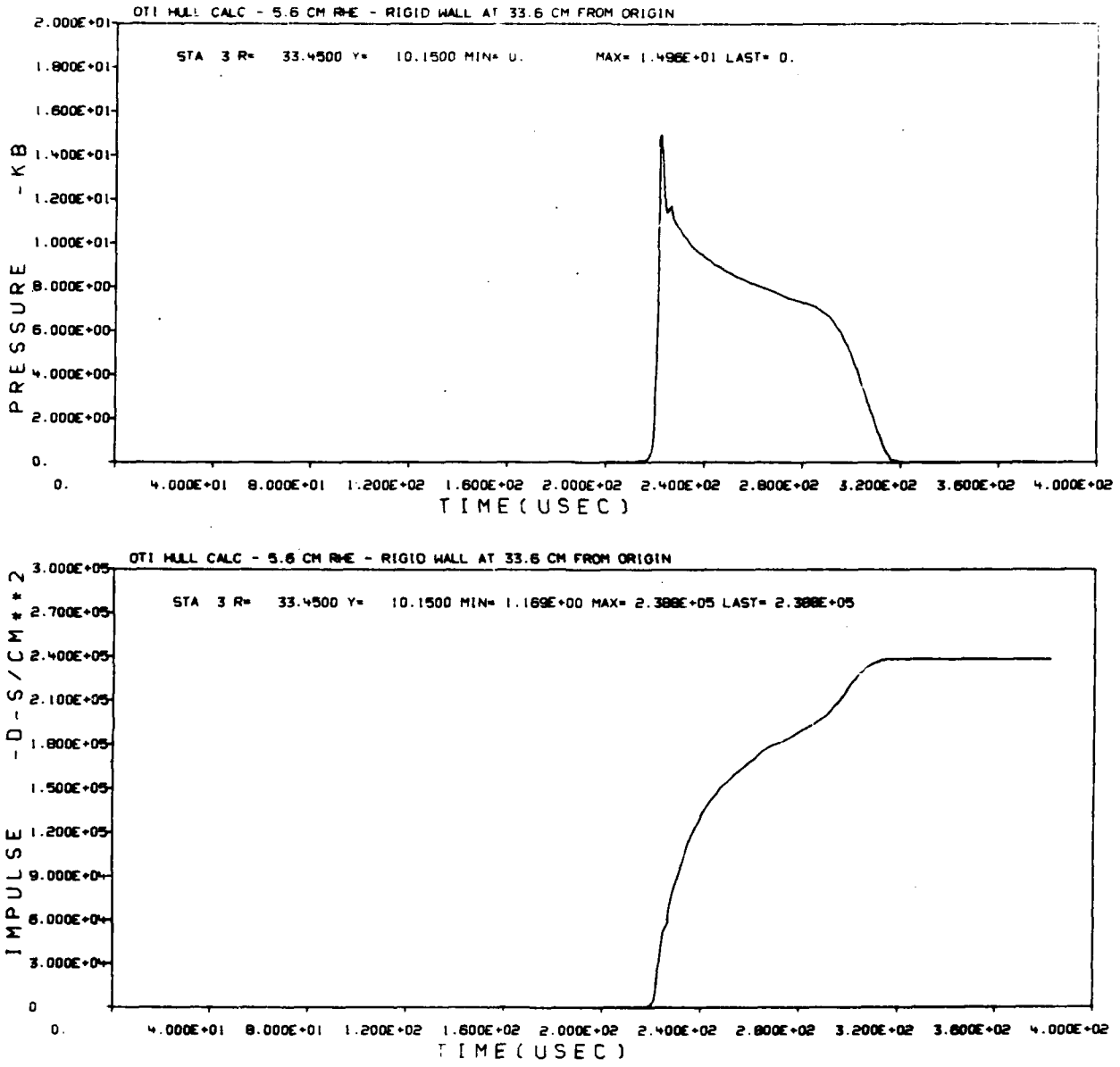

Figure 50. Station 3 Pressure/Impulse at Rigid Wall

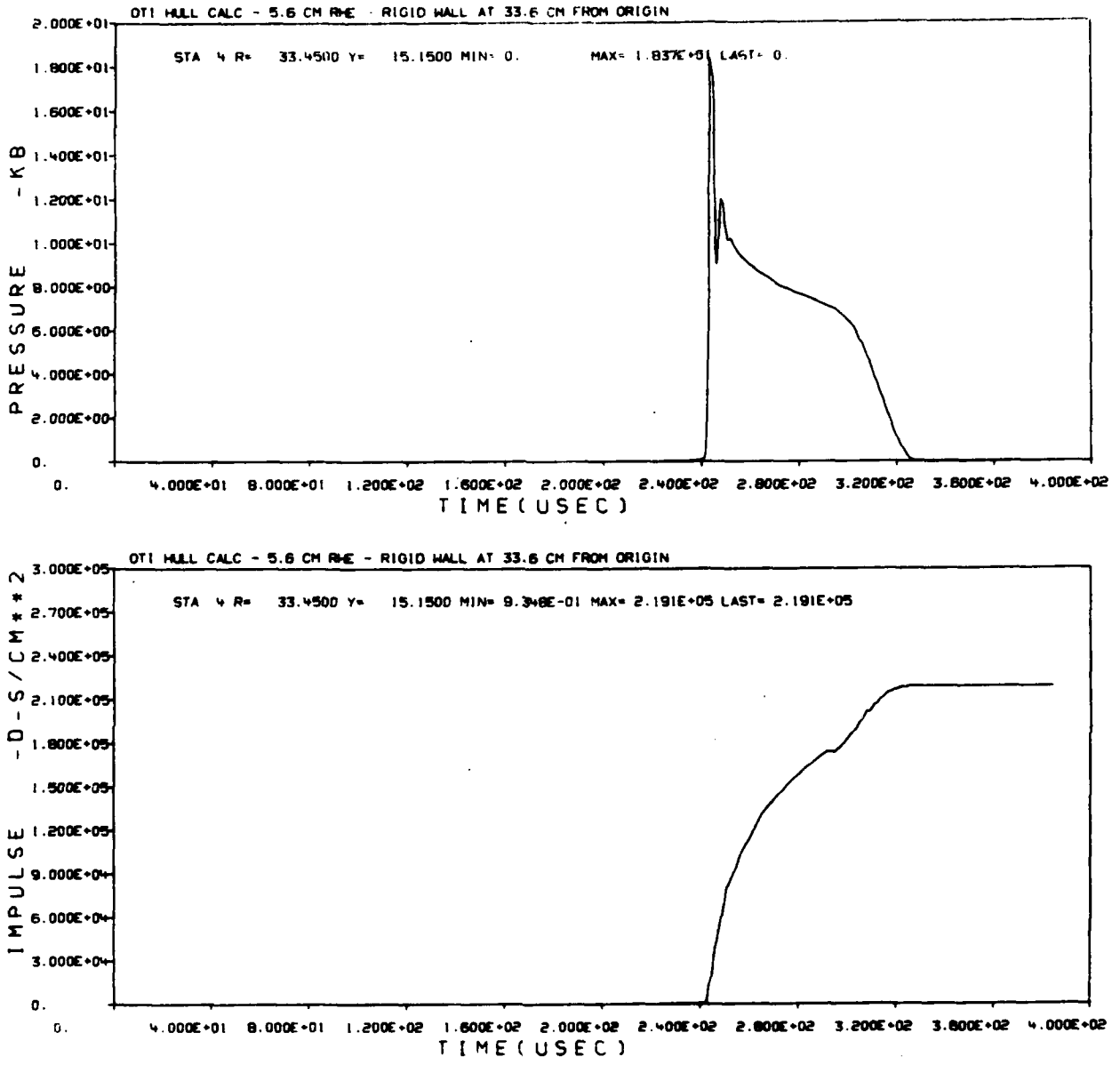

Figure 51. Station 4 Pressure/Impulse at Rigid Wall

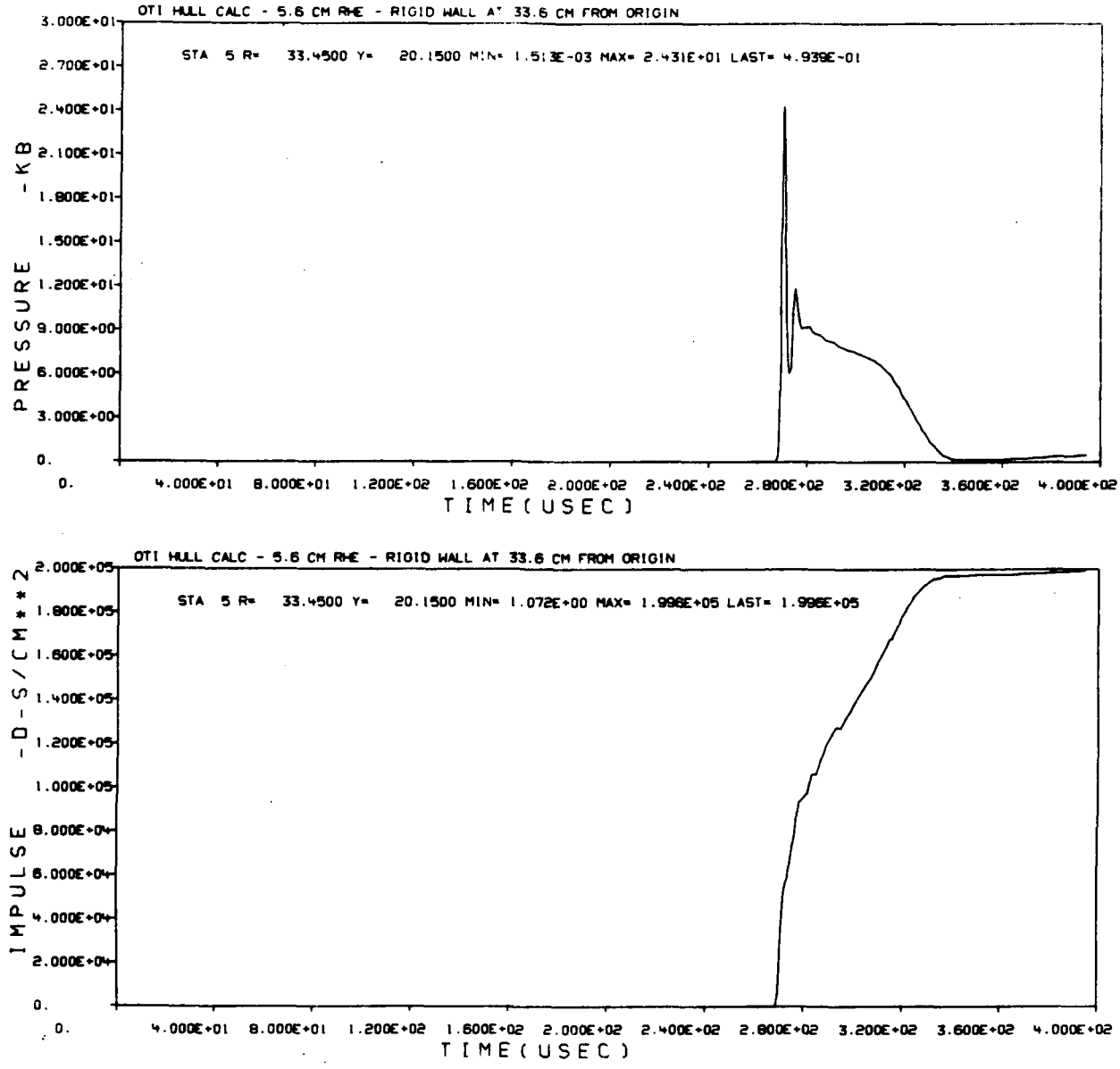

Figure 52. Station 5 Pressure/Impulse at Rigid Wall

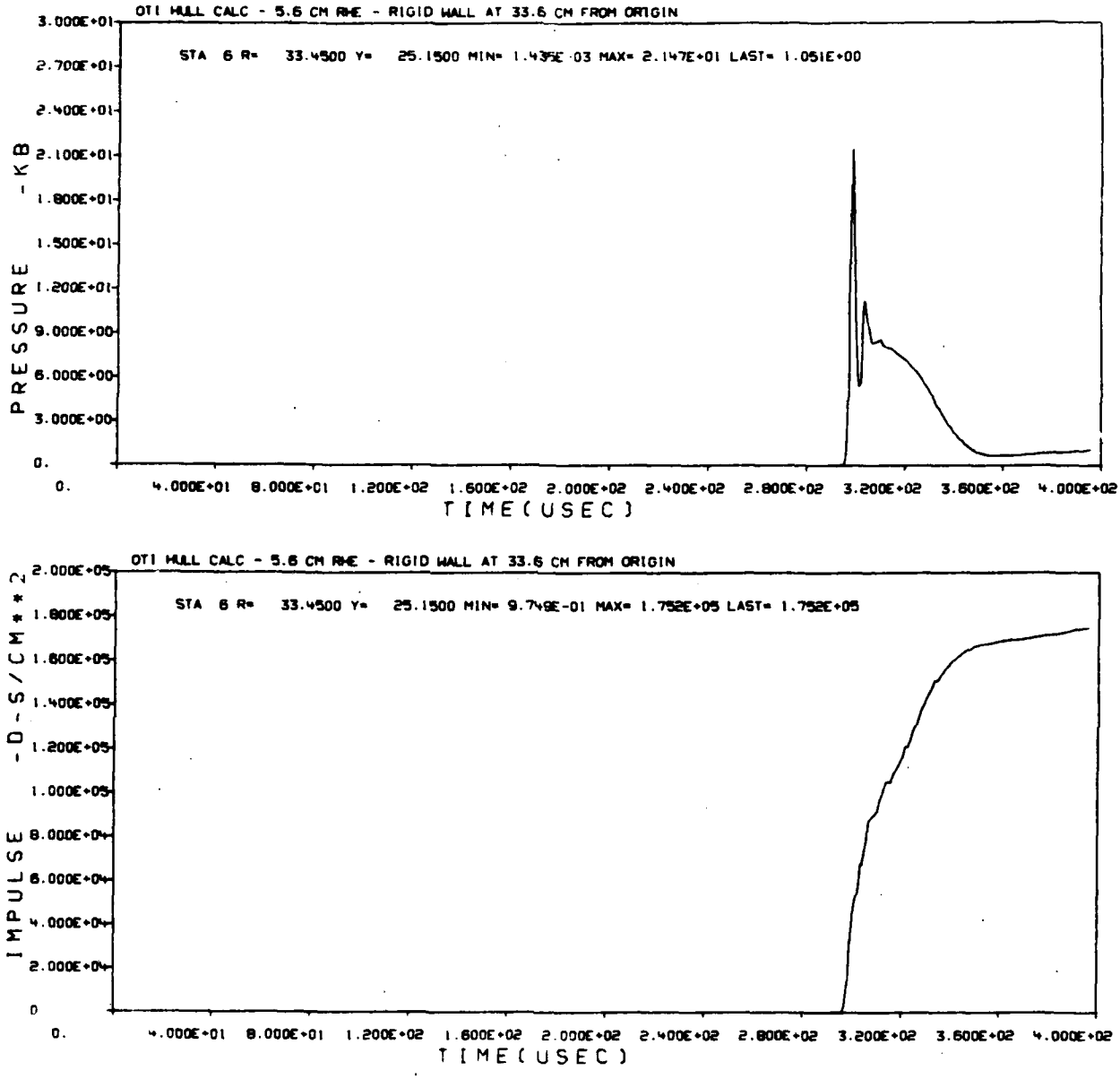

Figure 53. Station 6 Pressure/Impulse at Rigid Wall

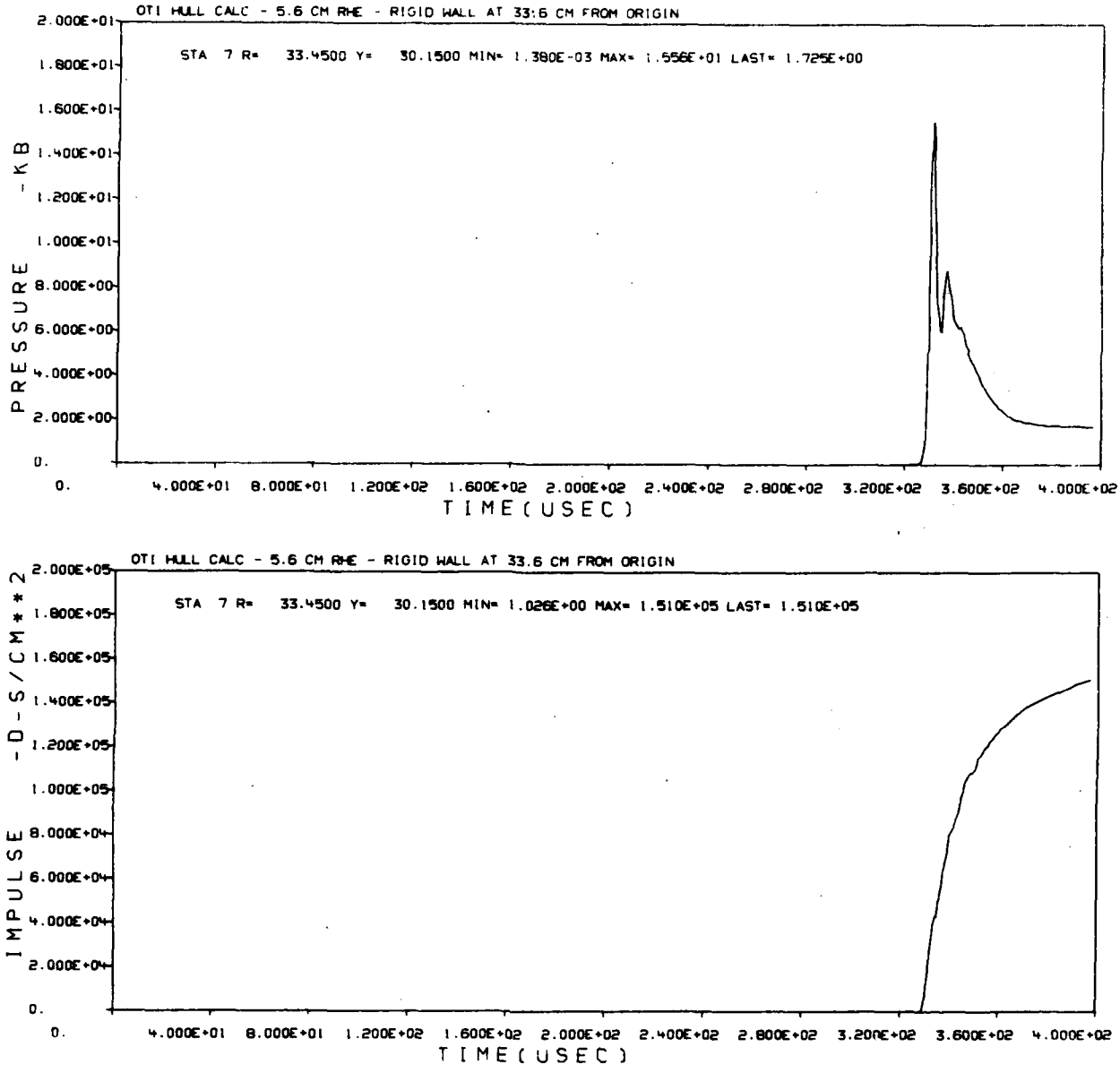

Figure 54. Station 7 Pressure/Impulse at Rigid Wall

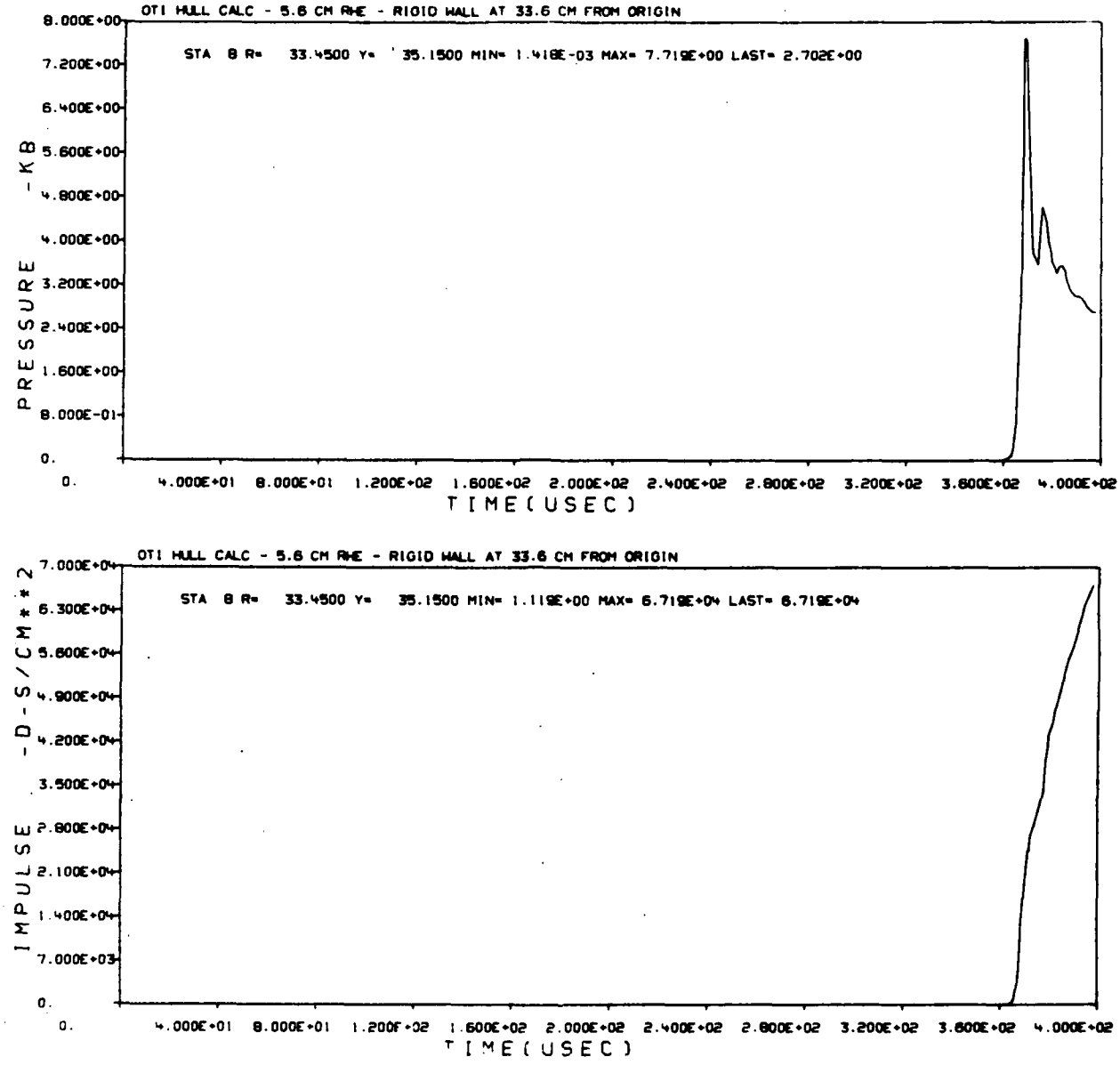

Figure 55. Station 8 Pressure/Impulse at Rigid Wall

TABLE 4. REFLECTED PRESSURE AT THE WALL

STATION NUMBER	STATION Y POSITION (CM)	REFLECTED PRESSURE (KB)	REFLECTED PRESSURE (PSI)
1	0.15	10.91	158,116
2	5.15	11.75	170,290
3	10.15	12.0	173,913
4	15.15	11.9	172,464
5	20.15	11.0	159,420
6	25.15	10.5	152,174
7	30.15	10.0	144,928
8	35.15	4.8	69,565

Examination of Table 4 data shows that reflected pressure increases away from the normal incidence point and then decreases again. This is due to the effect of the Mach-stem formation. Table 5 presents incident pressure computed from the previous scaled range equation using distance from charge center to the station. The incident pressure is seen to drop from 35,530 PSI at station 1 to 13,045 PSI at station 8. Using this incident pressure value and actual station pressure, values of P_R/P_I were calculated. Multiplying this ratio by the cosine of the angle the flow makes with the normal to the wall at the station location further smooths the data.

TABLE 5. REFLECTED PRESSURE VS ANGLE

STATION NUMBER	Y POSITION (CM)	ANGLE (DEG)	P_I (PSI)	P_R/P_I	$\frac{P_R}{P_I}\cos\theta$
1	0.15	0	35,530	4.45	4.45
2	5.15	8.75	34,953	4.88	4.82
3	10.15	16.88	32,438	5.36	5.13
4	15.15	24.37	28,813	5.98	5.45
5	20.15	31.06	24,642	6.47	5.54
6	25.15	36.94	20,419	7.46	5.96
7	30.15	42.02	16,490	8.79	6.53
8	35.15	46.42	13,045	5.34	3.68

SECTION IV
CONCLUSIONS

The calculations presented in the previous section must be applied to test results with caution since they all assume infinitely long cylindrical charges. End effects will obviously have some influence if the charge is of finite length. However, it is believed that they can be used to help interpret test data. The calculations clearly show that very large reflections can be expected at scaled distances of 6 or less from the charge and that pressure will vary across a steel plate placed in the flow due to varying distance from the charge, varying flow angle with respect to the plate, and Mach-stem formation.

REFERENCES

1. J. W. Swegle, TOODY IV - A Computer Program for Two-Dimensional Wave Propagation, Sandia Laboratories Report SAND-78-0552, September 1978.

2. R. E. Durrett and D. A. Matuska, The HULL Code, Finite Difference Solution to the Equations of Continuum Mechanics, AFATL-TR-78-125, November 1978.

3. M. Van Thiel, Compendium of Shock Wave Data, Lawrence National Laboratory, UCRL-50108, June 1966.

4. W. A. Allen, E. B. Mayfield and H. L. Morrison, Journal of Applied Physics, 28, 1957.